IDENTIFICATION OF FACTORS INVOLVED IN 18S NONFUNCTIONAL RIBOSOMAL RNA DECAY AND A METHOD FOR DETECTING 8-OXOGUANOSINE BY RNA-SEQ

A Dissertation Presented

By

Kelly Ann Limoncelli

Submitted to the Faculty of the
University of Massachusetts Graduate School of Biomedical Sciences, Worcester
in partial fulfillment of the requirements for the degree of

DOCTOR OF PHILOSOPHY

December 18, 2017

Neuroscience

IDENTIFICATION OF FACTORS INVOLVED IN 18S NONFUNCTIONAL RIBOSOMAL RNA DECAY AND A METHOD FOR DETECTING 8-OXOGUANOSINE BY RNA-SEQ

A Dissertation Presented
By

Kelly Ann Limoncelli

This work was undertaken in the Graduate School of Biomedical Sciences
Neuroscience Graduate Program

Under the mentorship of

Melissa J. Moore, Ph.D., Thesis Advisor

Andrei A. Korostelev, Ph.D., Member of Committee

Elisabet C. Mandon, Ph.D., Member of Committee

Sean P. Ryder, Ph.D., Member of Committee

Michael R. Volkert, Ph.D., Member of Committee

Hani S. Zaher, Ph.D., External Member of Committee

Fen-Biao Gao, Ph.D., Chair of Committee

Anthony Carruthers, Ph.D.,
Dean of the Graduate School of Biomedical Sciences

December 18, 2017

Dedicated to my friends and family.
Thank you for all your support.

ACKNOWLEDGEMENTS

I thank my mentor and role model Professor Melissa J. Moore, Ph.D. You taught me how to ask the right questions and how to be a critical thinker. You also pushed me to be a better scientist and supported me every step of the way. I am forever in your debt.

I thank all members of the Moore Laboratory, both past and present, for all of your support and guidance.

I thank all members of my small group meeting, Qualifying committee, and TRAC committee for your valuable input and providing me critical feedback throughout the years.

I thank all faculty mentors and members of the GSBS Diversity Interest Group.

I thank the National Institute of General Medical Sciences of the National Institutes of Health for the Ruth L. Kirschstein National Research Service Award (F31GM109753).

I thank my family and friends for all of your support.

I thank my husband, Nathan C. Carnes, Ph.D. You are the love of my life, my partner in crime, my other half. Without you, I would not be who I am today. You lighten my day with humor, you give me a shoulder to cry on, and you cheer me on. I look forward to raising children and growing old with you. And finally, I thank my daughter Amelia Mae Carnes. You gave me new meaning to my life. I will always love you.

ABSTRACT

The translation of mRNA into functional proteins is essential for all life. In eukaryotes, aberrant RNAs containing sequence features that stall or severely slow down ribosomes are subject to translation-dependent quality control. Targets include mRNAs encoding a strong secondary structure (No-Go Decay; NGD) or stretches of positively-charged amino acids (Peptide-dependent Translation Arrest/Ribosome Quality Control; PDTA/RQC), mRNAs lacking an in-frame stop codon (Non-Stop Decay; NSD), or defective 18S rRNAs (18S Nonfunctional rRNA Decay; 18S NRD). Previous work from our lab showed that the *S. cerevisiae* NGD factors *DOM34* and *HBS1*, and PDTA/RQC factor *ASC1*, all participate in the kinetics of 18S NRD. Upon further investigation of 18S NRD, our research revealed the critical role of ribosomal protein S3 (*RPS3*), thus adding to the emerging evidence that the ribosome senses its own translational status.

While aberrant mRNAs mentioned above can occur endogenously, damaging agents, such as oxidative stress or UV irradiation, can negatively affect the chemical integrity of RNA. Such lesions could lead to translation errors and ribosome stalling. However, current tools to monitor the fate of damaged RNA are quite limited and only provide a low-resolution picture. Therefore, we sought to develop a deep-sequencing method to detect damaged RNA, taking advantage of reverse transcriptase's ability to insert a mutation across a damaged site. Using oxidized RNA as a model damaged RNA, our preliminary data showed increased G>T mutations in oxidized RNA. This method provides the foundation for future work aimed at understanding how cells deal with damaged RNA.

TABLE OF CONTENTS

SIGNATURE PAGE......iii
DEDICATION......iv
ACKNOWLEDGEMENTS......v
ABSTRACT......vii
TABLE OF CONTENTS......ix
LIST OF FIGURES......xi
LIST OF TABLES......xii
LIST OF COPYRIGHTED MATERIALS......xiii
LIST OF ABBREVIATIONS......xiv
CHAPTER I. INTRODUCTION 1
  Translation-dependent quality control 1
    Translation-dependent quality control in bacteria 5
      Trans-translation......5
      ArfA and ArfB......6
    Translation-dependent quality control in eukaryotes......8
      No-go Decay (NGD) 8
      Non-stop Decay (NSD)......12
      Peptide-Dependent Translation Arrest (PDTA) 15
      Ribosome Quality Control (RQC) 18
      Nonfunctional rRNA Decay (NRD) 24
  RNA Damage......28
    Types of damage and molecular consequences......29
      Ultraviolet (UV) radiation 29
      Platination......31
      Alkylation 33
      Oxidation 34
    Relationship between damaged RNA and translation-dependent quality control 38
    Current tools to study damaged RNA 40
CHAPTER II. *ASC1* and *RPS3*: New actors in 18S nonfunctional rRNA decay 43
  Abstract 45
  Introduction......46
  Results......51
    A simplified system for monitoring 18S NRD 51
    DOM34 paralogs are not involved in 18S NRD......53
    Asc1p contributes to 18S NRD 54
    Increased non-functional 80S monosomes in *dom34Δ;asc1Δ* lysates......56

    - Variable effects of Ski proteins on 18S NRD 57
    - The Rps3p C-terminal tail 57
  - **Discussion** **61**
    - 18S NRD, NGD, PDTA and RQC: Different outcomes of ribosome stalling 61
    - Multiple kinetic contributors to 18S NRD targeting and decay 64
    - A central role for *RPS3* 66
    - Multiple pathways for resolving stalled ribosomes across domains 68
  - **Methods and Materials** **70**
  - **Acknowledgements** **74**
- **CHAPTER III. A deep-sequencing approach to detect oxidized RNA** **88**
  - **Introduction** **89**
  - **Results** **93**
  - **Discussion** **101**
  - **Methods and Materials** **105**
- **CHAPTER IV. DISCUSSION** **119**
  - **Part 1. *ASC1* and *RPS3*: New actors in 18S nonfunctional rRNA decay** **119**
  - **Part 2. A deep-sequencing approach to detect oxidized RNA** **127**
- **REFERENCES** **136**

LIST OF FIGURES

Figure 1.1: Aberrant RNA sequence features 9
Figure 1.2: Structure of Dom34p:Hbs1p in complex with the ribosome 16
Figure 1.3: Ribosome Quality Control pathway 21
Figure 1.4: Shared mechanisms among 18S NRD and other translation-dependent quality control pathways 27
Figure 1.5: Types of RNA damage 29
Figure 2.1: System for studying 18S NRD 75
Figure 2.2: *ASC1* contributes to 18S NRD 77
Figure 2.3: Polysome profiles and growth rates 79
Figure 2.4: Variable effects of Ski proteins on 18S NRD 81
Figure 2.5: Hbs1p N-terminal domain is dispensable for 18S NRD 83
Figure 2.6: Rps3p C-terminal tail is crucial for 18S NRD 85
Figure 2.7: Current model of 18S NRD 87
Figure 3.1: Reverse transcription of oxidized RNA 115
Figure 3.2: cDNA variant sequencing of yeast treated with H_2O_2 117

LIST OF TABLES

Table 3.1: Absorbance of untreated and oxidized RNA..............................118

LIST OF COPYRIGHTED MATERIAL

Excluding the figure titles, all contents of Chapter II appear as they were accepted for publication at RNA, September 27, 2017.

Limoncelli KA, Merrikh CN, Moore MJ. 2017. ASC1 and RPS3: New actors in 18S nonfunctional rRNA decay. *RNA* rna.061671.117.

LIST OF ABBREVIATIONS

(+)-charged	Positively charged
8oxoG	8-oxoguanosine or 8-oxo-7,8-dihydroguanosine
ALS	Amyotrophic lateral sclerosis
A-site	Aminoacyl-site
bp	base pair
CAT-tail	Carboxy-terminal alanine and threonine extensions
eRF1	Eukaryotic release factor 1
eRF3	Eukaryotic release factor 3
E-site	Exit-site
G>T	Guanosine to thymidine mutation
GTP	Guanosine triphosphate
H_2O_2	Hydrogen peroxide
mRNA	messenger RNA
NGD	No-go decay
NRD	Nonfunctional rRNA decay
NSD	Non-stop decay
nt	nucleotide
ORF	Open reading frame
P-site	Peptidyl-site
Poly(a)	Polyadenosine
PDTA	Peptide-dependent translation arrest
RF1/2	Release factor 1 / Release factor 2
ROS	Reactive oxygen species
RQC	Ribosome quality control
rRNA	ribosomal RNA
RT	Reverse transcriptase
SHAPE	Selective 2'-hydroxyl acylation analyzed by primer extension
SNP	Single nucleotide polymorphism
tRNA	transfer RNA
UTR	Untranslated region

CHAPTER I. INTRODUCTION

Translation-dependent quality control

Precise and efficient flow of genetic information is essential for all life. Sequence information encoded in deoxyribonucleic acid (DNA) is transcribed and processed into ribonucleic acid (RNA), which then serve as either functional molecules – such as ribosomal RNA (rRNA) and transfer RNA (tRNA) – or become templates for protein translation (messenger RNA; mRNA). The translation of mRNA into protein is a multistep process coordinated by a myriad of associated factors. At the core of translation is the highly conserved, ribonucleoprotein complex known as the ribosome. In eukaryotes, the ribosome consists of a small (40S) and large (60S) subunit that join together to form translationally competent 80S particles. Translation can be divided into four distinct steps: 1) initiation; 2) elongation; 3) termination; and 4) recycling. Translation initiation commences with the assembly of the 40S subunit, initiator methionyl-tRNA (Met-tRNA$_i$) positioned at the P-site, and eukaryotic initiation factors to form the pre-initiation complex (PIC). The PIC binds to the 5' end of the mRNA and proceeds to scan the mRNA until it encounters a start codon (Aitken and Lorsch 2012). Recognition of the start codon results in the dissociation of initiation factors, joining of the 60S subunit, and entrance into the elongation phase. Elongation describes the iterative process starting with the delivery of aminoacylated tRNA to the A-site, followed by peptide-bond formation (catalyzed by the ribozyme activity within the 60S subunit), and translocation to the adjacent mRNA codon (Dever and Green 2012).[1]

Canonical translation termination begins when the ribosome encounters an in-frame stop codon (UAG, UAA, or UGA). In bacteria, release factors RF1 or RF2 (RF1/2) associate with the ribosome at the A-site and sense the presence of a stop codon. This recognition step induces a conformational change in RF1/2 such that the conserved GGQ motif moves to the peptidyl-transferase center to catalyze peptidyl-tRNA hydrolysis and peptide release (Korostelev 2011). The GTPase RF3 binds to the ribosome and catalyzes the release of RF1/2 and RF3 upon GTP hydrolysis. Finally, the ribosome recycling factor RRF and elongation factor EF-G associate with the ribosome and catalyze ribosome subunit dissociation (Schmeing and Ramakrishnan 2009). Once initiation factor-3 (IF3) binds to the small subunit and facilitates mRNA and deacylated-tRNA release, both subunits are ready to be recycled for subsequent rounds of translation

---

[1] For a more in-depth review of eukaryotic initiation and elongation, refer to (Rodnina and Wintermeyer 2009; Aitken and Lorsch 2012; Dever and Green 2012; Voorhees and Ramakrishnan 2013).

(Dever and Green 2012; Keiler 2015). In eukaryotes, release factors eRF1 and eRF3, which bear no sequence homology to bacteria RF1/2, bind to the ribosome at the A-site (Schmeing and Ramakrishnan 2009; Korostelev 2011). eRF1 consists of three domains that fold into a tRNA-like structure and recognizes the stop codon (Song et al. 2000; Brown et al. 2015). The N-terminal domain (domain I) is similar to the tRNA anticodon loop, the middle domain (domain II) is similar to the tRNA acceptor arm and contains the catalytic GGQ motif, and the C-terminal domain (domain III) is similar to the tRNA T stem (Song et al. 2000; Graille and Séraphin 2012). Stop codon recognition triggers the GTPase activity of eRF3, which is followed by the dissociation of GDP-bound eRF3 and accommodation of eRF1 into the catalytically active state. The ATPase ABCE1 binds to the ribosome and holds eRF1 in the active state to promote eRF1-mediated peptidyl-tRNA hydrolysis and peptide release. Finally, ABCE1 and eRF1 dissociate the ribosome subunits in a ATPase-dependent manner (Shoemaker and Green 2011; Graille and Séraphin 2012; Preis et al. 2014). Individual subunits are then recycled for new rounds of translation (Dever and Green 2012).

Given the highly complex, multistep process, it is no surprise that cells possess quality control mechanisms to ensure the functional integrity of mRNA-to-protein translation. And while overt issues, such as mRNAs lacking a 5' cap, are readily detected and dealt with during mRNA and ribosome maturation (Jiao et al. 2010; Peña et al. 2017), subtle errors, such as those embedded within the mRNA or rRNA sequences (**Figure 1.1**), can still make their way into the translation cycle. Aberrant sequence features include mRNAs lacking a stop codon, encoding strong secondary structures, containing stretches of polyadenosine (poly(A)), etc., all of which could lead to the stalling of the associated ribosome (Shoemaker and Green 2012).[2] Ribosome stalling events are frequent, with reports indicating that two to four percent of *E. coli* ribosomes are stalled and in need of rescue (Ito et al. 2011; Keiler 2015). The complexity of the eukaryotic translation machinery suggests that ribosome stalling is also problematic in higher organisms. Without quality control, stalled ribosomes could potentially deplete the pool of translationally available ribosomes. Ribosome stalling can also lead to the generation of truncated, nonfunctional proteins, whose accumulation can activate cellular stress response (Gregersen et al. 2006; Walter and Ron 2011). Thus, rapid clearance of aberrant mRNA and the associated nascent peptide prevents ribosomes from reengaging on the same mRNA and protects cells against the accumulation of defective protein products.

---

[2] A premature stop codon within the mRNA open reading frame (ORF) triggers quality control known as nonsense-mediated decay (NMD). Although NMD depends on ongoing translation, the mechanism of ribosome rescue and mRNA decay largely deviates from other translation-dependent quality control pathways and, thus, will not be discussed here. Instead, see (Kervestin and Jacobson 2012) for a detailed review.

Translation-dependent quality control in bacteria

Trans-translation

Bacteria mRNAs lacking a stop codon can arise from ribosomal frameshifting, read-through of intact stop codons, premature transcription termination of the mRNA, endonucleolytic cleavage of the mRNA, etc. Consequently, ribosomes associated with non-stop mRNAs become stuck at the 3' end. There are currently three known mechanisms in bacteria that rescue ribosomes stalled on non-stop mRNAs (Keiler 2015). The first one, the trans-translation pathway, was initially discovered with the observation that nascent peptides containing a specific 11-amino acid tag were rapidly degraded. The gene responsible for the peptide tag (*E. coli ssrA*) encodes a unique RNA sequence that contains both mRNA- and tRNA-like properties, coined transfer-messenger RNA (tmRNA) (Keiler et al. 1996; Keiler 2015). The mRNA-like domain encodes the peptide tag while the 5' and 3' ends fold into a secondary structure – similar to a tRNA acceptor arm – that is aminoacylated with alanine. The complex formed by tmRNA and its binding partner small protein B (SmpB) resembles a complete tRNA molecule (Keiler et al. 1996; Karzai et al. 1999;

Bessho et al. 2007; Neubauer et al. 2012; Keiler 2015). Together with GTP-bound EF-Tu, the tmRNA-SmpB complex binds to the empty A-site of the stalled ribosome (Neubauer et al. 2012; Keiler 2015). Structural studies place the SmpB protein at the ribosome decoding center normally occupied by the tRNA anticodon loop, with the SmpB C-terminal tail positioned downstream of the A-site well into the mRNA entrance channel (Neubauer et al. 2012). SmpB acts as a sensor for non-stop complexes since the presence of an mRNA within the entrance channel would sterically clash with the SmpB C-terminal tail (Neubauer et al. 2012). The ribosome resumes translation on the tmRNA's mRNA-like domain that encodes the peptide tag, and continues elongating until it reaches the tmRNA stop codon sequence. The ribosome subsequently undergoes canonical termination and subunit dissociation (Keiler 2015). In addition, the associated non-stop mRNA is usually cleaved and rapidly degraded to prevent further translation of the aberrant transcript (Yamamoto et al. 2003; Ivanova et al. 2004; Keiler 2015; Ferrin and Subramaniam 2017).

ArfA and ArfB

In addition to trans-translation, some bacteria contain redundant pathways that rescue ribosomes stalled on non-stop mRNAs. In the ArfA pathway, the ArfA (yhdL) protein associates with stalled ribosomes and recruits RF2 for the hydrolysis of the peptidyl-tRNA (Keiler 2015; Demo et al. 2017). ArfA recognizes an empty A-site, with its N-terminus positioned near the decoding center and its C-terminus occupying the mRNA channel. Recent electron cryomicroscopy (cryo-EM) structures of ArfA bound to non-stop complexes suggest ArfA functionally mimics a stop codon, and its binding allows for stable association of a compact, inactive RF2 with the ribosome (James et al. 2016; Demo et al. 2017). Rearrangement of the ArfA N-terminus is coupled to the conformational change of RF2 from the compact, inactive state to an open, active state. Only in the active state is the RF2 GGQ motif positioned at the peptidyl-transferase center and primed for catalyzing the hydrolysis of peptidyl-tRNA (James et al. 2016; Demo et al. 2017; Huter et al. 2017; Ma et al. 2017). In *E. coli*, ArfA is essential for viability in the absence of a functional trans-translation pathway (*ssrA*$^-$) (Chadani et al. 2010), and evidence suggests the ArfA pathway functions as a backup to the trans-translation pathway via a negative feedback loop. Due to its secondary structure, the ArfA mRNA is cleaved by RNase III and the resulting mature mRNA lacks a stop codon. The ArfA mRNA forms non-stop ribosome complexes and is targeted for the trans-translation pathway. However, when the trans-translation pathway is limited, ArfA evades tmRNA peptide tagging and functional ArfA protein remains intact (Chadani et al. 2011a; Garza-Sánchez et al. 2011).

The ArfB pathway was discovered only when both the trans-translation and ArfA pathways were inactivated during a screen of multicopy suppressors of the lethal *ssrA*Δ *arfA*Δ phenotype (Chadani et al. 2011b). ArfB (YaeJ), which has homology to the GGQ catalytic domain of RF1/2, binds to the stalled ribosome and initiates peptidyl-tRNA hydrolysis (Handa et al. 2011). Structural studies place the ArfB C-terminal tail downstream of the A-site in the mRNA entrance channel, suggesting this domain acts as a sensor for non-stop complexes. Stable association of the C-terminal tail induces conformational changes in ArfB that leads to the placement of the GGQ motif in the peptidyl-transferase center (Gagnon et al. 2012). Unlike the trans-translation pathway, ArfA and ArfB do not promote the rapid degradation of the nascent peptide or associated mRNA (Keiler 2015).

Translation-dependent quality control in eukaryotes

No-go Decay (NGD)

Eukaryotes also possess surveillance mechanisms that resolve stalled ribosomes. No-go decay occurs when an mRNA sequence feature stalls or severely slows down associated ribosomes. These aberrant mRNAs are targeted by surveillance machinery, starting with the endonucleolytic cleavage of the mRNA in the vicinity of the stall site, followed by rapid degradation by the cytoplasmic 5' → 3' (Xrn1p) and 3' → 5' (exosome) decay factors (Shoemaker and Green 2012). This process was initially discovered in *S. cerevisiae* when researchers expressed a plasmid encoding a *pgk1* variant that contained a stem loop within the ORF (PGK1-SL) (Doma and Parker 2006); this strong secondary

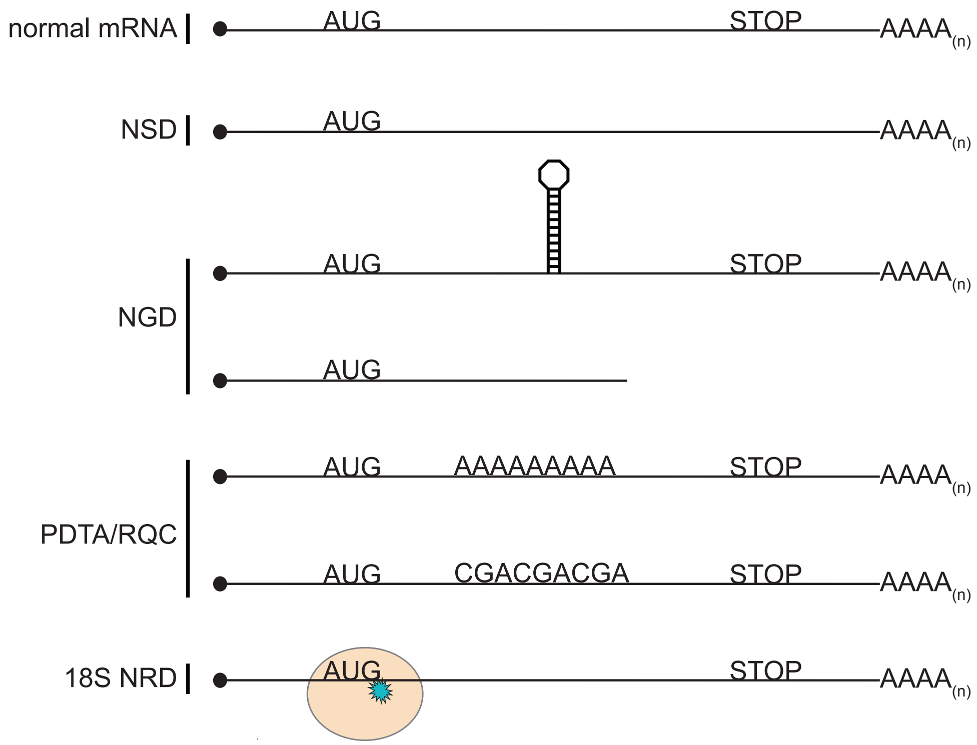
normal mRNA
AUG
STOP
AAAA(n)
NSD
AUG
AAAA(n)
NGD
AUG
STOP
AAAA(n)
AUG
PDTA/RQC
AUG
AAAAAAAAA
STOP
AAAA(n)
AUG
CGACGACGA
STOP
AAAA(n)
18S NRD
AUG
STOP
AAAA(n)

Figure 1.1: Aberrant RNA sequence features
Aberrant RNA sequence features that trigger non-stop decay (NSD), no-go decay (NGD), peptide dependent translation arrest (PDTA) or ribosome quality control (RQC), and 18S nonfunctional rRNA decay (18S NRD). mRNAs lacking a stop codon but contain a poly(A) tail are subject to NSD. mRNAs containing a strong secondary structure within the ORF or mRNAs lacking both a stop codon and poly(A) tail are subject to NGD. mRNAs containing stretches of poly(A) or rare codons within the ORF are subject to PDTA/RQC. 18S rRNA containing mutations within the decoding center is subject to 18S NRD.

structure was previously shown to stall ribosomes (Hosoda et al. 2003). Yeast rapidly degraded PGK1-SL, even in the absence of *DCP2* (decapping complex) or *SKI7* (Ski complex; 3' → 5' decay). However, strains lacking *XRN1* or components of the Ski complex accumulated 5' and 3' PGK1-SL fragments, which disappeared when translation initiation on the PGK1-SL mRNA was prevented (Doma and Parker 2006). This suggests NGD occurs during translation elongation and is initiated by an endonucleolytic cleavage event. Other sequence features that stall ribosomes (including pseudoknots, rare codons, GC-rich regions, and abasic sites) also induce a cleavage event (Doma and Parker 2006; Gandhi et al. 2008; Passos et al. 2009; Kuroha et al. 2010; Tsuboi et al. 2012).

The discovery of NGD led to the finding that Dom34p (mammalian Pelota) and Hbs1p, homologs to eRF1 and eRF3 respectively, are required for the release of stalled ribosomes (Shoemaker et al. 2010; Tsuboi et al. 2012). In *S. cerevisiae*, the Dom34p:Hbs1p heterodimer binds to the ribosome at the A-site (**Figure 1.2**), and GTP hydrolysis by the GTPase activity of Hbs1p promotes subunit dissociation (Shoemaker et al. 2010; Pisareva et al. 2011). Similar to eRF1, Dom34p consists of three domains: N-terminal domain (N), middle domain (M), and the C-terminal domain (C) (Graille et al. 2008; Pisareva et al. 2011). The M and C domains are homologous to the eRF1 domains II and III, but the

Dom34p N domain differs in that it adopts an Sm-fold (Chen et al. 2010). Cryo-EM data of Dom34p:Hbs1p bound to non-stop ribosome complexes place the Dom34p N domain at the A-site, occupying the same space as the tRNA anticodon region. The N domain also contains a loop that extends into the mRNA channel, suggesting that Dom34p recognizes an empty A-site (Hilal et al. 2016). Alternatively, this extension may destabilize shortened mRNA, as in the case of NGD complexes with mRNAs occupying the A-site and the downstream entrance channel (Shoemaker et al. 2010; Becker et al. 2011; Pisareva et al. 2011; Hilal et al. 2016; Shao et al. 2016). Unlike eRF1 domain II, the M domain of Dom34p lacks the catalytic GGQ motif (Graille et al. 2008; Hilal et al. 2016), consistent with the observation that subunit dissociation facilitates the release of an intact peptidyl-tRNA (Shoemaker et al. 2010). The body of Hbs1p folds similarly to the translational GTPase eRF3 and is organized into three domains: GTPase domain (G), domain II, and domain III. Hbs1p also contains a unique globular N-terminal domain that is attached to the body via a flexible linker. Hbs1p domains II and III interact with domains M and C of Dom34p, with their overall structural interaction comparable to that of eRF1-eRF3-GTP (Chen et al. 2010). Hbs1p holds Dom34p in the inactive state until GTP hydrolysis triggers the accommodation of Dom34p into the active state (Hilal et al. 2016). The N-terminal domain of Hbs1p resides near the mRNA entrance channel, between h16 and ribosomal protein S3 (Rps3p; uS3), possibly acting as another sensor for an empty A-site or truncated mRNA (Becker et al. 2011; Pisareva et al. 2011; Shoemaker and Green 2011; Franckenberg et al. 2012; Hilal et al. 2016). While Dom34p:Hbs1p alone can dissociate ribosome subunits, biochemical experiments not only demonstrate that the ATPase Rli1p (mammalian ABCE1) can function with Dom34p in subunit dissociation, but that Rli1p binding significantly accelerates the splitting rate (Pisareva et al. 2011; Shoemaker and Green 2011).

Non-stop Decay (NSD)

Non-stop decay targets ribosomes stalled at the 3' end of mRNAs lacking a stop codon (Shoemaker and Green 2012). Yeast genetic studies demonstrated rapid degradation of an mRNA reporter that lacks a stop codon in the ORF or 3' untranslated region (UTR). This degradation was dependent on on-going translation since the addition of cycloheximide or depletion of charged tRNAs stabilized the non-stop transcript. Studies also showed that rapid degradation occurred in the absence of the major turnover factors, *XRN1* (5' → 3' exonuclease), *DCP1* (decapping complex), or *CCR4* (deadenylase complex) (Frischmeyer et al. 2002). Rather, the Ski complex and the 3' → 5' exosome was found to mediate the degradation of non-stop transcripts (van Hoof et al. 2002; Wilson et al. 2007).

The Ski complex binds to the small subunit of non-stop ribosomes and directs the exosome 3' → 5' degradation of non-stop mRNAs (Wang et al. 2005; Kowalinski et al. 2016; Schmidt et al. 2016a). The Ski complex consists of three proteins: Ski2p, Ski3p, and Ski8p. Structural data place Ski2p, a DExH-box helicase, near the mRNA entrance channel where it is positioned to feed the mRNA substrate into the exosome (Halbach et al. 2013; Schmidt et al. 2016b). The N-terminal region of the tetratricopeptide (TRP) protein Ski3p, and one copy of the WD-repeat[3] protein Ski8p, make additional interactions with the 40S subunit; a second copy of Ski8p binds to the surface-exposed Ski3p (Schmidt et al. 2016a). Mediating the physical interaction between the Ski complex and the exosome is the eRF3-like factor Ski7p (Araki et al. 2001; Wang et al. 2005; Kowalinski et al. 2016). The Ski7p GTP-binding domain, domain II, and domain III all reside in the C-terminus, whereas the N-terminus houses distinct regions for exosome- and Ski complex-binding (Kowalinski et al. 2015; 2016). Immunoprecipitation experiments demonstrated direct binding of Ski7p to Ski8p and to multiple regions of Ski3p; these interactions allow for the indirect binding of Ski7p to Ski2p (Brown et al. 2000; Araki et al. 2001; Wang et al. 2005). With Ski7p being a stable component of the cytoplasmic exosome – and the observation that the Ski complex directly interacts with the ribosome in the absence of *SKI7* – the Ski complex likely recruits a preassembled Ski7p-exosome complex to the ribosome to initiate non-stop mRNA degradation (Kowalinski et al. 2016; Schmidt et al. 2016a).

---

[3] Tryptophan (W) and aspartic acid (D) repeats

Non-stop complexes can form from a variety of aberrant mRNA species. The read-through or complete lack of an in-frame stop-codon would result in ribosomes associated with the 3' UTR, poly(A) tail, or the 3' end of the mRNA. Alternatively, an endonucleolytic cleavage event within the ORF (as in the case with NGD substrates) would result in a ribosome complex stuck at the very 3' end of the mRNA. The formation of non-stop complexes from a NGD substrate have led researchers to speculate that the same NGD factors might also play a role in NSD. Indeed, both Dom34p and Hbs1p function in NSD by dissociating ribosomes stalled at the 3' end of the mRNA (Tsuboi et al. 2012; Saito et al. 2013a; Guydosh and Green 2014). This suggests NSD and NGD describe the same surveillance mechanism and differ only in the type of stalled ribosome complex that initiated the pathway.

Peptide-Dependent Translation Arrest (PDTA)

While NGD and NSD were discovered by examining the fate of aberrant mRNA, PDTA was discovered by examining the fate of the nascent peptide. Yeast expression of a plasmid encoding either stretches of positively-charged ((+)-charged) amino acids, poly(A) stretches, or rare codons resulted in rapid degradation of the associated nascent peptide (Dimitrova et al. 2009; Ikeuchi and Inada 2016). PDTA mRNAs likely stall or severely slow down ribosomes since stretches of (+)-charged amino acids can make electrostatic interactions with the ribosome's negatively-charged peptide channel (Lu et al. 2007; Requião et al. 2016), and rare codons reduce translation efficiency (Letzring et al. 2010; 2013; Wolf and Grayhack 2015). Furthermore, PDTA mRNAs are subject to endonucleolytic cleavage (Kuroha et al. 2010; Chen et al. 2010; Tsuboi et al. 2012; Guydosh and Green 2017), suggesting they are also targets for NGD. Indeed, NGD factors Dom34p and Hbs1p facilitate endonucleolytic cleavage and dissociate the 60S and 40S subunits of stalled PDTA complexes (Kuroha et al. 2010; Tsuboi et al. 2012).

A screen of *S. cerevisiae* mutants suppressing PDTA activity identified *ASC1* (mammalian RACK1) as a required factor. Asc1p is a highly conserved, stoichiometric component of the 40S ribosomal subunit (**Figure 1.2**) (Coyle et al. 2009). Without *ASC1*, protein products from PDTA mRNAs are stabilized

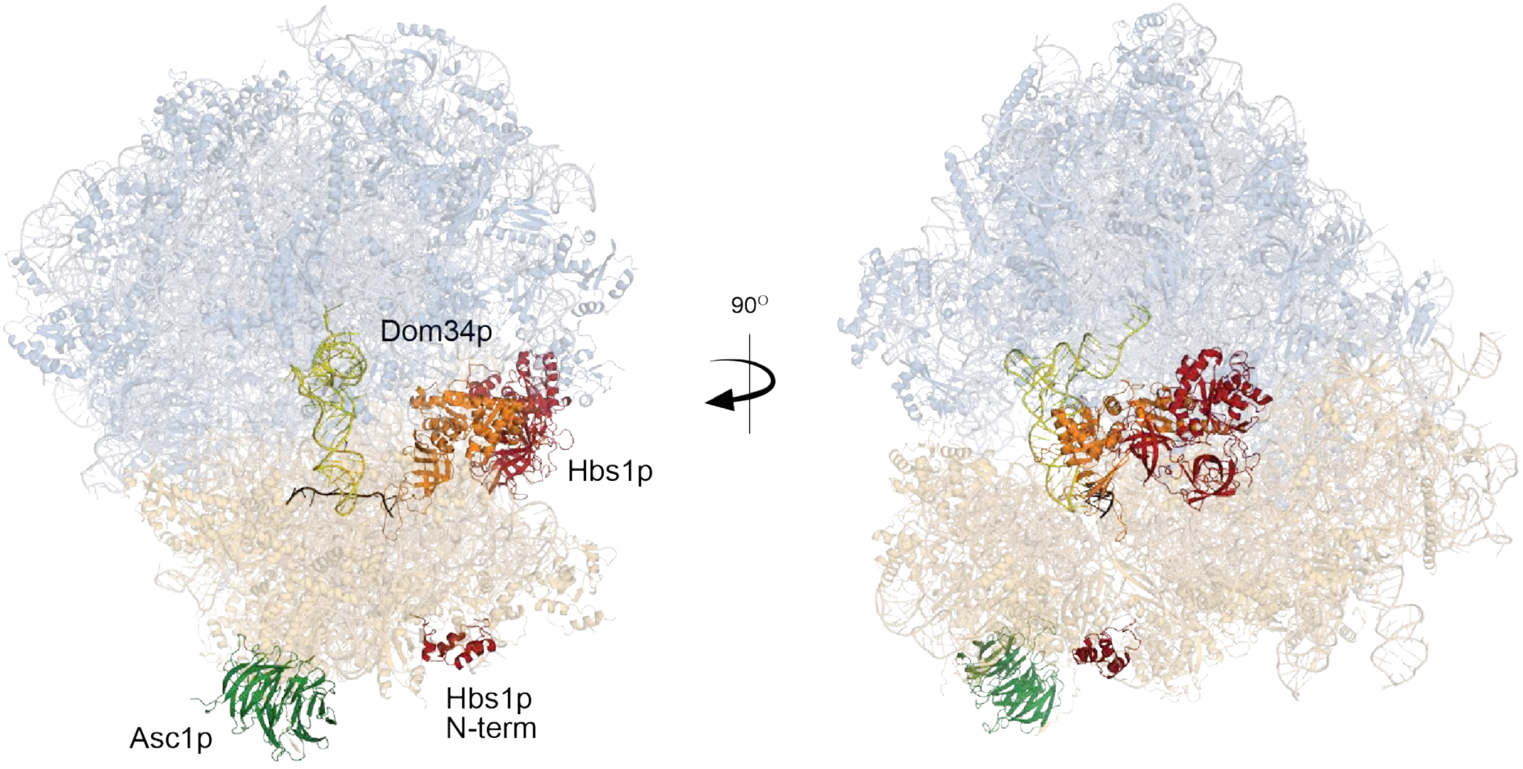
Dom34p
Hbs1p
Hbs1p
N-term
Asc1p
90°

Figure 1.2: Structure of Dom34p:Hbs1p in complex with the ribosome
Cryo-EM structure of the yeast 80S ribosome in complex with Dom34p (orange), Hbs1p (red), P-site tRNA (yellow), and mRNA (black). Shown in green is the ribosomal protein Asc1p (PDB: 5M1J) (Hilal et al. 2016).

(Kuroha et al. 2010; Ikeuchi and Inada 2016). It was thought that Asc1p promoted stalling of the ribosome (Kuroha et al. 2010; Inada 2013; Letzring et al. 2013), but more recent data suggest Asc1p is involved in targeting stalled ribosomes for quality control (Sitron et al. 2017).

Asc1p belongs to a class of WD-repeat (Trp-Asp) proteins and folds into a seven-bladed beta-propeller structure (Coyle et al. 2009). It was originally identified as an activator of Protein Kinase C (PKC), hence its mammalian name Receptor for Activated C Kinase 1 (RACK1) (Ron et al. 1994; 1999). This eukaryotic-specific factor is highly conserved from yeast to humans and, like other WD proteins, acts as a scaffold for multiple proteins. Indeed, RACK1 has been implicated in many signal transduction pathways, including the Src kinase, MAP kinase, and cAMP-specific phosphodiesterase PDE_4D_5 pathways (McCahill et al. 2002; Rachfall et al. 2013). In higher eukaryotes, loss of RACK1 is embryonic lethal with disruptions to neural tube closure, post-synaptic function in neurons, and cell migration (Ron et al. 1999; Yaka et al. 2002; Kiely et al. 2009; Wehner et al. 2011). In yeast, deletion of *ASC1* leads to slow growth, loss of cell wall integrity, loss of invasive growth (glucose sensing), and mitochondrial dysfunction (Valerius et al. 2007; Coyle et al. 2009; Melamed et al. 2010; Rachfall et al. 2013). Both RACK1 and Asc1p primarily exist as ribosome-bound factors, specifically associating with 40S subunits in proximity to the mRNA exit channel (Coyle et al. 2009; Ben-Shem et al. 2010; Anger et al. 2013). Studies in mammalian cells show RACK1 participating in translation initiation by directing PKC phosphorylation of eIF6[4] (Ceci et al. 2003). RACK1 has also been shown to promote ubiquitination of various proteins (Liu et al. 2007; Subauste et al. 2009; Sundaramoorthy et al. 2017). In yeast, loss of *ASC1* increases ribosome frameshifting at CGA repeats (Wolf and Grayhack 2015). Finally (as mentioned above), RACK1/Asc1p functions in ribosome quality control, where it promotes the degradation of nascent peptides associated with stalled ribosomes (Kuroha et al. 2010; Juszkiewicz and Hegde 2017; Sundaramoorthy et al. 2017).

Ribosome Quality Control (RQC)

RQC is similar to PDTA in that both describe the fate of nascent peptides associated with stalled ribosomes; however, RQC expands on the mechanism of peptide targeting and degradation (Brandman and Hegde 2016). RQC was originally discovered during a genome-wide screen of *S. cerevisiae* loss-of-function strains exhibiting high Heat Shock Factor 1 (Hsf1p) transcriptional activity. This was accomplished by expressing a reporter encoding GFP driven by Hsf1p promoter elements, and monitoring Hsf1p activity by high-throughput flow cytometry. The Hsf1p transcription factor activates genes in response to various stressors (e.g. heat shock); thus, the reporter system allowed for the identification of genes contributing to cellular homeostasis. A prominent subset of translationally-related genes modulating Hsf1p activity included those of the RQC pathway. Further experiments revealed Asc1p, Hel2p (an E3 ubiquitin ligase), Rqc1p, Rqc2p/Tae2p, Ltn1p (an E3 ubiquitin ligase), Cdc48p (an AAA ATPase), Npl4p (a cofactor of Cdc48p), and Ufd1p (a cofactor of Cdc48p) as protein components of the RQC pathway (Brandman et al. 2012).

---

[4] Dephosphorylated eIF6 prevents premature formation of 80S ribosomes by stably associating with free 60S subunits (Ceci et al. 2003; Brina et al. 2015).

In the current model (**Figure 1.3**), Asc1p functions with Hel2p and the recently identified RQT complex (Slh1p:Cue3p:Rqt4p) in targeting stalled ribosomes for RQC engagement (Saito et al. 2015; Matsuo et al. 2017; Sitron et al. 2017). Upon expression of a reporter mRNA encoding stretches of (+)-charged amino acids, deletion of either *ASC1*, *HEL2*, or the RQT proteins led to the increased stability of associated nascent peptides (Kuroha et al. 2010; Brandman et al. 2012; Matsuo et al. 2017; Sitron et al. 2017). Hel2p (along with its cofactors E2 ubiquitin-conjugating enzyme Ubc4p, E1 ubiquitin-activating enzyme Ube1p, and ubiquitin) ubiquitinates 40S proteins Rps3p (uS3; amino acid K212) and Rps20p (uS10; amino acids K6 and K8). Notably, the K6/K8 ubiquitination is required for RQC engagement (Matsuo et al. 2017). Hel2p co-sediments with polysomes, even in the absence of its RING domain or its Ubc4p binding-site, suggesting Hel2p associates with ribosomes prior to ubiquitination (Matsuo et al. 2017). The RQT complex associates with Hel2p-bound ribosomes and likely functions in recognizing Rps20p (uS10) ubiquitination via the ubiquitin-binding CUE domain of Cue3p. The ATPase activity of the RecA helicase Slh1p is required for targeting and subsequent RQC engagement, but the exact role of the ATPase activity is still unknown (Matsuo et al. 2017). Work in mammalian cells using a poly(A) mRNA reporter demonstrates that the targeting of stalled ribosomes by Asc1p and Hel2p is highly conserved. Both ZNF598 (yeast *HEL2*) and RACK1 (yeast *ASC1*) facilitate the ubiquitination of specific 40S proteins in stalled ribosomes. ZNF598 primarily functions in RPS20 (uS10) and RPS10 (eS10) ubiquitination, whereas RACK1 functions in RPS3 (uS3) and RPS2 (uS5) ubiquitination. A similar ubiquitination pattern was apparent in cells treated with inhibitors of translation elongation or activators of the unfolded protein response (Higgins et al. 2015; Juszkiewicz and Hegde 2017; Sundaramoorthy et al. 2017). Finally, the current model places targeting upstream of ribosomal subunit dissociation given the evidence that *DOM34* and *HBS1* function in splitting ribosomes and that peptidyl-tRNA is stabilized in yeast lacking either factor (Tsuboi et al. 2012; Shao et al. 2013; Verma et al. 2013; Osuna et al. 2017).

Once targeted, the RQC factors Rqc1p, Rqc2p, and Ltn1p associate with nascent-chain containing 60S subunits to tag the nascent peptide for

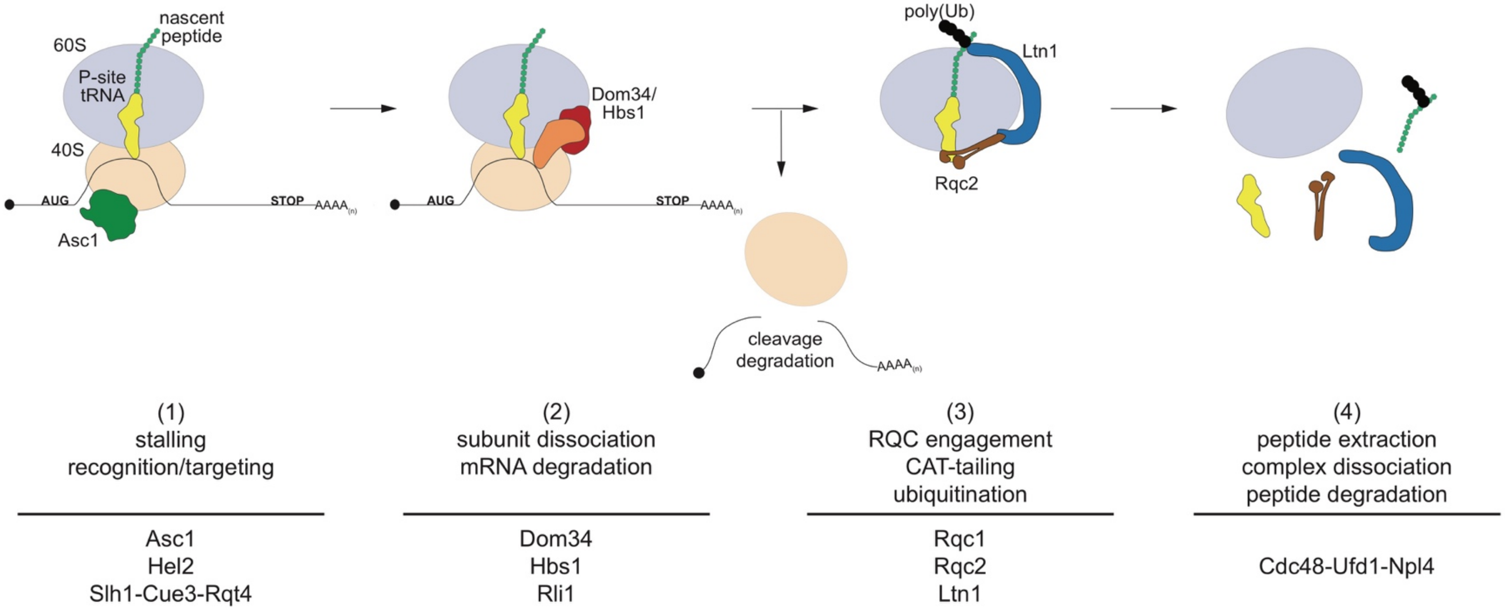
nascent
peptide
60S
P-site
tRNA
40S
AUG
STOP
AAAA(n)
Asc1
Dom34/
Hbs1
cleavage
degradation
poly(Ub)
Ltn1
Rqc2
(1)
stalling
recognition/targeting
Asc1
Hel2
Slh1-Cue3-Rqt4
(2)
subunit dissociation
mRNA degradation
Dom34
Hbs1
Rli1
(3)
RQC engagement
CAT-tailing
ubiquitination
Rqc1
Rqc2
Ltn1
(4)
peptide extraction
complex dissociation
peptide degradation
Cdc48-Ufd1-Npl4

Figure 1.3: Ribosome Quality Control pathway
Current model of Ribosome Quality Control (RQC). Step 1) Recognition and targeting by Asc1p, Hel2p, and the RQT complex (Slh1p:Cue3p:Rqt4p). Step 2) Subunit dissociation by Dom34p:Hbs1p and Rli1p. Endonucleolytic cleavage and degradation of mRNA. Step 3) Assembly of remaining RQC factors. CAT-tailing by Rqc2p, nascent peptide ubiquitination by Ltn1p. Step 4) Peptide extraction by Cdc48p:Ufd1p:Npl4p, complex dissociation, and peptide degradation by the proteosome. Figure adapted from (Brandman and Hegde 2016).

degradation. This is accomplished by CAT-tail synthesis and/or ubiquitination. Rqc2p directs the template-independent addition of alanine and threonine extensions (CAT-tails) to the C-terminus of the nascent peptide (Shen et al. 2015). Rqc2p interacts with alanine- or threonine-charged tRNA, bringing the A-site tRNA to the peptidyl-transferase center for the ribosome to catalyze peptide bond formation (Shao et al. 2015; Osuna et al. 2017). Cryo-EM data revealed extensive interactions between the P-site tRNA and the N- and C-terminal domains of Rqc2p, suggesting that Rqc2p stabilizes P-site tRNA after 40S dissociation (Shao et al. 2015; Shen et al. 2015). CAT-tailing also promotes Hsf1p transcriptional activation and is abrogated in the absence of Rqc2p in vivo and in vitro (Shen et al. 2015; Osuna et al. 2017).

CAT-tailing appears to facilitate ubiquitination of the nascent chain (Brandman and Hegde 2016; Kostova et al. 2017; Osuna et al. 2017). For example, when ribosomes stall due to stretches of (+)-charged amino acids, lysine residues would be enclosed within ribosome's exit channel and, therefore, would be unavailable for ubiquitination. The addition of alanine and threonine residues to the nascent chain would move the lysine residues through the channel, eventually exposing them for post translational modification. Alternatively, if sufficient lysine residues were already exposed, ubiquitination and degradation of the nascent peptide proceeds regardless of CAT-tails (Shao and Hegde 2014; Shen et al. 2015; Choe et al. 2016; Defenouillère et al. 2016; Yonashiro et al. 2016; Kostova et al. 2017; Osuna et al. 2017). In addition to CAT-tail synthesis, Rqc2p functions in CAT-tail termination by promoting hydrolysis of the peptidyl-tRNA. Although the exact mechanism remains unclear, it was shown that peptidyl-tRNA was stabilized in the absence of *RQC2* (Osuna et al. 2017).

While Rqc2p promotes CAT-tailing, the E3 ubiquitin ligase Ltn1p ubiquitinates the nascent peptide of stalled complexes in an Rqc1p-dependent manner (Osuna et al. 2017).[5] Biochemical experiments showed that Ltn1p is able to distinguish nascent chains associated with 60S subunits from 80S ribosomes; therefore, ribosomal subunit dissociation must occur before ubiquitination by Ltn1p (Shao et al. 2013; Shao and Hegde 2014). Structural studies place the RING domain (the binding site of E2 ubiquitin-conjugating enzyme) near the peptide exit channel (Shao et al. 2015), priming Ltn1p to ubiquitinate the emerging nascent chain. Of note, the positioning of both Rqc2p and Ltn1p on the 60S subunit effectively blocks the 40S subunit from re-associating (Shao et al. 2015; Shen et al. 2015).

---

[5] The role of Rqc1p in ubiquitination remains elusive, but authors have speculated that Rqc1p either helps position the nascent chain near the Ltn1p RING domain, stimulates Ltn1p's ligase activity, or promotes E2 binding (Osuna et al. 2017).

The final steps of the current model describe the degradation of the peptide. Tagging by polyubiquitination initiates the association of the AAA+ ATPase Cdc48p and its cofactors Ufd1p and Npl4p for extraction of the nascent peptide. Based on its role in the endoplasmic reticulum associated protein degradation (ERAD), it is believed that Cdc48p uses its ATPase activity to pull the tagged nascent peptide from the 60S subunit, consequently freeing the peptide for degradation by the proteasome (Brandman et al. 2012; Wolf and Stolz 2012; Verma et al. 2013; Brandman and Hegde 2016).

Nonfunctional rRNA Decay (NRD)

NRD describes the surveillance of nonfunctional 18S (18S NRD) and 25S (25S NRD) ribosomal RNAs (LaRiviere et al. 2006; Cole and LaRiviere 2008; Cole et al. 2009). Previous work from our laboratory monitored the fate of mature but functionally defective *S. cerevisiae* rRNAs that contained inactivating mutations in the 18S rRNA decoding center (equivalent to G530U, U534G, or A1492C in *E. coli* 16S rRNA) or the 25S rRNA peptidyl-transferase center (equivalent to A2451G, C2452U, or U2585A in *E. coli* 23S rRNA). These mutations were embedded in a plasmid encoding the entire 35S pre-rRNA sequence driven by the polymerase II promoter GAL7. The plasmid-derived rRNA also contains benign sequence tags that enable specific detection of the reporter rRNA amongst total rRNA via northern blot analysis (LaRiviere et al. 2006; Cole and LaRiviere 2008). Induction of transcription by galactose produces reporter rRNA that makes up only 1% of total rRNA (LaRiviere et al. 2006). Thus, 18S NRD kinetics can be monitored by performing a transcriptional pulse chase (Cole and LaRiviere 2008). Like their corresponding wild-type rRNAs, mutant rRNAs are synthesized, processed, and assembled into structurally intact ribosomes. However, the mutant 18S and 25S rRNAs are eliminated by mechanistically distinct pathways (LaRiviere et al. 2006; Cole et al. 2009).

In 25S NRD, 60S subunits containing mutant 25S rRNA cannot form stable 80S monosomes, and mutant 25S rRNA localize to perinuclear foci. Further, yeast preserve 25S NRD in the presence of the translation elongation inhibitor cycloheximide, indicating 25S NRD is not dependent on ongoing translation (LaRiviere et al. 2006; Cole et al. 2009). Finally, 25S NRD involves DNA damage repair factors *MMS1* and *RTT101* (an ubiquitin E3 ligase) (Fujii et al. 2009). 60S subunits containing mutant 25S rRNA are tagged with ubiquitin in a Mms1p:Rtt101p-dependent manner, which is subsequently recognized by the Cdc48p:Ufd1p:Npl4p complex and the proteasome (Fujii et al. 2012). Since 25S NRD still occurs in yeast lacking *XRN1* or *SKI7* (Cole et al. 2009), it remains unknown how exactly mutant 25S rRNA is removed from the 60S subunit and degraded.

In contrast, 18S NRD exhibits similar characteristics of other translation-dependent pathways (**Figure 1.4**). Like wild-type rRNA in translating ribosomes, mutant 18S rRNA displays diffuse cytoplasmic localization, and co-sediments with 40S subunits and 80S monosomes – mutant 18S rRNA also co-sediments with polysomes but to a much lesser extent (LaRiviere et al. 2006; Cole et al. 2009). Treatment with cycloheximide completely abrogates 18S NRD, demonstrating its dependence on ongoing translation (Cole et al. 2009). Furthermore, 18S NRD involves a number of factors implicated in other translation-dependent surveillance pathways. 18S NRD kinetics is significantly reduced in the absence of either *DOM34*, *HBS1*, *ASC1*, *or SKI7* (Cole et al. 2009). Double deletion of *DOM34* and *HBS1* only partially stabilizes mutant 18S rRNA (Cole et al. 2009), consistent with the model that the Dom34p:Hbs1p heterodimer function in the same pathway by dissociating ribosomal subunits. On the other hand, a *dom34*Δ strain lacking *ASC1* completely abrogates 18S NRD (Merrikh 2012). Thus, 18S NRD appears to consist of two genetically separable pathways, one involving *ASC1* and the other involving *DOM34*:*HBS1*. Examination of the cryo-EM structure of the yeast 80S ribosome in complex with Dom34p:Hbs1p revealed that the ribosomal protein S3 (uS3) structurally

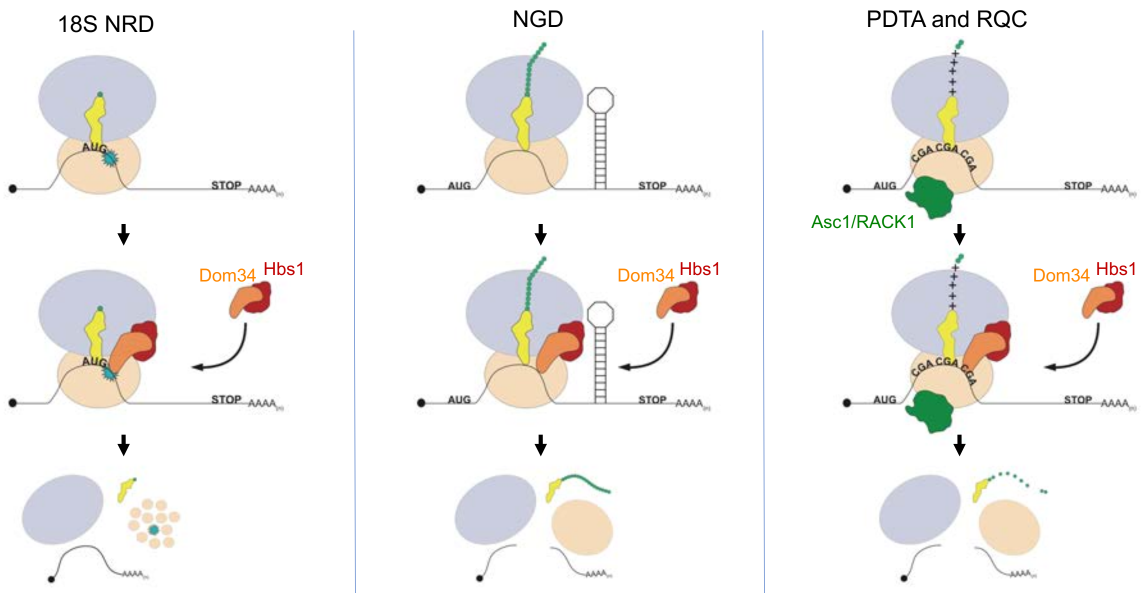

Figure 1.4: Shared mechanisms among 18S NRD and other translation-dependent quality control pathways
18S NRD, NGD, PDTA, and RQC are all initiated by ribosomal stalling. Mutations within the 18S rRNA decoding center lead to ribosomal stalling, whereas aberrant mRNAs containing strong secondary structures (NGD), stretches of CGA repeats, or basic amino acids (PDTA/RQC) stall ribosomes. Ribosome stalling is recognized by the splitting factors Dom34p:Hbs1p in all pathways. After subunit dissociation, cytoplasmic exonucleases degrade problematic RNAs (18S NRD and NGD), while the proteasome degrades the nascent peptide (PDTA/RQC).

interacts with Hbs1p and Asc1p, leading us to predict that *RPS3* might be involved in 18S NRD. *Chapter II of this thesis investigates whether RPS3 contributes to the rapid decay of mutant 18S rRNA and confirms the role of ASC1 in 18S NRD.*

RNA Damage

Normal metabolic byproducts and environmental factors can negatively affect cellular function by damaging macromolecules. Although a considerable amount of work has focused on pathways that deal with damaged proteins, lipids, and DNA (Doetsch and Cunningham 1990; Demple and Harrison 1994; Gros et al. 2002; Niki 2014), little is known about the cellular responses to RNA damage. Numerous studies have shown that RNA is highly susceptible to oxidation, alkylation, and irradiation that result in aberrant RNA modifications (Wurtmann and Wolin 2009) (**Figure 1.5**); such lesions could lead to ribosome stalling and protein miscoding (Simms and Zaher 2016). Since translation-dependent quality control mechanisms target stalled ribosomes, recent data implies that damaged RNA may stand in as a possible substrate (Simms et al. 2014; Calabretta et al. 2015; Hudson and Zaher 2015; Jamar et al. 2017). In addition, damaged RNA has been linked to many diseases, including amyotrophic lateral sclerosis (ALS), Alzheimer's, and Parkinson's (Zhang et al. 1999; Shan et al. 2003; Chang et al. 2008; Nunomura et al. 2009), but whether this is merely an outcome of the pathology, or part of the cause, remains elusive. The amount of unanswered questions points to a need for higher-resolution tools to further our knowledge on how cells deal with damaged RNA.

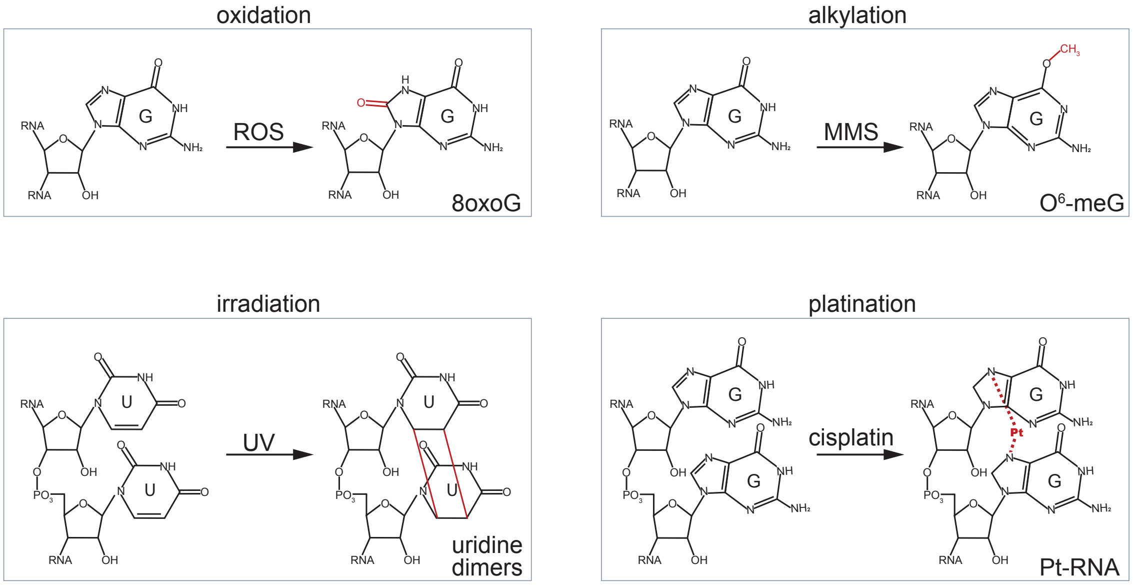
oxidation

alkylation

irradiation

platination

Figure 1.5: Types of RNA damage
Different types of damaging agent-induced adducts. ROS: reactive oxygen species; 8oxoG: 8-oxoguanosine; MMS: methyl methanesulfonate; O^6-meG: O^6-methylguanosine; UV: ultraviolet; Pt-RNA: platinated RNA.

Types of damage and molecular consequences

Ultraviolet (UV) radiation

Irradiation of purified RNA induces several types of photoproducts, including cyclobutane pyrimidine dimers, uridine hydrate, and cytidine hydrate. These products are more likely to occur in single-stranded RNA than double-stranded RNA (Pearson and Johns 1966; Pearson et al. 1966; Miller and Cerutti 1968; Remsen et al. 1970; Holmes and Singer 1971; Wurtmann and Wolin 2009; Kladwang et al. 2012). Several lines of work suggest UV-irradiated RNA can substantially impact RNA-based methods, cellular components, and cellular function. For instance, one group noted significant RNA damage upon UV-shadowing (Kladwang et al. 2012). Gel-purification of RNA is routinely practiced during the preparation of RNA deep-sequencing libraries, and many laboratories use hand-held UV lamps to visualize RNA within gels. However, even at low-energy settings, UV-shadowing induces damaging photo lesions in RNA samples (Kladwang et al. 2012). Moreover, gel-purification of size-selected RNA often precedes the reverse transcription step for some specialized deep-sequencing libraries (Ingolia et al. 2012). Since reverse transcriptase tends to stop at pyrimidine dimers (Iordanov et al. 1998; Kladwang et al. 2012), incomplete cDNA synthesis can bias downstream analyses.[6]

In vivo studies of cells irradiated with UV revealed extensive cross-linking between ribosomal proteins and RNA that coincides with reduced global translation (Stiege et al. 1986; Iordanov et al. 1998; Casati 2004). UV-irradiation also induces the conserved ribotoxic stress response[7]. Upon exposure to UV radiation, mammalian 28S rRNA acquired specific sites of damage, notably in the peptidyl transferase center and the sarcin-ricin loop (SRL). Furthermore, cellular response to UV-exposure requires actively translating ribosomes as a prerequisite for the activation of several kinases and the transcriptional induction of stress-related genes (Iordanov et al. 1998). Another study demonstrated a connection between UV-irradiated RNA and skin inflammation (i.e. sunburn) (Bernard et al. 2012). Exposing keratinocytes to UV radiation induces cytokine production from neighboring, non-irradiated keratinocytes via activation of the Toll-like receptor 3 (TLR3). UV-exposure also induces changes to RNA secondary structure, specifically the noncoding snU1 RNA. The authors were able to show that purified UV-irradiated snU1 RNA, as well as lysate from UV-exposed cells, was sufficient to induce TLR3 activation. Therefore, irradiated cells release damaged snU1 RNA, which then serves as a signaling molecule for TLR3-mediated inflammatory response (Bernard et al. 2012).

---

[6] On the other hand, the cross-linking effects of UV-irradiation have proven to be an asset in certain experimental designs, such as those aimed at identifying sequence targets of RNA-binding proteins (Greenberg 1979; Hafner et al. 2010).

[7] A signaling pathway that is initiated in response to treatment with ribotoxins ricin A chain or alpha-sarcin (Iordanov et al. 1997). Ribotoxins cleave the 60S sarcin-ricin loop (SRL), a highly conserved rRNA domain that facilitates elongation by anchoring EF-G to the ribosome during translocation (Wool et al. 1992; Shi et al. 2012); thus, ribotoxins essentially inactivate ribosomes.

Platination

Cisplatin, carboplatin, and oxaliplatin are platinum-based chemotherapeutic drugs often used for the treatment of numerous cancers. Their utility has earned them a spot on the World Health Organization (WHO) List of Essential Medicines. Platinum-based molecules react primarily with the N7 position of guanosine to form intrastrand and interstrand crosslinks in nucleic acids. The cross-linking properties of platinum-based molecules can lead to cell-cycle arrest and programmed cell-death (Rosenberg 1985). While some literature attribute the antitumor activity of platinum-based molecules on their ability to damage DNA (Roberts and Thomson 1979; Rosenberg 1985; Siddik 2003), emerging evidence indicates platination effects the chemical and functional integrity of RNA and RNA-related processes. For instance, cisplatin treatment reduced the splicing activity of HeLa nuclear extracts in a dose-dependent manner (Schmittgen et al. 2003). Further, *S. cerevisiae* treated with micromolar amounts of cisplatin accumulated 4- to 20-fold more platinum-RNA products than DNA. Most platinum-RNA products occurred on rRNA at functionally-relevant sites, with estimates of one to two platinum products occurring every three ribosomes (Hostetter et al. 2012; Osborn et al. 2014; Melnikov et al. 2016). Cisplatin appears to inhibit both translation initiation and elongation. An in vitro translation study using rabbit reticulocyte lysate demonstrated that cisplatin prevented the joining of 60S and 48S particles to form stable 80S complexes (Rosenberg and Sato 1993), while another study found that cisplatin arrested elongation (Heminger et al. 1997). Although a direct link has yet to be shown, it is possible that the platinum effects on RNA-related processes might contribute to the neuropathies many cancer patients experience from cisplatin treatment (Windebank and Grisold 2008).

Alkylation

Aberrant methylation of RNA can stem from endogenous sources, such as *S*-adenosyl methionine (SAM), or exogenous sources, such as methyl halides (found in pesticides and tobacco smoke) and many chemotherapeutic drugs (Drabløs et al. 2004; Sedgwick 2004; Simms and Zaher 2016). The nitrogenous bases and phosphate backbone are all susceptible to methylation, with the 7-methylguanosine being the most prevalent (Sedgwick 2004). O^6-methylguanosine is highly mutagenic due to its ability to base pair with thymidine or uridine. Kinetic studies using a reconstituted in vitro translation system determined the effects of O^6-methylguanosine on the ribosome decoding process (Hudson and Zaher 2015). The authors monitored peptide-bond formation by incubating purified bacteria-initiation complexes (carrying fMet-tRNA[8] in the P-site) with elongation factors, charged tRNA, and mRNA (with or without O^6-methylguanosine positioned at the A-site). Cytidine:O^6-methylguanosine pairs in the first and second codon:anticodon positions slowed ribosome decoding by 100- to 1000-fold. Uridine:O^6-methylguanosine pairs in the second position also slowed ribosome decoding. Conversely, ribosomes readily translated uridine:O^6-methylguanosine pairs occupying the first position, and cytidine:O^6-

---

[8] N-formyl-methionyl tRNA (fMet-tRNA) is the bacteria-specific initiator tRNA

methylguanosine pairs in the third position (Hudson and Zaher 2015). Thus, depending on the position of the modified codon, methyl adducts can either slow ribosome transit or permit incorrect tRNA selection. Another study examined other types of methylated adducts on translation fidelity. Depending on the location of the methyl group and the codon position of the methylated base, some adducts had no effect on translation whereas others inhibited it (You et al. 2017). Overall, these data suggest that mRNA containing methylated bases can severely slow down ribosomes or lead to the production of aberrant peptides.[9]

Oxidation

Cells generate reactive oxygen species (ROS) as a normal metabolic byproduct. For example, the mitochondria electron chain transporter can prematurely leak oxygen, giving rise to the superoxide radical ($\cdot O_2^-$) (Turrens 2003). Neutrophils also generate superoxide radicals during phagocytosis of invading microorganisms (Rada and Leto 2008). Finally, peroxisomes produce many precursors of ROS, including hydrogen peroxide (H_2O_2) and nitric oxide (·NO)[10], which can both pass through the peroxisomal membrane (Bonekamp et al. 2009).[11] Many exogenous stressors can lead to the intracellular production of ROS. UV radiation, inflammation, heat shock, or treatment with carcinogens or chemotherapeutic drugs have all been shown to increase intracellular ROS (Fiala et al. 1989; Nunoshiba and Demple 1993; Bruskov et al. 2002; Cadet et al. 2005; Rada and Leto 2008; Carozzi et al. 2010). Bacteria, yeast, and mammalian cells treated with oxidizing agents have yielded more oxidized RNA than DNA. 8-oxo-7,8-dihydroguanosine (8-oxoguanosine; 8oxoG) is the most prevalent product, however, 8-oxo-7,8-dihydroadenosine (8oxoA), 5-hydroxycytidine (5-HO-C), and 5-hydroxyuridine (5-HO-U) have also been observed; 8oxoG is particularly mutagenic due to its ability to base pair with adenosine (Fiala et al. 1989; Yanagawa et al. 1990; 1992; Shen et al. 2000; Weimann et al. 2002; Hsu et al. 2004; Hofer et al. 2005; 2006; Kim et al. 2006; Liu et al. 2012; Simms et al. 2014).

---

[9] Interestingly, members of the AlkB-like family have been shown to demethylate RNA (Aas et al. 2003; Ougland et al. 2004; Jia et al. 2011; Vågbø et al. 2013), implicating a repair mechanism for methylated RNA. However, RNA methylation is wide-spread and a normal part of the maturation and function of noncoding RNA (Decatur and Fournier 2002; Duechler et al. 2016; Liu et al. 2016). Methylated mRNA, such as N^6-methyladenosine (m^6A), has been recently implicated in regulating gene expression (Fu et al. 2014; Gilbert et al. 2016; Hoernes et al. 2016). Therefore, it is unclear whether these enzymes necessarily repair methylated RNA or assist in the dynamic regulation of post transcriptional methylation (Wu et al. 2016).

---

[10] H_2O_2 reacts with iron to produce the hydroxyl radical ($\cdot OH^-$) via Fenton's reaction (Walling 1975), and nitric oxide reacts with superoxide radicals to produce the oxidant peroxynitrite ($ONOO^-$) (Bonekamp et al. 2009).

[11] It should be noted that cells contain a variety of enzymes that neutralize ROS. For instance, catalase breaks down H_2O_2, while superoxide dismutase (SOD1) catalyzes the disproportionation of the superoxide radical.

High levels of 8oxoG RNA have been linked with many neurodegenerative diseases. For example, a mouse model of ALS (SOD1^{G93A}) contained high levels of 8oxoG in the spinal cord motor neurons and oligodendrocytes. This increase in oxidation occurred before the onset of behavioral symptoms associated with ALS (Chang et al. 2008).[12] Human tissue samples from the spinal cord and motor cortices of ALS patients also contained high levels of 8oxoG RNA (Chang et al. 2008). In addition, RNA oxidation has been observed in tissue samples of Alzheimer's patients (Nunomura et al. 1999; Abe et al. 2002; Shan et al. 2003; Ding et al. 2005; Shan and Lin 2006; Nunomura et al. 2012). Hippocampal tissue immunostained with an antibody that specifically recognizes 8oxoG exhibited greater RNA oxidation in patient samples compared to age-matched tissues, where the amount of 8oxoG RNA positively correlated with cognitive decline (Nunomura et al. 1999; 2012). These studies treated samples with RNAase prior to immunostaining to verify that the signal comes from 8oxoG RNA as opposed to 8oxoG DNA (Nunomura et al. 1999; 2002; Chang et al. 2008). Finally, other studies have found increased 8oxoG RNA in neurons of the substantia nigra and in the cerebrospinal fluid of patients with Parkinson's disease (Zhang et al. 1999; Abe et al. 2003). Despite its prevalence, however, it remains unclear whether RNA oxidation directly contributes to the pathogenesis or is just a byproduct.

---

[12] Interestingly, another group treated cultured neurons with oxidizing agents and observed an increase in 8oxoG RNA that preceded neuronal cell death (Shan et al. 2007).

Emerging evidence suggests RNA oxidation can have profound effects on translation. In vitro translation of an oxidized mRNA substrate results in fewer protein products compared to non-oxidized mRNA (Shan et al. 2007). A similar outcome was observed in mammalian cells transfected with oxidized mRNA (Shan et al. 2007; Tanaka et al. 2007). Other studies have examined ribosome decoding kinetics on 8oxoG bases. Using a high-resolution reconstituted translation system, one group demonstrated that cytidine:8oxoG or adenosine:8oxoG pairs in the first, second, or third codon:anticodon positions significantly slowed peptide-bond formation anywhere from 100- to 1000-fold (Simms et al. 2014). The same group studied the translational effects of an mRNA reporter containing a single 8oxoG in eukaryotic extract. The reporter yielded very little protein, even in the presence of protease inhibitors (Simms et al. 2014). Another study developed an mRNA reporter containing a single oxidized base (8oxoG, 8oxoA, 5-HO-C, or 5-HO-U) upstream of a puromycin unit[13] (Calabretta et al. 2015). Translation of this reporter results in a peptide product covalently linked to the mRNA, allowing for direct analysis of translation products on a denaturing gel (Roberts and Szostak 1997; Calabretta et al. 2015). The authors showed that in vitro translation of the reporter mRNA produced fewer full-length proteins while simultaneously increased the amount of abortive peptides whose length corresponded to the site of the lesion (Calabretta et al. 2015). Overall, these data indicate that oxidized mRNA can severely slow down ribosomes and prevent the production of full-length proteins.

---

[13] Since puromycin functionally mimics the aminoacyl end of tRNA, ribosomes readily incorporate puromycin into the peptide chain. Adding a puromycin unit to

Relationship between damaged RNA and translation-dependent quality control

As the above-mentioned studies suggest, certain damaging adducts in RNA can inhibit protein production by severely slowing (or stalling) ribosome elongation; therefore, one might predict that damaged RNA could trigger translation-dependent quality control. Indeed, some research has provided evidence of a possible link between the two. One study found that *dom34Δ* and *xrn1Δ* yeast had increased levels of 8oxoG RNA (Simms et al. 2014). The *dom34Δ* lysates were enriched for 8oxoG RNA in the monosome and polysome fractions (Simms et al. 2014), implicating that Dom34p resolves ribosomes

---

the 3' end of an mRNA generates stable mRNA-peptide fusions that can be assayed directly on a denaturing polyacrylamide gel (Roberts and Szostak 1997).

stalled on 8oxoG RNA. Yeast lacking components of the Ski complex (*ski2Δ, ski3Δ*, or *ski8Δ*) are highly sensitive to oxidative stress, and while single deletion of either *SKI7*, *DOM34*, or *HBS1* tolerated H_2O_2 treatment similarly as wild-type yeast, the *dom34Δ;ski7Δ* or *hbs1Δ;ski7Δ* double-deletion strains exhibited increased sensitivity (Jamar et al. 2017). These data suggest NGD and NSD factors help reduce the effects of oxidative stress. The screen that eventually uncovered the RQC pathway was originally designed to find genetic elements regulating the yeast heat-shock stress response. The authors showed that the translation-dependent activation of Hsf1p required the CAT-tailing activity of Rqc2p (Brandman et al. 2012). Yeast deleted for *LTN1* contain insoluble protein aggregates, indicating a role for RQC in mitigating proteotoxic stress; proteotoxicity might also explain why null mutations in Listerin (yeast *LTN1*) cause neurodegeneration in mice (Chu et al. 2009; Choe et al. 2016). Since heat shock can increase the intracellular levels of reactive oxygen species (Bruskov et al. 2002), and that ribosomes stall at oxidized sites within the mRNA ORF (Simms et al. 2014; Calabretta et al. 2015), such data raise the possibility that the RQC pathway could target oxidized mRNA and the associated nascent peptide for rapid degradation. Another study showed that mRNA containing an abasic site within the ORF stalled ribosomes and initiated NGD (Gandhi et al. 2008). This is consistent with the observation that in vitro translation of abasic mRNA prevents synthesis of full-length proteins (Calabretta et al. 2015). Finally, as mentioned before, UV-irradiation triggers the ribotoxic stress response (Iordanov et al. 1998). Overall, these data point to a model wherein damaged RNA might serve as a substrate for translation-dependent quality control.

Current tools to study damaged RNA

There are a limited number of tools that have been used to detect damaged RNA. Several groups have employed HPLC-MS/MS[14] or HPLC-ECD[15] to quantify 8oxoG in total RNA from mammalian tissue samples (Fiala et al. 1989; Park et al. 1992; Abe et al. 2002; Weimann et al. 2002; Abe et al. 2003; Hofer et al. 2006). These methods are highly sensitive, but require molecular standards and several micrograms of nucleic acid (Hofer et al. 2006). Antibodies specific for 8oxoG also exist and have been successfully used for immunohistochemistry and competitive ELISA[16] (Park et al. 1992; Yin et al. 1995; Nunomura et al. 1999; 2002; Shan et al. 2007; Chang et al. 2008; Simms et al. 2014). A few studies immunoprecipitated RNA from cells using 8oxoG antibodies and performed low- or high-throughput sequencing. The authors identified transcripts that were more susceptible to oxidation in vivo, but did not analyze sequence features[17] (Shan et al. 2007; McKinlay et al. 2012). To examine methylated RNA, a recently developed method takes advantage of the demethylation activity of *E. coli* AlkB, coined ARM-seq. By comparing deep-sequencing results from demethylated and untreated (methylated) RNA, one can determine the in vivo methylation landscape (Cozen et al. 2015).

---

[14] High performance liquid chromatography coupled to electrospray tandem mass spectrometry

[15] High performance liquid chromatography coupled to electrochemical detection

[16] Enzyme-linked immunosorbent assay

Many groups have used reverse transcription to detect the presence of damaging adducts (Rhee et al. 1995; Iordanov et al. 1998; Gong et al. 2006; Hostetter et al. 2012; Kladwang et al. 2012). Depending on the type of enzyme and reaction conditions, reverse transcriptase (RT) tends to stop at modified sites, such as adducts formed by UV-irradiation, oxidation, methylation, or cisplatin treatment (Iordanov et al. 1998; Gong et al. 2006; Hostetter et al. 2012; Wilusz 2015). Analysis of cDNA products on a sequencing gel reveals prominent bands corresponding to RT stops. This approach has been used to determine 18S rRNA regions that are prone to cisplatin- or UV-induced adduct formation (Iordanov et al. 1998; Hostetter et al. 2012; Kladwang et al. 2012); RT stops also revealed oxidized-prone sites on 16S rRNA (Gong et al. 2006). Nevertheless, monitoring adduct formation via RT stops is very low-throughput since only one sequence can be analyzed at a time. More recently, however, researchers have determined that changing the enzyme and reaction conditions can permit read-through of modified sites. For example, the high-processing power of the thermostable group II intron reverse transcriptase (TGIRT™) allows for the read-through of methylated adducts (Mohr et al. 2013; Katibah et al. 2014). Another group determined conditions that allow SuperScript™ II to read through SHAPE[18]-adducts and introduce either a deletion or mutation across the modified site. The authors were able to quantify mutations in the deep-sequencing data to determine the secondary structures of several species of RNA (Siegfried et al. 2014). This raises the possibility that RT can incorporate mutations across damaged sites given the appropriate enzyme and reaction conditions. If so, one can use a deep-sequencing approach to examine sequence features that are more susceptible to damaging agents. *Chapter III of this thesis describes the development of a deep-sequencing approach to detect oxidized RNA.*

---

[17] Regions or motifs within the sequence, such as secondary structures or UTRs. For example, if single stranded RNA is more susceptible to oxidation, do regions encoding secondary structures exhibit fewer oxidized bases compared to unstructured regions?

---

[18] Selective 2'-Hydroxyl Acylation analyzed by Primer Extension (SHAPE) uses reagents that preferentially modify RNA 2'-hyroxyls within flexible regions (Merino et al. 2005).

CHAPTER II. *ASC1* and *RPS3*: New actors in 18S nonfunctional rRNA decay

Excluding the figure titles, all contents of Chapter II appear as they were accepted for publication at RNA, September 27, 2017.

Limoncelli KA, Merrikh CN, Moore MJ. 2017. ASC1 and RPS3: New actors in 18S nonfunctional rRNA decay. *RNA* rna.061671.117.

Author contributions:

M.J.M, K.A.L, and C.N.M conceived of the project. K.A.L and C.N.M performed the experiments and analyzed the data. M.J.M and K.A.L wrote the main manuscript text and K.A.L prepared the figures. All authors edited and reviewed the manuscript.

ASC1 and *RPS3*: New actors in 18S nonfunctional rRNA decay

Kelly A. Limoncelli[1*], Christopher N. Merrikh[1,2*], and Melissa J. Moore[1,3]

[1] RNA Therapeutics Institute, Department of Biochemistry and Molecular Pharmacology, University of Massachusetts Medical School, Worcester, MA 01605

[2] Current Address: Department of Microbiology, University of Washington, Seattle, WA 98195

* These authors contributed equally to this work.

[3] Correspondence: melissa.moore@umassmed.edu

Abstract

In budding yeast, inactivating mutations within the 40S ribosomal subunit decoding center lead to 18S rRNA clearance by a quality control mechanism known as nonfunctional 18S rRNA decay (18S NRD). We previously showed that 18S NRD is functionally related to No-Go mRNA Decay (NGD), a pathway for clearing translation complexes stalled on aberrant mRNAs. Whereas the NGD factors Dom34p and Hbs1p contribute to 18S NRD, their genetic deletion (either singly or in combination) only partially stabilizes mutant 18S rRNA. Here we identify Asc1p (aka RACK1) and Rps3p, both stable 40S subunit components, as additional 18S NRD factors. Complete stabilization of mutant 18S rRNA in *dom34Δ;asc1Δ* and *hbs1Δ;asc1Δ* strains indicates the existence of two genetically separable 18S NRD pathways. A small region of the Rps3p C-terminal tail known to be subject to post-translational modification is also crucial for 18S NRD. We combine these findings with the effects of mutations in the 5' → 3' and 3' → 5' decay machinery to propose a model wherein multiple targeting and decay pathways kinetically contribute to 18S NRD.

Introduction

Accurate and efficient flow of information from nucleic acids to proteins is essential for all life. Central to this process is protein synthesis, which requires the coordinated action of myriad components including mRNAs and rRNAs. As with any complex manufacturing process, tight quality control is crucial for both ensuring functional products and eliminating defective machine parts. Therefore, numerous mechanisms exist to ensure the overall integrity of the translation machinery (Shoemaker and Green 2012). In eukaryotes, the best understood quality control pathways are those that eliminate mRNAs that contain a premature stop codon (subject to Nonsense Mediated Decay; NMD) (Amrani et al. 2006), lack a stop codon altogether (subject to Non-Stop Decay; NSD) (Frischmeyer et al. 2002; van Hoof et al. 2002; Saito et al. 2013b; Horikawa et al. 2016), or have some structural feature that leads to ribosome stalling (subject to No-Go Decay; NGD) (Doma and Parker 2006; Tsuboi et al. 2012). Each of these pathways involves specific factors that recognize and target the defective mRNA for degradation by the general mRNA decay machinery. Decay is often initiated via endonucleolytic cleavage of the mRNA at or adjacent to the ribosome stall site, followed by 5' → 3' and 3' → 5' degradation by Xrn1p and the exosome, respectively (Gatfield and Izaurralde 2004; Doma and Parker 2006; Eberle et al. 2009; Dimitrova et al. 2009; Tsuboi et al. 2012).

Other eukaryotic quality control pathways monitor and target rRNA. Previous work from our laboratory examined the fate of *S. cerevisiae* rRNAs containing inactivating mutations in either the 18S rRNA decoding center or the 25S rRNA peptidyl-transferase center (LaRiviere et al. 2006). These mutant rRNAs are synthesized, processed, and assembled into ribosomal subunits similarly to wild-type rRNAs. The functionally-defective mature subunits, however, are cleared by mechanistically distinct pathways known respectively as 18S and 25S Nonfunctional rRNA Decay (18S NRD and 25S NRD). Large ribosomal subunits containing defective 25S rRNAs fail to form stable 80S monosomes (LaRiviere et al. 2006) and localize to perinuclear foci (Cole et al. 2009). Elimination of these particles by 25S NRD can occur in the absence of ongoing translation (Cole et al. 2009), requires the DNA damage repair factors, Mms1p and Rtt101p, and involves ubiquitination of 60S subunit proteins (Fujii et al. 2009; 2012). Therefore, 25S NRD appears to occur via a mechanism unrelated to mRNA quality control. In contrast, 18S NRD shares many similarities with NGD. Mutant 18S rRNAs exhibit diffuse cytoplasmic localization and co-sediment with 40S subunits, 80S monosomes and, to a lesser extent, polysomes (LaRiviere et al. 2006; Cole et al. 2009). Further, 18S NRD does not occur in the presence of translation elongation inhibitors and is substantially reduced in yeast strains lacking the known NGD factors *DOM34* and *HBS1* (Cole et al. 2009). Structurally related to eRF1 and eRF3, the Dom34p:Hbs1p heterodimer recognizes the A-site of stalled ribosomes and functions to both dissociate the ribosomal subunits and initiate decay of the associated mRNA (Lee et al. 2007; Passos et al. 2009; van den Elzen et al. 2010; Shoemaker et al. 2010; Becker et al. 2011; Pisareva et al. 2011; Shoemaker and Green 2011; Tsuboi et al. 2012; Guydosh and Green 2014; van den Elzen et al. 2014; Hilal et al. 2016).

Whereas translation inhibitors completely abrogate 18S NRD, elimination of either *DOM34* or *HBS1* only slows its kinetics (Cole et al. 2009); therefore, additional factors must contribute. Although we previously demonstrated that NMD factors are not required for 18S NRD (Cole et al. 2009), other candidates include proteins involved in nascent peptide-dependent translation arrest (PDTA) (Dimitrova et al. 2009; Kuroha et al. 2010) or ribosome quality control (RQC) (Brandman et al. 2012). PDTA targets mRNAs containing rare codons or encoding stretches of positively charged amino acids, whereas RQC mediates the degradation of nascent peptide chains associated with stalled ribosomes. One factor known to participate in NGD, PDTA, and RQC is the WD-repeat protein Asc1p (Dimitrova et al. 2009; Brandman et al. 2012). Asc1p (aka RACK1 in mammals) is a stoichiometric component of the small ribosomal subunit located in the vicinity of the mRNA exit channel (Coyle et al. 2009; Ben-Shem et al. 2010). *ASC1* deletion increases the ability of ribosomes to read through rare codons and stretches encoding positively charged amino acids (Kuroha et al. 2010; Brandman et al. 2012; Letzring et al. 2013). Deletion of *ASC1* also increases ribosome frameshifting at CGA repeats (Wolf and Grayhack 2015). Although these observations led to a model wherein Asc1p somehow promoted ribosomal stalling (Kuroha et al. 2010; Inada 2013; Letzring et al. 2013), more recent data suggest Asc1p functions instead to target stalled ribosomes for quality control (Sitron et al. 2017). Asc1p may also promote endonucleolytic cleavage of NGD substrates (Ikeuchi and Inada 2016).

Another set of factors implicated in NGD, PDTA and NSD are the Ski proteins. Ski2p, Ski3p, and Ski8p form the Ski complex which binds tightly to ribosomes stalled on mRNA 3' ends (van Hoof et al. 2002; Wang et al. 2005; Schmidt et al. 2016a). The central component Ski2p is a DExH-box helicase located near the mRNA entrance channel where it is well positioned to feed the mRNA 3' end into the exosome (Schmidt et al. 2016a). Exosome recruitment is mediated by Ski7p, which bridges the exosome to Ski3p and Ski8p (Wang et al. 2005; Kowalinski et al. 2016; Schmidt et al. 2016a). We previously showed that elimination of *SKI7* in combination with *HBS1* completely abrogates 18S NRD (Cole et al. 2009), but we did not examine the requirement of other Ski proteins.

The major goal of this study was to identify additional 18S NRD factors and elucidate their genetic and mechanistic relationships. Here we show that both *ASC1* and *SKI2* contribute to the rate of mutant 18S decay, and we identify a small region of Rps3p, an essential 40S subunit protein physically residing between Asc1p and the mRNA entrance channel, as crucial for 18S NRD.

Results

A simplified system for monitoring 18S NRD

The system we use to monitor 18S NRD employs a galactose-inducible (GAL7 promoter) URA$^+$ plasmid encoding the entire 35S pre-rRNA (**Figure 2.1, A**). Benign sequence tags within the 18S and 25S regions allow for specific northern blot detection of plasmid-derived rRNAs, which, when fully induced, account for only ~1% of total rRNA in BY4741 yeast (LaRiviere et al. 2006). Introduction of an A to C mutation at position 1755 in the decoding center (equivalent to A1492C in *E. coli* 16S rRNA) renders the 40S subunit incapable of carrying out efficient elongation and therefore subject to NRD (LaRiviere et al. 2006; Cole et al. 2009). Whereas wild-type 18S rRNA (18S:WT) has no discernible decay over a six-hour time course (data not shown), mutant 18S rRNA (18S:A1492C[19]) decays with a half-life of <100 minutes (LaRiviere et al. 2006; Cole et al. 2009).

---

[19] Although 18S:A1755C would be a more accurate name for this mutation in *S. cerevisiae*, we originally chose to dub it 18S:A1492C in our first NRD paper (LaRiviere et al. 2006) to call particular attention to the fact that this position is equivalent to *E. coli* 16S rRNA nucleotide A1492, about which the effects of mutations on ribosome decoding were well understood. In the time since, multiple papers using our plasmids have continued to use the 18S:A1492C nomenclature (e.g., (Fujii et al. 2009; van den Elzen et al. 2010; Fujii et al. 2012).

In previous studies, we monitored 18S NRD by normalizing 18S:A1492C to endogenous *SCR1* RNA after correcting for cell growth (LaRiviere et al. 2006; Cole and LaRiviere 2008; Cole et al. 2009). However, knowledge that 18S NRD is an entirely post-ribosome synthesis process (LaRiviere et al. 2006) raised the possibility that the tagged wild-type 25S rRNA (25S:WT) derived from the same 35S pre-rRNA transcript as 18S:WT or 18S:A1492C might be a better (or at least equivalent) normalization control. An added advantage of normalizing tagged 18S to tagged 25S:WT is that there is no need to correct for cell growth or variable plasmid copy number. To test the reliability of this 18S:25S ratio approach, we grew parental BY4741 yeast harboring either the 18S:WT or 18S:A1492C plasmid (both paired with 25S:WT) to mid-log phase in synthetic complete minus uracil media (SC-ura) plus raffinose, induced tagged pre-rRNA expression for 90 minutes with galactose, turned off transcription by adding glucose, then collected samples over time (**Figure 2.1, B**). Our results demonstrate that normalizing tagged 18S:WT or 18S:A1492C to the tagged 25S:WT yielded similar findings as normalizing to endogenous *SCR1* RNA. That is, whereas there was no apparent decay of 18S:WT, 18S:A1492C had a half-life of 76 minutes in the parental strain (**Figure 2.1, B** and **2.2, B**). The 18S:25S

Therefore, to avoid compounding any confusion, we will retain the 18S:A1492C nomenclature here.

ratio also reproduced previous findings that individual deletion of either *DOM34* or *HBS1* resulted in partial 18S:A1492C stabilization (**Figure 2.1, B**) (Cole et al. 2009).

Because time courses are inherently low throughput, we also tested the feasibility of monitoring a single time point. After inducing expression for 90 minutes, cells were immediately harvested and subjected to northern analysis. As expected, 18S:A1492C was substantially lower than 18S:WT in the parental BY4741 yeast, with the decrease being less drastic, but still statistically significant ($p = 0.0022$, unpaired t test), in the *dom34Δ* strain (**Figure 2.1, D**). Thus, a single-time point assay proved sufficient as an initial mutant screen.

***DOM34* paralogs are not involved in 18S NRD**

Whereas deletion of *DOM34*, *HBS1*, or both slows 18S:A1492C decay, small molecule translation inhibitors completely abrogate decay (Cole et al. 2009); this suggests the existence of a second, kinetically separable 18S NRD pathway. Consistent with the multiple-pathway hypothesis, we previously showed that double deletion of *HBS1* and *SKI7* completely stabilizes 18S:A1492C (**Figure 2.1, C**) (Cole et al. 2009). Since Hbs1p and Dom34p form a heterodimer and their simultaneous deletion had no additive effect on 18S NRD (Cole et al. 2009), we reasoned that double deletion of *DOM34* and *SKI7* would also completely stabilize 18S:A1492C. Unexpectedly, however, no synthetic effect was apparent in the *dom34Δ;ski7Δ* strain (**Figure 2.1, C** and **2.4**). One possible explanation for this result was the existence of a cross-functional Dom34p paralog. Dom34p consists of three domains: N (1-131 aa), M (136-268 aa), and C (271-370 aa), with M and C serving as the binding sites for Hbs1p (Chen et al. 2010; van den Elzen et al. 2010). *S. cerevisiae* contains two genes of unknown function, *YCL001W-A* and *YCL001W-B*, and a multiple sequence alignment showed both having high similarity with the M and C domains of Dom34p (data no shown). However, no decrease in 18S NRD efficiency was observed in either a *YCL001W-A* or *YCL001W-B* knockout strain, and when either deletion was combined with the *DOM34* deletion, there was no enhancement of the *dom34Δ* phenotype (**Figure 2.1, E**). Thus, we conclude that neither *YCL001W-A* nor *YCL001W-B* contribute to 18S NRD.

Asc1p contributes to 18S NRD

To identify additional 18S NRD factors, we performed a small screen in strains lacking proteins previously implicated in other degradation pathways (**Figure 2.1, F**). Among these, only the *ASC1* knockout diminished 18S NRD (**Figure 2.1, F** and **2.2, A**). Substantially more 18S:A1492C was observed in the *asc1Δ* strain than the parental strain, with the level being comparable to the *dom34Δ* strain. In the *dom34Δ;asc1Δ* double-deletion strain, 18S:A1492C levels were indistinguishable from 18S:WT (**Figure 2.2, A**). Time course data confirmed that, whereas deletion of either *ASC1* or *DOM34* alone resulted in a two-fold increase in 18S:A1492C half-life, deletion of both led to its complete stabilization (**Figure 2.2, B**). *ASC1* was also synthetic with *HBS1* (**Figure 2.4**), and in no strain was 18S:WT detectably degraded (**Figure 2.2, B** and **2.4**). Although the *dom34Δ;asc1Δ* and *hbs1Δ;asc1Δ* strains grew more slowly than the parental strain, neither grew more slowly than the *asc1Δ* single deletion strain (**Figure 2.3, B**). Therefore, slower cell growth could not account for the observed synthetic effects.

To confirm that the 18S NRD defect observed in the *asc1Δ* strain was due to the loss of the *ASC1* protein and not the *snR24* snoRNA that derives from the *ASC1* intron, we transformed the *asc1Δ* strain with different plasmids containing the *ASC1* gene with or without the intron, both under control of the endogenous *ASC1* promoter. The intron-less version completely restored 18S NRD (**Figure 2.2, C**). Further, when transformed into the parental strain, neither plasmid enhanced 18S:A1492C decay. Thus, we conclude that Asc1p is an 18S NRD factor, and its endogenous levels are sufficient for optimal 18S NRD. Taken together, these data indicate the existence of two genetically separable pathways contributing to 18S NRD kinetics: one involving *DOM34* and *HBS1,* and another involving *ASC1*.

Increased non-functional 80S monosomes in *dom34Δ;asc1Δ* lysates

In a wild-type background, 18S:A1492C rRNA predominantly co-sediments on sucrose gradients with 40S subunits (**Figure 2.3, A**) (LaRiviere et al. 2006). This suggests highly efficient resolution of stalled 80S monosomes containing the 18S:A1492C mutation. Since both Asc1p and Dom34p have been implicated in targeting and resolving stalled ribosomes (Shoemaker et al. 2010; Tsuboi et al. 2012; Sitron et al. 2017), we next examined sucrose gradients of *asc1Δ, dom34Δ*, and *dom34Δ;asc1Δ*. The sedimentation pattern in *asc1Δ* lysates revealed a slight increase in the amount of 18S:A1492C co-sedimenting with 80S monosomes, and this increase was more noticeable in *dom34Δ* lysates. This effect was further amplified in the *dom34Δ;asc1Δ* double-mutant (**Figure 2.3, A**). While there was some increase in bulk 80S monosomes in both the *dom34Δ* and *dom34Δ;asc1Δ* profiles (data not shown), this increase was much less pronounced than the change in 80S co-sedimentation of 18S:A1492C in the *dom34Δ;asc1Δ* lysate (**Figure 2.3, A**). Thus, cells lacking both *ASC1* and *DOM34* are substantively impaired in their ability to resolve non-functional 80S ribosomes.

Variable effects of Ski proteins on 18S NRD

Having identified a new *ASC1*-dependent pathway contributing to 18S NRD, we next tested whether *ASC1* was synthetic with *SKI7*. However, we could detect no difference in the rate of 18S:A1492C decay between the *asc1Δ* single deletion and *asc1Δ;ski7Δ* double deletion strain (**Figure 2.4**). To investigate whether the Ski complex itself contributes to 18S NRD, we examined 18S:A1492C decay kinetics in *ski2Δ* strains (**Figure 2.4**). Deletion of *SKI2* alone had no effect on cell doubling time (**Figure 2.3, B**), but it slowed 18S:A1492C decay to a similar extent as deletion of either *DOM34* or *ASC1* alone. No further decrease in decay rate was observed, however, in either a *dom34Δ*;*ski2Δ* or *asc1Δ*;*ski2Δ* strain (**Figure 2.4**) despite decreased growth rates of these double mutant strains (**Figure 2.3, B**). Thus, while both *SKI7* and *SKI2* contribute to the rate of 18S:A1492C decay, neither is synthetic with *DOM34* or *ASC1*. Further, there is no clear relationship between cell doubling time and the rate of 18S:A1492C decay.

The Rps3p C-terminal tail

On the ribosome, the binding sites for Dom34p:Hbs1p and Asc1p are separated by >75 angstroms (Becker et al. 2011; Hilal et al. 2016). Whereas

Dom34p:Hbs1p interact with the A-site at the interface between the large and small subunits, Asc1p resides on the opposite (solvent-exposed) surface of the small subunit in the general area of the mRNA exit channel. Physically linking these two sites is a single protein: Rps3p (**Figure 2.5, A**). The body of Rps3p consists of an N-terminal type II KH domain (three-stranded 🚲-sheet backed by three ✔-helices; amino acids 1-88) attached via a nine-amino acid linker to a central RRM-like domain (four-stranded 🚲-sheet backed by two ✔-helices; amino acids 98-189); together these form part of the mRNA entrance channel adjacent to the A-site. Intriguingly, cryo-EM studies indicate that the body of Rps3p contacts the N-terminal 90-amino acid globular domain of Hbs1p, which is attached via a 62-amino acid flexible linker to the GTPase core (Becker et al. 2011; Hilal et al. 2016). A 50-amino acid C-terminal tail extends from the body of Rps3p along the outer surface of the small ribosomal subunit and contacts the fourth WD repeat in Asc1p (Ben-Shem et al. 2010). This network of structural contacts between Hbs1p, Rps3p, and Asc1p suggested to us that *RPS3* might be a component of the 18S NRD pathway.

Because *RPS3* encodes an essential protein, it was impossible to monitor 18S NRD in an *RPS3* knockout strain. We therefore implemented a 5-FOA plasmid shuffle approach in a *rps3Δ* background to test the effects of various *rps3* mutations (**Figure 2.5, B** and **2.6, A**). Validating this approach, a LEU$^+$

plasmid encoding wild-type *RPS3* complemented the knockout strain, whereas the empty LEU$^+$ vector did not. For point mutations, we chose positions that were highly conserved across all eukaryotes (data not shown) and were previously proposed to make specific interactions with the Hbs1p N-terminal domain (**Figure 2.5, A**) (Becker et al. 2011). All point mutations tested complemented the *rps3Δ* strain, indicating that none of the amino acids we mutated were required for viability. All four mutations also had 18S:A1492C/25:WT ratios similar to wild-type *RPS3* (**Figure 2.5, B**), suggesting that the mutations fail to compromise the interaction between Rps3p and Hbs1p or that the interaction might be dispensable for 18S NRD.

To more rigorously test the functionality of the Rps3p:Hbs1p interaction, we next mutated *HBS1*. Earlier work had shown that an *hbs1* protein variant lacking the entire N-terminal domain (amino acids 1-152) retains its ability to bind to ribosomes in complex with Dom34p (Becker et al. 2011). When we complemented the *hbs1Δ* strain with plasmids encoding either full-length *HBS1* (1-611) or *hbs1* lacking either the first 90 or 152 amino acids ($hbs1_{1\text{-}90\Delta}$ and $hbs1_{1\text{-}152\Delta}$, respectively), we observed no difference in the rate of 18S:A1492C decay (**Figure 2.5, C**). Therefore, we conclude that the interaction of the Hbs1p N-terminus with Rps3p is dispensable for 18S NRD.

We next examined the Asc1p:Rps3p interaction. The Rps3p C-terminal tail (amino acids 190-240) exhibits much lower sequence conservation than the N-terminal domains (data not shown). To test the essentiality of the tail, we made a series of C-terminal truncation mutants. Whereas *rps3*$_{1-200}$ proved inviable, cells expressing either *rps3*$_{1-211}$ or *rps3*$_{1-217}$ grew equally well as cells expressing full-length *RPS3* (amino acids 1-240) (**Figure 2.3, B** and **2.6, A**). Thus, amino acids 1-211 of *S. cerevisiae* Rps3p are sufficient for both survival and wild-type cell growth. We did, however, observe a significant difference between the two truncation mutants with regard to 18S NRD efficiency: whereas yeast expressing *rps3*$_{1-217}$ degraded 18S:A1492C at a rate indistinguishable from cells expressing the full-length protein, 18S:A1492C decay in *rps3*$_{1-211}$ yeast was >11-fold slower (**Figure 2.6, B**). The magnitude of this effect is so far the largest we have observed for any single mutation or gene deletion tested (this study) (Cole et al. 2009). Thus, a small region of the Rps3p C-terminal tail is crucial for efficient 18S NRD. Of the six amino acids (KEEEPI), the first three (KEE) are highly conserved across eukaryotic species (**Figure 2.6, C**).

Discussion

Here we identified Asc1p, Ski2p, and Rps3p as factors contributing to 18S:A1492C rRNA decay kinetics. We found that *ASC1* is synthetic with *DOM34* and *HBS1,* but not with *SKI7* (**Figure 2.2, B** and **2.4**). Further, whereas deleting *SKI2* slowed 18S:A1492C rRNA decay similarly to deletion of *ASC1*, *DOM34*, or *HBS1*, no synthetic effects were detectable upon combining a *SKI2* deletion with deletion of *ASC1* or *DOM34* (**Figure 2.4**). Finally, we found that mutant 18S rRNA is substantially stabilized upon deletion of a six-amino acid region within the C-terminal tail of Rps3p (**Figure 2.6, B**), implicating Rps3p as a central player in targeting nonfunctional 40S subunits for preferential elimination by 18S NRD. We synthesize these findings with previous data to propose a model wherein 18S NRD is the result of multiple independent targeting and decay pathways (**Figure 2.7**).

18S NRD, NGD, PDTA and RQC: Different outcomes of ribosome stalling

The data in this paper strengthen and extend our previous findings that 18S NRD is functionally related to the mRNA and protein quality control pathways associated with ribosome stalling (this study) (Cole et al. 2009). NGD, PDTA, 18S NRD, and RQC were all discovered independently by examining the fate of mRNAs (NGD and PDTA) or rRNAs (18S NRD) with features that inhibit protein production, or by a genome-wide screen for deletions that over-activate the heat-shock stress response pathway (RQC) (Doma and Parker 2006; LaRiviere et al. 2006; Cole et al. 2009; Dimitrova et al. 2009; Kuroha et al. 2010; Brandman et al. 2012). Subsequent investigation of the identified RQC genes led to the finding that this increased stress response was due to accumulation of aberrant nascent peptides associated with stalled ribosomes (Brandman et al. 2012; Choe et al. 2016). Evidence accumulating since these initial discoveries suggests that all four pathways are simply alternate outcomes of the same initiating event – a stalled or slowly elongating ribosome (Shoemaker and Green 2012; Brandman and Hegde 2016). Whether an individual stall event leads to all or only a subset of these outcomes may depend on both the nature of the stall and the kinetic stability of the stalling event (i.e., whether the ribosome is completely halted or is simply moving slowly).

A recently proposed unifying model (Brandman and Hegde 2016) suggests the following order of events for the resolution of stalled ribosomes: (1) recognition and targeting of the stalled ribosome by Asc1p, Hel2p (an E3 ubiquitin ligase), and the recently identified RQT complex (Brandman et al. 2012; Sitron et al. 2017; Matsuo et al. 2017); (2) subunit dissociation by Dom34p, Hbs1p, and Rli1p (mammalian ABCE1) (Shoemaker et al. 2010; Shoemaker and

Green 2011; Pisareva et al. 2011; Tsuboi et al. 2012); (3) degradation of the associated aberrant mRNA (Frischmeyer et al. 2002; van Hoof et al. 2002; Doma and Parker 2006; Tsuboi et al. 2012); (4) assembly of the remaining RQC components onto the 60S subunit (Brandman et al. 2012; Shao et al. 2015); (5) CAT-tailing by Rqc2p and/or ubiquitination of the nascent peptide chain by Ltn1p (another E3 ubiquitin ligase) (Bengtson and Joazeiro 2010; Shao and Hegde 2014; Shen et al. 2015; Shao et al. 2015; Osuna et al. 2017); and (6) extraction and degradation of the ubiquitinated nascent peptide (Brandman et al. 2012; Defenouillère et al. 2013; Verma et al. 2013; Kostova et al. 2017; Osuna et al. 2017). Missing from this model is the fate of the 40S subunit. In cases where ribosome stalling was not due to any specific 40S dysfunction, it would seem reasonable that the subunit would simply be released to return to the translationally active pool. However, when stalls are due to a specific 40S defect (such as the decoding center mutation used here), the defective subunit is ultimately dismantled and the 18S rRNA decayed. Since *ASC1* and *DOM34*:*HBS1* are additive for 18S:A1492C kinetics (**Figure 2.2, B** and **2.4**), our data suggest that initial targeting of the 40S subunit for decay occurs prior to or concurrent with 80S ribosome dissociation. However, the lack of an 18S NRD defect in the *ltn1Δ* strain (**Figure 2.1, F**) suggests that the 40S subunit fate is not tied to the process of dismantling of the nascent peptide-60S complex.

Multiple kinetic contributors to 18S NRD targeting and decay

While we were successful in identifying additional 18S NRD factors (Asc1p, Rps3p, and Ski2p), some of the single- and double-mutant results were confounding. For example, while the deletion of *SKI2* partially stabilizes mutant 18S rRNA, it is not synthetic with either *DOM34* or *ASC1* (**Figure 2.4**). Furthermore, whereas a HFY1200 strain lacking *XRN1* exhibits decreased 18S NRD kinetics, this same deletion in a BY4741 background is without apparent consequence (Cole et al. 2009). Finally, we previously observed no substantial decrease in 18S NRD kinetics in a temperature-sensitive exosome strain (Cole et al. 2009). To explain these apparent inconsistencies, we propose a model wherein multiple parallel and sequential pathways kinetically contribute to 18S NRD (**Figure 2.7**). In this model, Asc1p and the Dom34p:Hbs1p heterodimer sit at the top of the pathway where they function independently to target non-functional 40S subunits for decay. Once targeted, 18S rRNA decay likely involves subunit disassembly and both endonucleolytic and exonucleolytic activities, with the relative kinetic contributions of 5' → 3' decay by Xrn1p and 3' → 5' decay by the exosome being highly dependent on strain background and growth conditions (Cole et al. 2009).

Whereas the half-lives of NGD, NSD, and PDTA mRNAs range from 2 to 9 minutes in wild-type yeast (Frischmeyer et al. 2002; Doma and Parker 2006; Tsuboi et al. 2012; Sweet et al. 2012), the half-life of 18S:A1492C rRNA ranges from 41 to 96 minutes (this study) (LaRiviere et al. 2006; Cole et al. 2009). Since the 18S:A1492C half-lives are of similar magnitude to the doubling time of wild-type yeast (87 minutes), a simple explanation could have been that 18S NRD is somehow tied to the cell cycle. However, we observed no consistent relationship between 18S:A1492C decay kinetics and cell growth rate over multiple strain backgrounds (**Figure 2.3, B**). What can account for the 10-fold slower kinetics of 18S NRD compared to defective mRNA decay? Is 18S NRD targeting slow, with non-functional 40S subunits going through multiple rounds of initiation prior to being tagged for decay, or is targeting efficient and decay slow? What steps are involved in decay? Does decay first require 40S disassembly (i.e., removal of some or all of the proteins) to allow for 18S rRNA decay, or is 18S rRNA decay initiated within the intact subunit with protein disassembly occurring concomitant with rRNA degradation? While the available data do not address these questions directly, the observation of no 18S:A1492C decay in the presence of elongation inhibitors (Cole et al. 2009) suggests that targeting of non-functional 40S subunits to 18S NRD is relatively inefficient and may require multiple rounds of initiation. Slow targeting would also be consistent with the variable kinetic effects of eliminating individual components of the degradation machinery.

A central role for *RPS3*

Rps3p (a.k.a. uS3 in the recently adopted systematic ribosomal protein nomenclature (Ban et al. 2014)) is an essential component of the small ribosomal subunit. Along with Rps2p (uS5) and Rps30p (eS30), Rps3p forms part of the mRNA entrance channel (Ben-Shem et al. 2010). The type II KH and RRM-like domains of Rps3p are structurally conserved from bacteria to humans, whereas the C-terminal tail is more conserved in eukaryotes (data not shown). Proteomics studies in *S. cerevisiae* have identified C-terminal tail amino acids K200, T207, K212, S221, and T231 as sites of acetylation, phosphorylation, succinylation, and/or ubiquitination (Peng et al. 2003; Albuquerque et al. 2008; Seyfried et al. 2008; Holt et al. 2009; Soulard et al. 2010; Weinert et al. 2013; Fang et al. 2014). If 18S NRD consists of independent targeting and decay pathways, then post-translation modification of the Rps3p tail could serve as the mark that connects targeting to decay. Indeed, the significant decrease in 18S:A1492C rRNA half-life (>11-fold) observed upon removing Rps3p amino acids 212-217 (**Figure 2.6, B**) suggests a central role for one or more of these residues.

In *S. cerevisiae*, *Drosophila*, and human ribosomes, the Rps3p/RPS3 tail interacts with the WD40 blade IV of Asc1p/RACK1 (Ben-Shem et al. 2010; Anger et al. 2013), but functional relevance had been lacking. Recent studies in mammalian cells investigating ribosome read-through on poly(A) stretches now suggest a regulatory link between Asc1p and Rps3p (Sundaramoorthy et al. 2017; Juszkiewicz and Hegde 2017). RACK1 (yeast *ASC1*) and ZNF598 (yeast *HEL2*) are both involved in ubiquitination of stalled ribosomes (Saito et al. 2015; Sundaramoorthy et al. 2017; Juszkiewicz and Hegde 2017). *HEL2* was previously identified as a genetic component of the *S. cerevisiae* RQC pathway where it, along with *ASC1*, acts upstream of *LTN1* (Brandman et al. 2012; Letzring et al. 2013; Sitron et al. 2017). Both mammalian ZNF598 and RACK1 facilitate RPS3 (uS3) ubiquitination, although ZNF598 primarily participates in RPS10 (eS10) and RPS20 (uS10) ubiquitination, whereas RACK1 primarily participates in RPS2 (uS5) and RPS3 ubiquitination. Furthermore, inhibitors of translation elongation and activators of the unfolded protein response pathway also result in RPS3 ubiquitination, with the ubiquitination site occurring on the yeast equivalent of K212 (Higgins et al. 2015; Sundaramoorthy et al. 2017; Juszkiewicz and Hegde 2017). Another recent study showed that yeast Hel2p ubiquitinates both Rps20p (uS10) K6/K8 and Rps3p K212 in stalled ribosomes (Matsuo et al. 2017). Collectively, these findings may explain why loss of *ASC1* only partially stabilizes 18S:A1492C, whereas deletion of *RPS3* amino acids 212-217 has a much stronger effect. It seems likely that Asc1p and Hel2p converge to ubiquitinate Rps3p K212, which in turn serves to target the mutant 18S rRNA for decay.

Multiple pathways for resolving stalled ribosomes across domains

The existence of multiple pathways in eukaryotes for detecting and eliminating functionally defective ribosomes parallels the situation in prokaryotes. Although the decoding center A1492C and G530U mutations are known to inactivate the 16S rRNA decoding center (Powers and Noller 1990; 1993; Yoshizawa et al. 1999a; Ogle et al. 2001), these mutant rRNAs are not subject to preferential degradation in *E. coli* (Paier et al. 2015). Nonetheless, *E. coli* does harbor three functionally redundant pathways for rescuing ribosomes stalled on truncated mRNAs: the trans-translation pathway, ArfB, and ArfA (Keiler et al. 1996; Karzai et al. 1999; Chadani et al. 2011b; 2010). In the trans-translation pathway, tmRNA/SmpB recognizes the empty A-site and acts as both a tRNA and mRNA to allow continued elongation and normal termination at the tmRNA stop codon. ArfB and ArfA act as backups to the tmRNA/SmpB system. ArfB, a release factor 2 (RF2) homolog, binds to the stalled ribosome and initiates peptidyl-tRNA hydrolysis and ribosome release. ArfA accomplishes the same thing, but does so by binding within the empty mRNA channel and directly recruiting RF2 to the A-site. Of particular note for our findings, the ArfA and ArfB pathways were discovered only upon tmRNA/SmpB inactivation (Chadani et al. 2010; 2011b). The existence of so many redundant mechanisms in bacteria to rescue stuck ribosomes suggests that ribosome stalling is a pervasive problem. Indeed, it has been estimated that 2-4% of all translating ribosomes in *E. coli* are in need of rescue at any given time (Ito et al. 2011; Keiler 2015). Given the greater complexity of their translation machinery, one might predict ribosome stalling to be even more problematic in eukaryotes. Thus, it would not be surprising if more pathways for resolving stalled translation complexes await discovery.

Methods and Materials

Yeast Strains and Plasmids:

All strains and plasmids used in this study are listed in **Table 2.1**. The *dom34Δ;asc1Δ*, *hbs1Δ;asc1Δ*, *asc1Δ;ski7Δ*, and *asc1Δ;ski2Δ* mutants were constructed by transforming a *dom34Δ*, *hbs1Δ*, *ski7Δ*, or *ski2Δ* strain with dsDNA encoding *asc1Δ::NATMX* and colony selection on G418;ClonNat plates. The *dom34Δ;ski7Δ* and *dom34Δ;ski2Δ* mutants were constructed by transforming a *ski7Δ* or *ski2Δ* strain with dsDNA encoding *dom34Δ::NATMX* and colony selection on G418;ClonNat plates. Homologous recombination at the *ASC1* or *DOM34* locus was confirmed by PCR. *rps3* mutant strains were constructed by plasmid shuffling. Briefly, a *RPS3/rps3Δ::KANMX* diploid strain was transformed with a *RPS3/URA3*$^{+}$ plasmid, sporulated, and selected on SC-ura;G418 plates to obtain a haploid *rps3Δ::KANMX* strain harboring the *URA3*$^{+}$ plasmid. *LEU2*$^{+}$ plasmids encoding *rps3* variants were then transformed into the *rps3Δ::KANMX;URA3*$^{+}$ haploid strain; *rps3* variants that had lost the *URA3*$^{+}$ plasmid were then selected on SC-leu;5-FOA plates. To generate *hbs1* N-terminal deletion strains, a *hbs1Δ* haploid strain was transformed with plasmids encoding either *HBS1*, *hbs1*$_{1\text{-}90\Delta}$, or *hbs1*$_{1\text{-}152\Delta}$; all variants were expressed under the endogenous *HBS1* promoter.

Single Time Point Assay:

Strains harboring pSC40-WT (18S:WT;25S:WT) or pSC40-A1492C (18S:A1492C;25S:WT) plasmids were grown at 30°C in SC-ura media plus 2% raffinose to mid-log phase (OD600 = 0.4-0.5). Following addition of 20% galactose (final concentration = 2%) to induce rRNA transcription, cells were incubated at 30°C for an additional 90 minutes. Pre-warmed SC-ura media plus 2% galactose was added as necessary to maintain OD600 = 0.5. Cells were then harvested by centrifugation and flash frozen in liquid nitrogen or a dry ice/EtOH mixture.

Pulse-chase Analysis:

Pulse-chase analysis was performed as previously described (Cole and LaRiviere 2008) with some modifications. Strains harboring pSC40-WT or pSC40-A1492C plasmids were grown at 30°C in SC-ura media plus 2% raffinose to mid-log phase (OD600 = 0.4-0.5). 20% galactose was added to a final concentration of 2% to induce rRNA transcription, and cells were incubated for an additional 90 minutes. 50% glucose was then added to a final concentration of 2% and the first-time point (T=0) was immediately harvested; subsequent time points were taken at indicated intervals post glucose addition. Samples were pelleted by centrifugation, and then flash frozen in liquid nitrogen or a dry ice/EtOH mixture. Pre-warmed SC-ura media plus 2% glucose was added as necessary to maintain an OD600 of 0.5 for the duration of the time course.

Northern Blot Analysis:

For each sample, 2.0-2.5 μg total RNA was electrophoresed on a 1% agarose-formaldehyde gel and transferred to a nitrocellulose membrane as previously described (Cole and LaRiviere 2008; Cole et al. 2009). Total RNA was detected via staining with Methylene Blue (Molecular Research). Membranes were hybridized with ^{32}P-end-labeled probes FL125 (anneals to plasmid-derived 18S rRNA) and FL126 (anneals to plasmid-derived 25S rRNA) for 12-24 hours at 42°C in ExpressHyb (BD Biosciences). Bands were visualized using a Typhoon Phosphorimager (Molecular Dynamics) and quantified via ImageQuant software (GE Lifesciences). Signal from the tagged-18S rRNA was normalized to the signal from the tagged-25S rRNA. Curve fitting was done using GraphPad Prism 7 software.

Sucrose Gradients:

The parental wild-type, *dom34Δ*, *asc1Δ*, and *dom34Δ;asc1Δ* strains were transformed with the pSC40-A1492C plasmid and grown to mid-log in SC-ura media plus 2% raffinose (80 mL culture volume per gradient). After a 90-minute induction with 2% galactose, cycloheximide was added to a final concentration of 0.1 mg/mL. Cells were immediately chilled on ice, harvested, and lysed in the presence of glass beads and lysis buffer (20 mM Tris-HCl pH=8.0, 140 mM KCl, 1.5 mM $MgCl_2$, 0.5 mM DTT, 1% Triton X-100, 0.1 mg/mL cycloheximide, 1 mg/mL heparin). Individual lysates (12 A260 units) were layered onto 5-47% sucrose gradients (sucrose, 20 mM Tris-HCl pH=8.0, 140 mM KCl, 5mM $MgCl_2$, 0.5 mM DTT, 0.1 mg/mL cycloheximide, 0.5 mg/mL heparin) and spun in an ultracentrifuge (35K rpm, 160 minutes, SW41 rotor). Individual fractions were then collected and subjected to northern blot analysis.

Multiple Sequence Alignments:

A multiple sequence alignment of the *DOM34*, *YCL001W-A*, or *YCL001W-B* protein sequences was performed using ClustalW (v1.83). A multiple sequence alignment of *RPS3* protein sequences across various species (from *E. coli* to *H. sapiens*) was also performed using ClustalW (v1.83).

Supplemental Material

Supplemental material includes a table of yeast strains, plasmids, and probe sequences used in this study.

Acknowledgements

We thank Dr. Andrei Korostelev, Dr. Nicholas Rhind, and Dr. Elisabet Mandon for their invaluable input, and members of the Moore lab for many helpful discussions. This research was supported by the Howard Hughes Medical Institute (M.J.M. was an HHMI Investigator when the research was conducted), Moderna Therapeutics, and the National Institute of General Medical Sciences of the National Institutes of Health under Award Number F31GM109753 (K.A.L.). The content is solely the responsibly of the authors and does not necessarily represent the official view of the National Institute of Health.

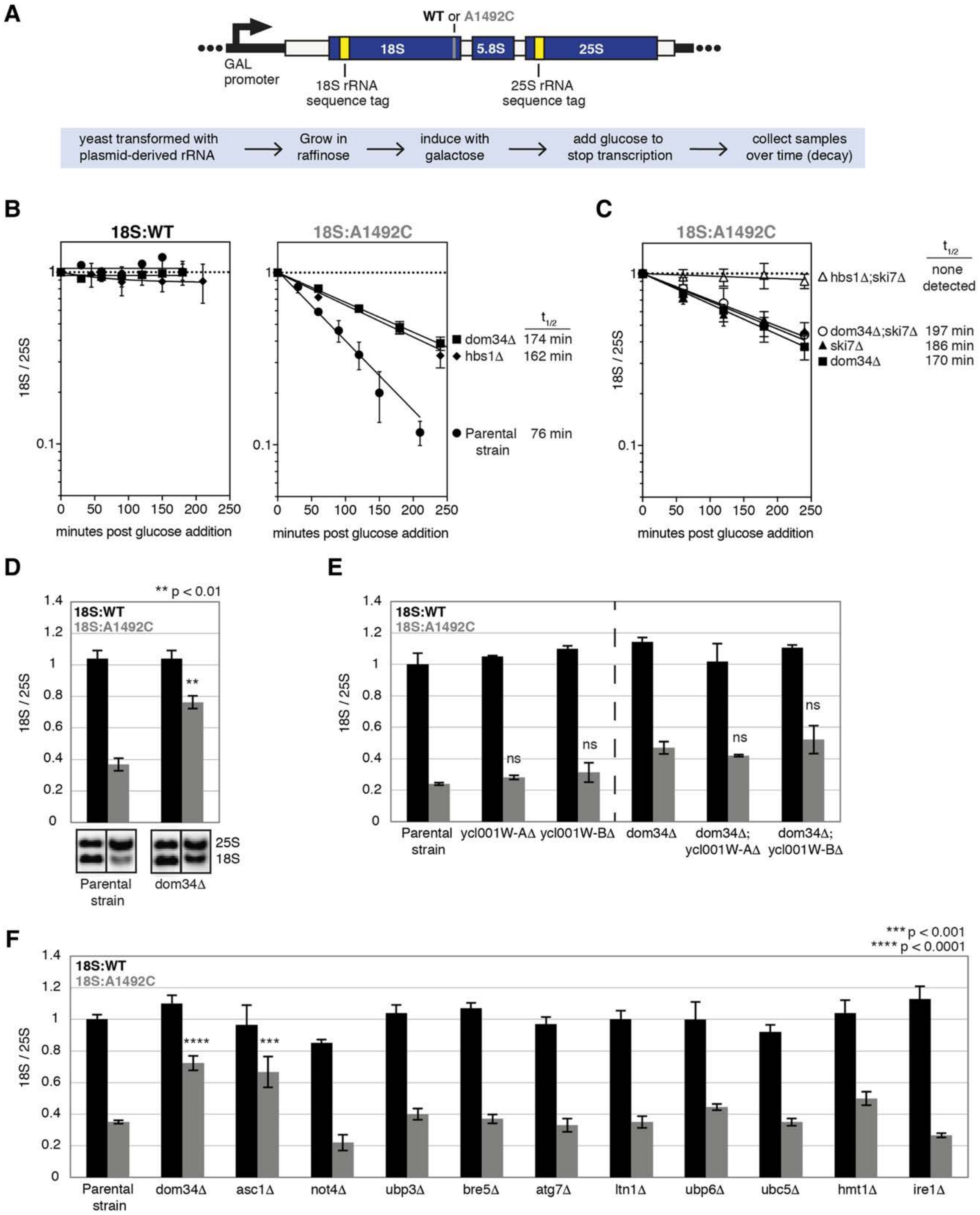
A
WT or A1492C
GAL promoter
18S
5.8S
25S
18S rRNA sequence tag
25S rRNA sequence tag
yeast transformed with plasmid-derived rRNA → Grow in raffinose → induce with galactose → add glucose to stop transcription → collect samples over time (decay)
B
18S:WT
18S:A1492C
18S / 25S
1
0.1
0 50 100 150 200 250
minutes post glucose addition
t1/2
■ dom34Δ 174 min
◆ hbs1Δ 162 min
● Parental strain 76 min
C
18S:A1492C
t1/2
Δ hbs1Δ;ski7Δ none detected
○ dom34Δ;ski7Δ 197 min
▲ ski7Δ 186 min
■ dom34Δ 170 min
D
** p < 0.01
18S:WT
18S:A1492C
18S / 25S
0 0.2 0.4 0.6 0.8 1 1.2 1.4
**
25S
18S
Parental strain
dom34Δ
E
18S:WT
18S:A1492C
18S / 25S
ns
ns
ns
ns
Parental strain
ycl001W-AΔ
ycl001W-BΔ
dom34Δ
dom34Δ; ycl001W-AΔ
dom34Δ; ycl001W-BΔ
F
*** p < 0.001
**** p < 0.0001
18S:WT
18S:A1492C
18S / 25S
****
***
Parental strain
dom34Δ
asc1Δ
not4Δ
ubp3Δ
bre5Δ
atg7Δ
ltn1Δ
ubp6Δ
ubc5Δ
hmt1Δ
ire1Δ

Figure 2.1: System for studying 18S NRD
(A) Diagram of rDNA plasmid reporter (top) and summary of experimental design (bottom). The reporter contains sequence tags for northern blot detection of plasmid-derived 18S and 25S rRNAs. **(B)** Time course analysis of tagged 18S and 25S rRNAs in parental, dom34Δ, and hbs1Δ yeast strains. **(C)** Same as (B), but for dom34Δ, ski7Δ, dom34Δ;ski7Δ, and hbs1Δ;ski7Δ strains. (B and C) Tagged 18S:tagged 25S ratios (18S/25S) were normalized to the T=0 time point; error bars represent standard error of the mean (n=3). 18S:A1492C half-life is indicated on the right. **(D, E, and F)** Single time-point analyses of tagged 18S rRNAs. Error bars represent standard error of the mean (n=3). **(D)** Unpaired t test was used for significance testing against parental strain 18S:A1492C levels. **(E)** One-way ANOVA with planned comparisons was used for significance testing comparing 18S/25S in parental strain to single mutants or in dom34Δ strain to double mutants. ns = not significant. **(F)** One-way ANOVA with planned comparisons was used for significance testing comparing 18S/25S in all mutant strains against the parental strain.

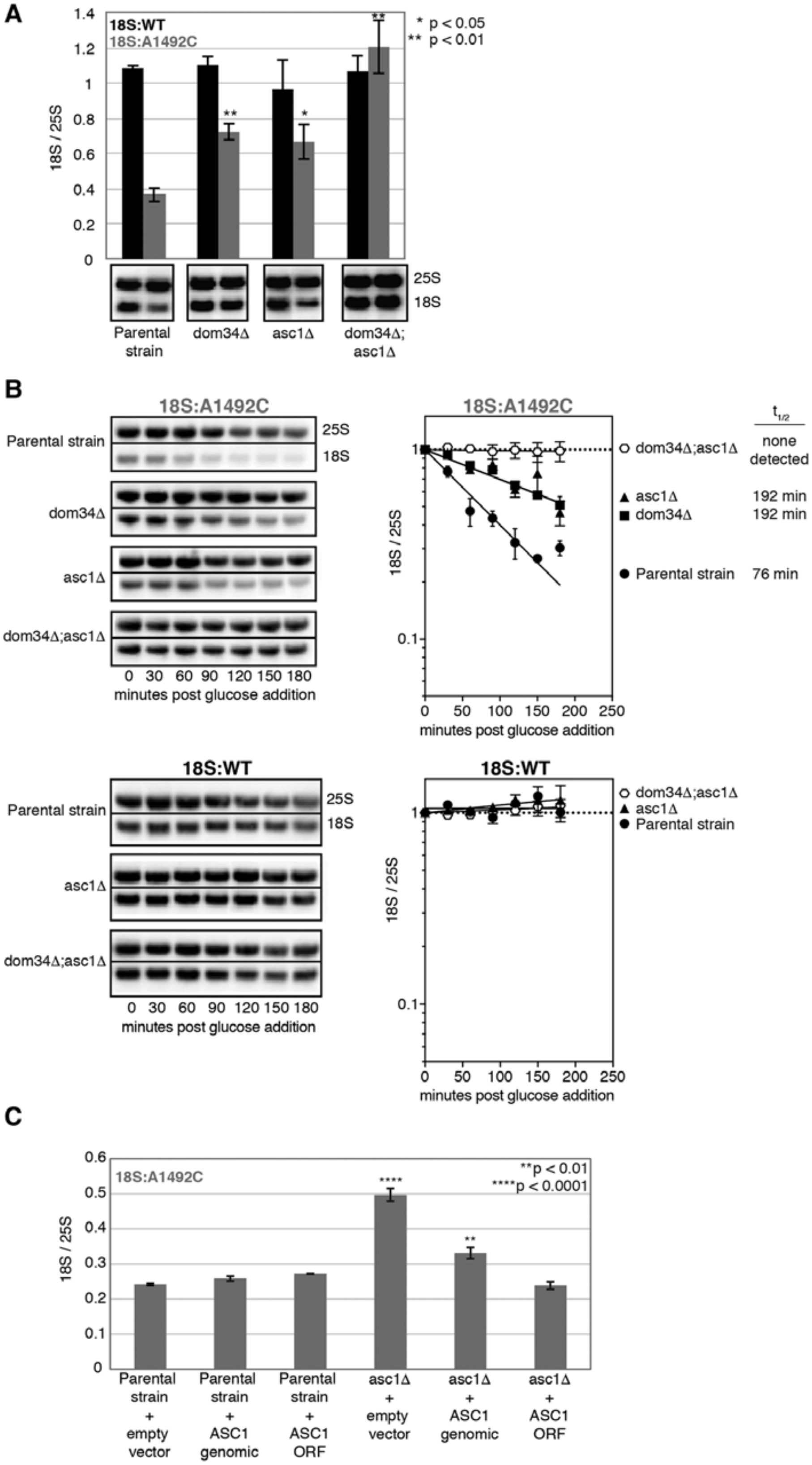
A
18S:WT
18S:A1492C
* p < 0.05
** p < 0.01
18S / 25S
1.4
1.2
1
0.8
0.6
0.4
0.2
0
**
*
**
25S
18S
Parental strain
dom34Δ
asc1Δ
dom34Δ; asc1Δ
B
18S:A1492C
Parental strain
dom34Δ
asc1Δ
dom34Δ;asc1Δ
25S
18S
0 30 60 90 120 150 180
minutes post glucose addition
18S / 25S
1
0.1
0 50 100 150 200 250
minutes post glucose addition
t1/2
dom34Δ;asc1Δ none detected
asc1Δ 192 min
dom34Δ 192 min
Parental strain 76 min
18S:WT
Parental strain
asc1Δ
dom34Δ;asc1Δ
25S
18S
0 30 60 90 120 150 180
minutes post glucose addition
18S / 25S
1
0.1
0 50 100 150 200 250
minutes post glucose addition
dom34Δ;asc1Δ
asc1Δ
Parental strain
C
18S:A1492C
**p < 0.01
****p < 0.0001
18S / 25S
0.6
0.5
0.4
0.3
0.2
0.1
0
****
**
Parental strain + empty vector
Parental strain + ASC1 genomic
Parental strain + ASC1 ORF
asc1Δ + empty vector
asc1Δ + ASC1 genomic
asc1Δ + ASC1 ORF

Figure 2.2: *ASC1* contributes to 18S NRD

(A) Single time-point analysis of tagged 18S and 25S rRNAs. One-way ANOVA with planned comparisons was used for significance testing comparing the parental strain and each single deletion 18S:A1492C/25S:WT ratio. Unpaired t test was used to compare the parental strain and *dom34∆;asc1∆* 18S:A1492C/25S:WT ratios. Error bars represent standard error of the mean (n=3)**.** **(B)** Time course analysis of 18S:A1492C and 18S:WT decay in *dom34∆* and *asc1∆* single and double deletion strains. Representative northern blots of tagged 18S:A1492C and 25S rRNAs and graphs summarizing multiple (n=3) biological replicates. Normalization and error bars as in Figure 2.1 B and C. **(C)** Single time-point analysis of tagged 18S:A1492C rRNA in parental and *asc1∆* strains harboring indicated plasmids. One-way ANOVA with planned comparisons was used for significance testing of all strains against the “Parental strain + empty vector” strain. Error bars represent standard error of the mean (n=3).

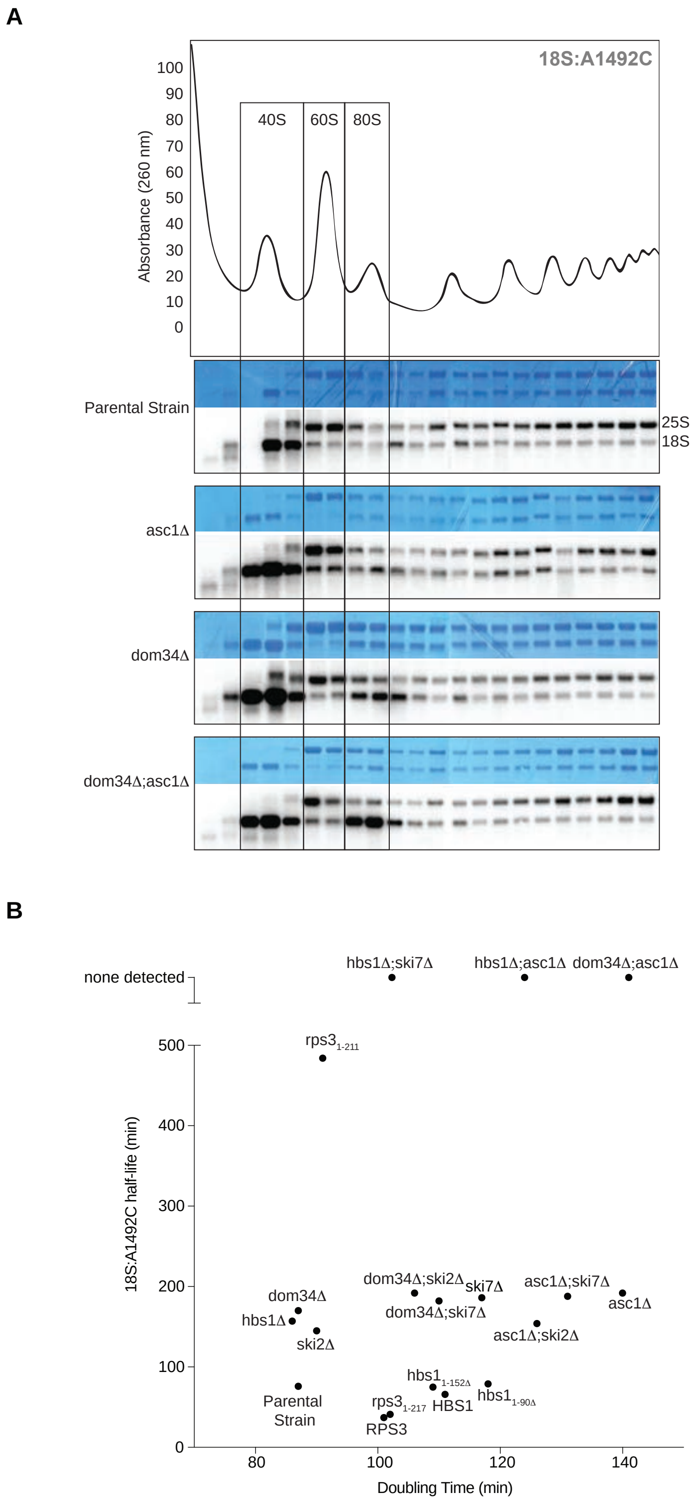
A
18S:A1492C
Absorbance (260 nm)
100
90
80
70
60
50
40
30
20
10
0
40S
60S
80S
Parental Strain
asc1Δ
dom34Δ
dom34Δ;asc1Δ
25S
18S
B
none detected
hbs1Δ;ski7Δ
hbs1Δ;asc1Δ
dom34Δ;asc1Δ
rps3 1-211
18S:A1492C half-life (min)
500
400
300
200
100
0
dom34Δ
hbs1Δ
ski2Δ
Parental Strain
dom34Δ;ski2Δ
ski7Δ
dom34Δ;ski7Δ
asc1Δ;ski7Δ
asc1Δ
asc1Δ;ski2Δ
hbs1 1-152Δ
HBS1
hbs1 1-90Δ
rps3 1-217
RPS3
80
100
120
140
Doubling Time (min)

Figure 2.3: Polysome profiles and growth rates
(A) Polysome profiles. Top: Representative sucrose gradient trace for the parental strain. Bottom: Methylene Blue stains and Northern blots of sucrose gradient fractions for the parental, *asc1*Δ, *dom34*Δ*,* and *asc1*Δ*;dom34*Δ strains harboring the 18S:A1492C plasmid. Boxes show positions of 40S, 60S and 80S ribosomes. **(B)** Scatter plot of mean 18S:A1492C half-lives (n=3) versus mean growth rates (doubling time; n=3) of various yeast strains used in current study.

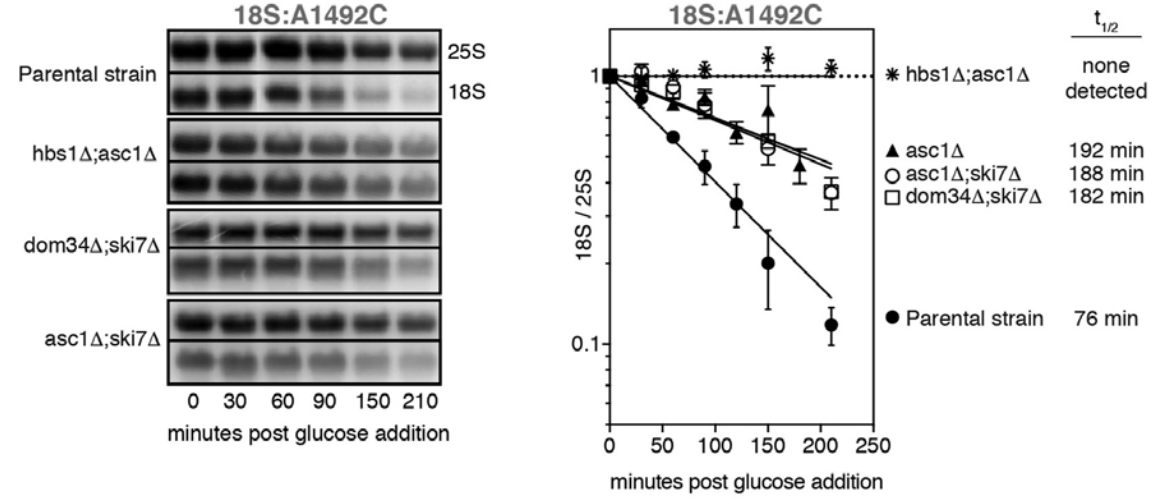
18S:A1492C
Parental strain
hbs1Δ;asc1Δ
dom34Δ;ski7Δ
asc1Δ;ski7Δ
25S
18S
0 30 60 90 150 210
minutes post glucose addition
18S:A1492C
18S / 25S
1
0.1
0 50 100 150 200 250
minutes post glucose addition
$t_{1/2}$
✱ hbs1Δ;asc1Δ none detected
▲ asc1Δ 192 min
○ asc1Δ;ski7Δ 188 min
□ dom34Δ;ski7Δ 182 min
● Parental strain 76 min

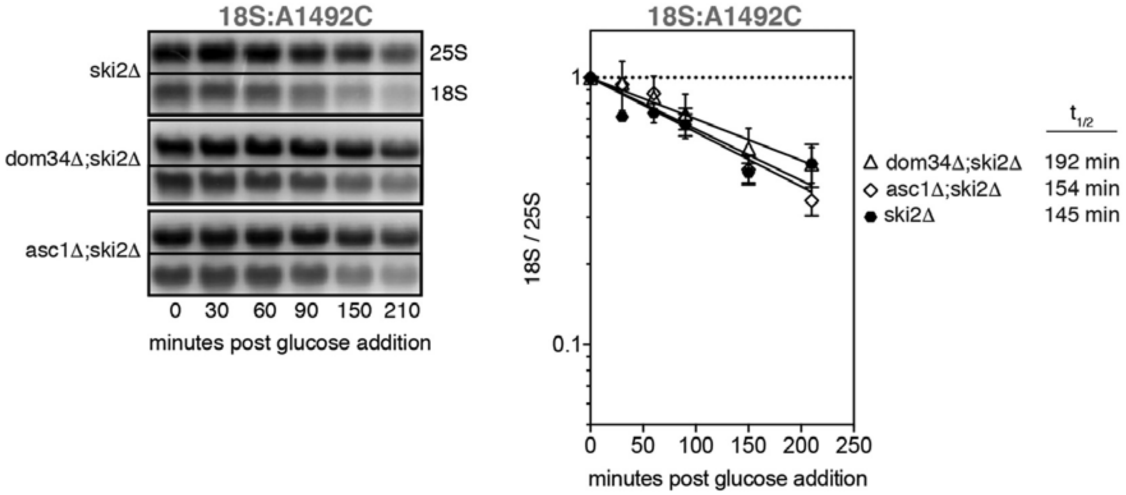
18S:A1492C
ski2Δ
dom34Δ;ski2Δ
asc1Δ;ski2Δ
25S
18S
0 30 60 90 150 210
minutes post glucose addition
18S:A1492C
18S / 25S
1
0.1
0 50 100 150 200 250
minutes post glucose addition
$t_{1/2}$
△ dom34Δ;ski2Δ 192 min
◇ asc1Δ;ski2Δ 154 min
● ski2Δ 145 min

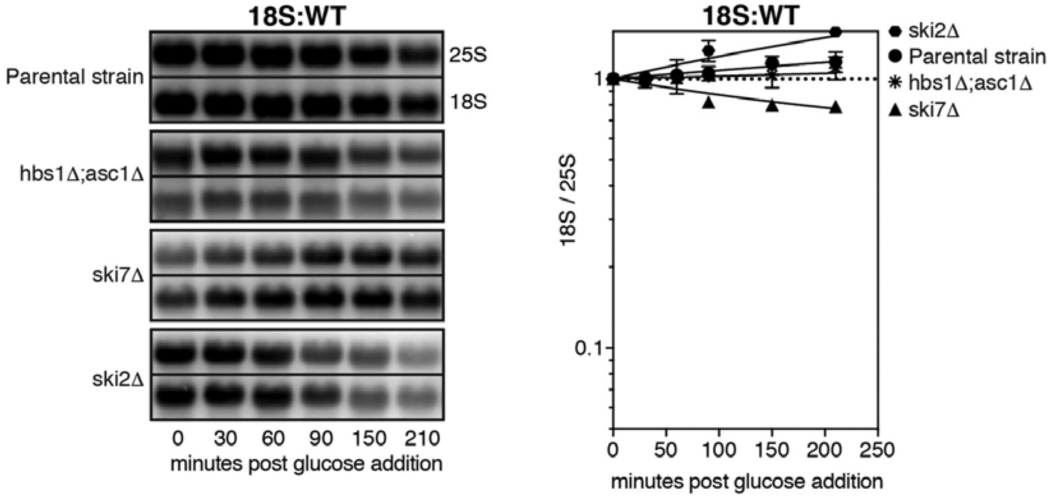
18S:WT
Parental strain
hbs1Δ;asc1Δ
ski7Δ
ski2Δ
25S
18S
0 30 60 90 150 210
minutes post glucose addition
18S:WT
18S / 25S
1
0.1
0 50 100 150 200 250
minutes post glucose addition
● ski2Δ
● Parental strain
✱ hbs1Δ;asc1Δ
▲ ski7Δ

Figure 2.4: Variable effects of Ski proteins on 18S NRD
Time course analysis of 18S:A1492C and 18S:WT in single and double deletion strains. Representative northern blots of tagged 18S:A1492C and 25S rRNAs and graphs summarizing multiple (n=2-3) biological replicates. Normalization and error bars as in Figure 2.1 B and C. 18S:A1492C data from the parental and *asc1*Δ single deletion strains are the same as Figure 2.1 B (parental) and Figure 2.2 B (*asc1*Δ).

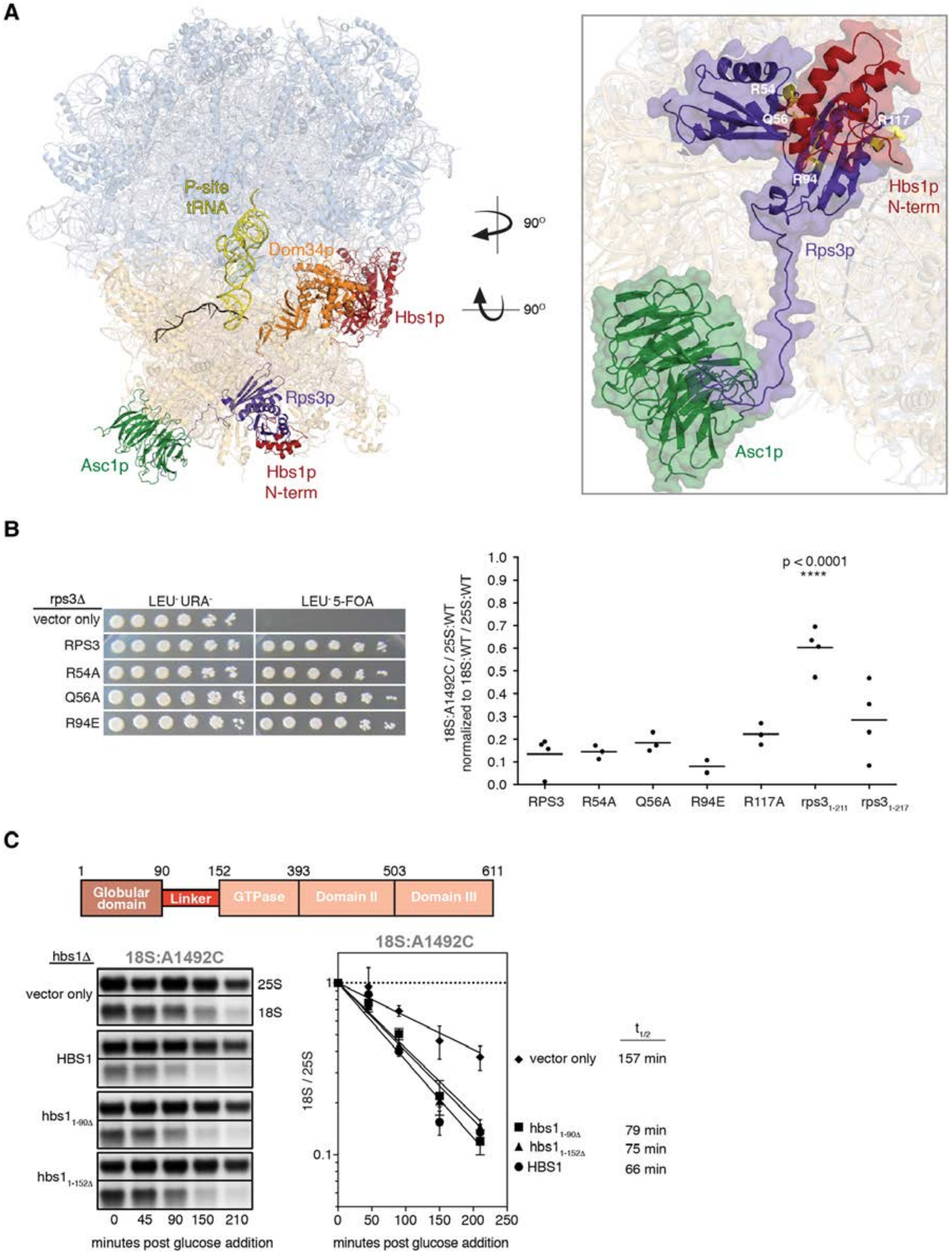
A
P-site
tRNA
Dom34p
Hbs1p
Rps3p
Asc1p
Hbs1p
N-term
90°
90°
R54
Q56
R117
R94
Hbs1p
N-term
Rps3p
Asc1p
B
rps3Δ
LEU⁻ URA⁻
LEU⁻ 5-FOA
vector only
RPS3
R54A
Q56A
R94E
18S:A1492C / 25S:WT
normalized to 18S:WT / 25S:WT
1.0
0.9
0.8
0.7
0.6
0.5
0.4
0.3
0.2
0.1
0.0
p < 0.0001
****
RPS3
R54A
Q56A
R94E
R117A
rps3$_{1-211}$
rps3$_{1-217}$
C
1
90
152
393
503
611
Globular domain
Linker
GTPase
Domain II
Domain III
hbs1Δ
18S:A1492C
vector only
25S
18S
HBS1
hbs1$_{1-90\Delta}$
hbs1$_{1-152\Delta}$
0
45
90
150
210
minutes post glucose addition
18S:A1492C
18S / 25S
1
0.1
0
50
100
150
200
250
minutes post glucose addition
t$_{1/2}$
◆ vector only
157 min
■ hbs1$_{1-90\Delta}$
79 min
▲ hbs1$_{1-152\Delta}$
75 min
● HBS1
66 min

Figure 2.5: Hbs1p N-terminal domain is dispensable for 18S NRD
(A) Left: Cryo-EM structure of the yeast 80S ribosome in complex with Dom34p:Hbs1p (orange:red), P-site tRNA (yellow), and nonstop mRNA (black) (PDB: 5M1J) (Hilal et al. 2016). Also highlighted are Asc1p (green) and Rps3p (purple). Right: Close up of the Hbs1p:Rps3p:Asc1p interaction. Positions of Rps3p point mutations at the Hbs1p:Rps3p interface are shown in yellow. Note that amino acids 3-225 of Rps3p have been resolved (Full-length: 240). **(B)** Left: Plasmid shuffle experiment showing growth of strains (10-fold dilution series) harboring plasmids expressing wild-type *RPS3* or indicated point mutations on a $LEU^{-}URA^{-}$ or LEU^{-}5-FOA plate. Right: Single time-point analyses of tagged 18S and 25S rRNAs. For all strains, 18S:A1492C/25S:WT ratio was normalized to the 18S:WT/25S:WT ratio. Error bars represent standard error of the mean. One-way ANOVA with planned comparisons was used for significance testing comparing all *rps3* variant strains against the wild-type *RPS3* strain; only $rps3_{1\text{-}211}$ was statistically different ($p<0.0001$). **(C)** Diagram of Hbs1p domains (top) and time course analysis of 18S:A1492C in *hbs1* strains (bottom). Data normalization as in Figure 2.1 B and C. Representative northern blots and graph of time course data with indicated 18S:A1492C rRNA half-lives. Error bars represent standard error of the mean (n=2).

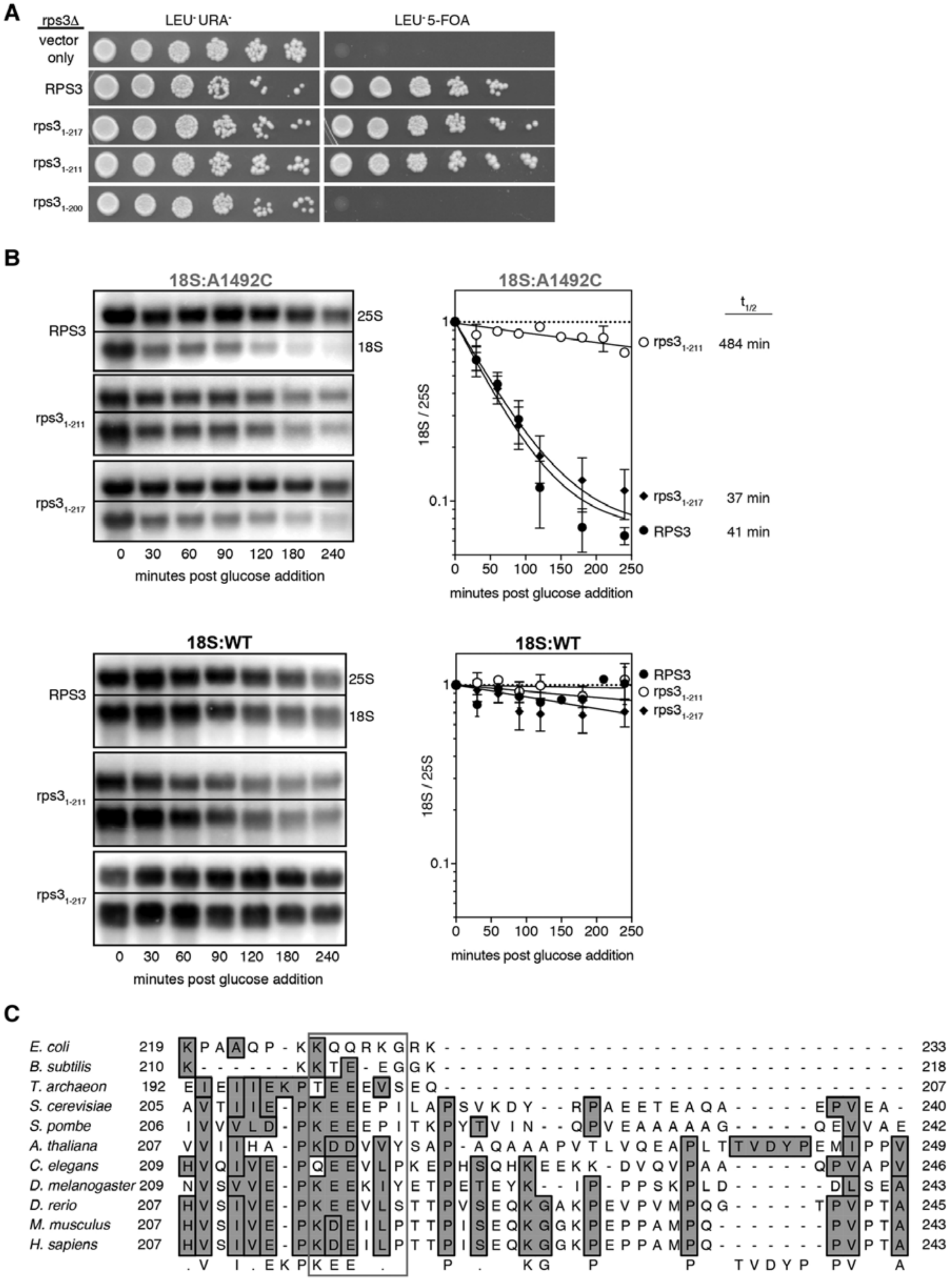
A
rps3Δ
LEU⁻ URA⁻
LEU⁻ 5-FOA
vector only
RPS3
rps3 1-217
rps3 1-211
rps3 1-200
B
18S:A1492C
RPS3
rps3 1-211
rps3 1-217
25S
18S
0 30 60 90 120 180 240
minutes post glucose addition
18S / 25S
t1/2
rps3 1-211 484 min
rps3 1-217 37 min
RPS3 41 min
1
0.1
0 50 100 150 200 250
18S:WT
C
E. coli 219 K P A A Q P - K K Q Q R K G R K - 233
B. subtilis 210 K - - - - - - K K T E - E G G K - 218
T. archaeon 192 E I E I I E K P T E E E V S E Q - 207
S. cerevisiae 205 A V T I I E - P K E E E P I L A P S V K D Y - - R P A E E T E A Q A - - - - - E P V E A - 240
S. pombe 206 I V V V L D - P K E E E P I T K P Y T V I N - - Q P V E A A A A A G - - - - - Q E V V A E 242
A. thaliana 207 V V I I H A - P K D D V V Y S A P - A Q A A A P V T L V Q E A P L T T V D Y P E M I P P V 249
C. elegans 209 H V Q I V E - P Q E E V L P K E P H S Q H K E E K K - D V Q V P A A - - - - - Q P V A P V 246
D. melanogaster 209 N V S V V E - P K E E K I Y E T P E T E Y K - - I P - P P S K P L D - - - - - - D L S E A 243
D. rerio 207 H V S I V E - P K E E V L S T T P V S E Q K G A K P E V P V M P Q G - - - - - T P V P T A 245
M. musculus 207 H V S I V E - P K D E I L P T T P I S E Q K G G K P E P P A M P Q - - - - - - - P V P T A 243
H. sapiens 207 H V S I V E - P K D E I L P T T P I S E Q K G G K P E P P A M P Q - - - - - - - P V P T A 243
. V I . E K P K E E . P . K G P P T V D Y P P V A

Figure 2.6: Rps3p C-terminal tail is crucial for 18S NRD
(A) Plasmid shuffle experiment showing growth of strains (10-fold dilution series) harboring plasmids expressing wild-type *RPS3* or indicated C-terminal truncation variant on a LEU$^-$URA$^-$ or LEU$^-$5-FOA plate. **(B)** Time course analysis of 18S rRNA in *rps3* yeast strains. Representative northern blots of tagged 18S and tagged 25S rRNA and graphs summarizing multiple (n=3) biological replicates. Normalization and error bars as in Figure 2.1 B and C. **(C)** Multiple sequence alignment of *RPS3* protein sequences.

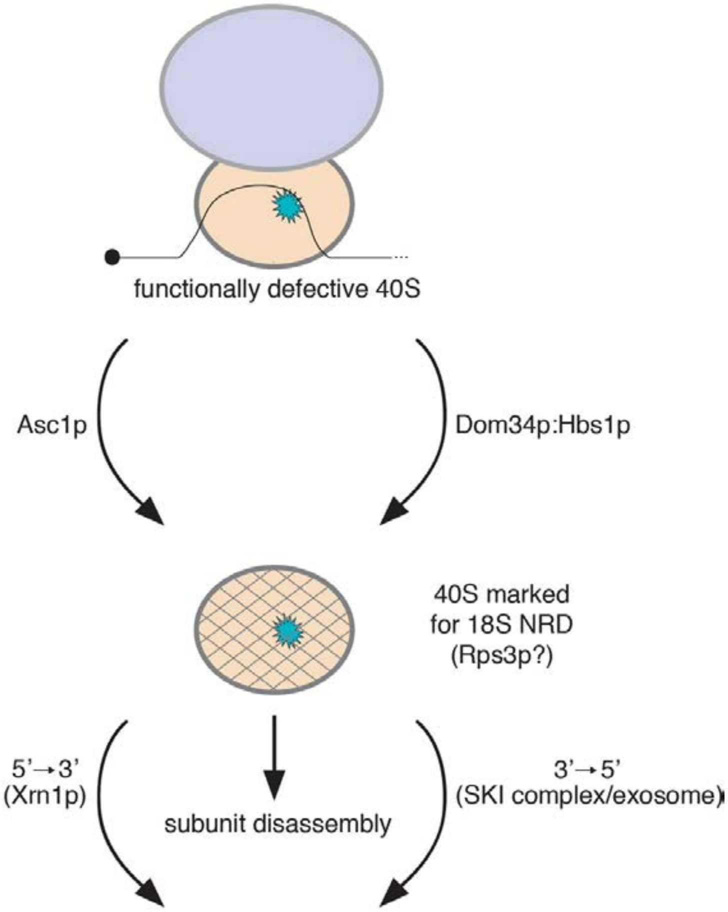
functionally defective 40S
Asc1p
Dom34p:Hbs1p
40S marked
for 18S NRD
(Rps3p?)
5'→3'
(Xrn1p)
subunit disassembly
3'→5'
(SKI complex/exosome)

Figure 2.7: Current model of 18S NRD
Proposed model depicting the contributions of multiple independent targeting and decay pathways to 18S NRD. A stalled ribosome harboring mutant 18S rRNA (blue splatter) can be marked for decay by two separate pathways involving either Asc1p or Dom34p:Hbs1p. Once marked (possibly by covalent modification of the Rps3p C-terminal tail), 40S ribosomes are disassembled and 18S rRNA degraded by 5' → 3' and 3' → 5' decay pathways.

CHAPTER III. A deep-sequencing approach to detect oxidized RNA

Melissa J. Moore, Ph.D., and I designed the study. I performed the reverse transcription experiments and prepared libraries for the 40mer oligos, 8oxoG oligos, and in vitro synthesized RNA. I also performed the yeast experiments and prepared libraries from yeast total RNA. Hakan Ozadam, Ph.D., processed the synthesized RNA dataset while I processed the yeast dataset. Nicholas Hathaway wrote the mutation counting script and I performed the analysis for all datasets.

Introduction

Many endogenous and exogenous stressors generate intracellular reactive oxygen species (ROS), which pose a threat to the chemical integrity of nucleic acids. While much is known about the effects of DNA oxidation, little is known about the effects of RNA oxidation. Accumulating evidence suggests RNA is more susceptible to ROS than DNA, with the prevailing ROS-induced adduct being 8-oxoguanosine (8oxoG) (Fiala et al. 1989; Shen et al. 2000; Hofer et al. 2005; 2006; Liu et al. 2012). The in vivo basal levels of 8oxoG RNA range from 0.2 to 60 8oxoG per 10^5 G's, with levels significantly increasing upon exposure to oxidizing agents (Hofer et al. 2005; 2006; Liu et al. 2012; Simms et al. 2014). The ability of 8oxoG to base pair with adenosine makes 8oxoG highly mutagenic and problematic (Yanagawa et al. 1992; Weimann et al. 2002; Hsu et al. 2004; Kim et al. 2004; 2006; Simms et al. 2014).

Interestingly, high levels of oxidized RNA have been observed in many neurodegenerative disease states, including ALS, Alzheimer's, and Parkinson's (Nunomura et al. 1999; Zhang et al. 1999; Abe et al. 2002; Nunomura et al. 2002; Abe et al. 2003; Shan et al. 2003; Chang et al. 2008; Nunomura et al. 2012; 2009). Although it is unknown whether oxidized RNA contributes to the pathology, some research has implicated a connection between oxidized RNA and reduced translation efficiency. For example, ribosomes purified from patients with Alzheimer's disease produced fewer protein products than ribosomes purified from aged-match controls (Ding et al. 2005). Furthermore, in vitro translation of oxidized mRNA produces fewer full-length peptides while simultaneously increases the production of abortive peptides (Shan et al. 2007; Tanaka et al. 2007; Calabretta et al. 2015). It has also been shown that the ribosome transit on 8oxoG is 100- to 1000-fold slower than on unmodified bases (Simms et al. 2014).

There are currently a limited number of techniques available for the study of oxidized RNA. HPLC-MS/MS and HPLC-ECD have been used to quantify 8oxoG adducts in RNA and in DNA (Fiala et al. 1989; Park et al. 1992; Abe et al. 2002; Weimann et al. 2002; Abe et al. 2003; Hofer et al. 2006). Despite being highly sensitive, these instruments require a lot of sample material and molecular standards (Hofer et al. 2006). Antibodies specific for 8oxoG also exist and have been used for immunohistochemistry and competitive ELISA (Park et al. 1992; Yin et al. 1995; Nunomura et al. 1999; 2002; Shan et al. 2007; Chang et al. 2008; Simms et al. 2014). These low-resolution techniques all share a common problem in that they fail to provide information regarding sequence features. For example, are specific motifs more prone to oxidation? Are sequences less likely to be oxidized if they are embedded within secondary structures?

Reverse transcription can be used to identify adducts within a given sequence. Reverse transcriptase (RT) inefficiently reads through base modifications (e.g. 8oxoG), giving rise to terminated cDNA products; analysis of cDNA lengths on a sequencing gel reveals the location of 8oxoG sites. Thus, RT stops can detect regions prone to oxidation (Rhee et al. 1995; Gong et al. 2006). A major drawback of this approach, however, is the sequence of the transcript must be known and only one transcript can be analyzed at a time.

The efficiency of RT read-through is more dynamic than a binary "stop" and "no-stop" action; rather, it is a parameter that can change depending on the type of RT and reaction conditions. For instance, SHAPE experiments depend on SuperScript™ III termination at modified 2'-hydroxyls. SHAPE reagents react with 2'-hydroxyls within flexible regions to form bulky adducts. Thus, careful analysis of RT stops can be used to ascertain the secondary structure of various RNA species (Merino et al. 2005; Mortimer and Weeks 2007; McGinnis et al. 2012). After adjusting RT conditions to increase read-through at SHAPE adducts, deep-sequencing is a feasible option to determine the secondary structures of various RNAs. Moreover, replacing $MgCl_2$ with $MnCl_2$ and using SuperScript™ II increases read-through events that manifest as quantifiable base substitutions and deletions in deep-sequencing data (Siegfried et al. 2014).

Here, we developed a high-throughput, high-resolution tool to detect and quantify oxidized RNA. Our approach relies on the ability of RT to read through and introduce mutations across 8oxoG sites. Analysis of oxidized in vitro synthesized RNA revealed increased G>T mutation rates compared to untreated RNA. Furthermore, preliminary analysis of yeast treated with the oxidizing agent H_2O_2 showed increased G>T mutations. Thus, we provide the foundation for a deep-sequencing approach to detect oxidized RNA.

Results

One of the initial steps in creating RNA-sequencing libraries is reverse transcription of the RNA samples. While it has been suggested that reverse transcriptase (RT) poorly reads through base adducts, this behavior appears to depend on the type of RT and the reaction conditions (Gong et al. 2006; Kladwang et al. 2012; Mohr et al. 2013; Siegfried et al. 2014). We, therefore, sought to determine which RT enzymes read through 8oxoG sites by performing reverse transcription using synthesized 40mer RNA oligos that contained either a single 8oxoG or an unmodified guanosine (**Figure 3.1, A**). A 21 nt DNA adaptor was ligated to the 3' end of the RNA oligos to serve as the priming site for a ^{32}P-end labeled oligo, and all reactions were performed according to manufacturer's instructions. Of the enzymes tested, cDNA products from SuperScript™ II had the weakest signal corresponding to the 8oxoG site (**Figure 3.1, B**), whereas cDNA products from SuperScript™ III had the strongest. These results suggest SuperScript™ II can read through 8oxoG sites.

We next determined which conditions permitted the insertion of a mutation across the 8oxoG site. SHAPE-Map experiments have successfully obtained mutations across SHAPE-modified bases by replacing 3 mM $MgCl_2$ with 6 mM $MnCl_2$ and allowing the reaction to run for three hours (Siegfried et al. 2014). We tested whether similar conditions would yield mutations at the 8oxoG site by generating deep-sequencing libraries from four different reverse transcription conditions (see **Chapter III/Methods and Materials/Reverse Transcription** for details). Our data revealed a high incidence of G>T mutations in the 8oxoG RNA for all RT conditions (**Figure 3.1, C**). The highest overall rate of G>T mutations resulted from using SuperScript™ II in buffer condition 1 (i.e. 3 mM $MgCl_2$, one-hour incubation), whereas substituting 3 mM $MgCl_2$ with 6 mM $MnCl_2$ decreased the G>T mutation rate at the 8oxoG site. SuperScript™ II also had high G>G fidelity (> 95 x 10^{-2}) in all reaction conditions containing the 40mer RNA. Finally, SuperScript™ III (condition 4) exhibited the lowest G>T mutation rate and the highest G>G fidelity in reactions containing either the 40mer or 8oxoG RNAs.

Our results suggest SuperScript™ II specifically produces G>T mutations at 8oxoG sites. The G>T mutation rate at G29 (which corresponds to the 8oxoG site) was 0.30 x 10^{-2} in the 40mer RNA and 74.92 x 10^{-2} in the 8oxoG RNA. Second, the fidelity of unmodified guanosine was relatively comparable between the 40mer RNA and 8oxoG RNA. The G>T mutation rate at G22 (unmodified in both the 40mer and 8oxoG RNAs) was 1.705 x 10^{-2} in the 40mer RNA and 0.885 x 10^{-2} in the 8oxoG RNA. Finally, the overall mutation rate of G>A or G>C was less than 3 x 10^{-2} for both RNAs. This observed specificity is consistent with previous reports suggesting 8oxoG preferentially base pairs with adenosine (Hsu et al. 2004; Kim et al. 2006; Simms et al. 2014).

To estimate the rate at which SuperScript™ II stops at 8oxoG, we subtracted reads containing C28 from reads containing C30 and normalized to the total number of reads containing both C28 and C30. This value corresponded to stops occurring immediately before or at the 8oxoG site (G29). Our calculation revealed a stopping rate of 2.61×10^{-2} for SuperScript™ II in buffer condition 1 (**Figure 3.1, C**). While the stopping rate improved with the 6 mM $MnCl_2$ substitution and longer incubation time, the lower G>T mutation rate in these conditions led us to conclude that buffer condition 1 offered the best outcome for detecting 8oxoG sites in RNA. We also note that SuperScript™ III had the highest – albeit marginal – stopping rate of 3.78×10^{-2}. Overall, our results suggest SuperScript™ II can read through 8oxoG modifications and introduce mutations.

To further test our deep-sequencing approach, we included two additional in vitro transcribed RNA species in our libraries. The in vitro transcribed RNAs (RP51A and P2-o41-o26) were oxidized using Fenton's reagent (Walling 1975).

$Fe^{2+} + H_2O_2 \rightarrow Fe^{3+} + OH^- + {}^{\cdot}OH$

$Fe^{3+} + H_2O_2 \rightarrow Fe^{2+} + {}^{\cdot}OOH + H^+$

Ferrous iron (Fe^{2+}) reacts with hydrogen peroxide (H_2O_2) to form ferric iron (Fe^{3+}), hydroxide (OH^-), and a hydroxyl radical ($^{\cdot}OH$). The reaction continues with the reduction of ferric iron to ferrous iron, producing a hydroperoxyl radical ($^{\cdot}OOH$) and a proton; the resulting free radicals oxidize susceptible substrates, such as RNA (Walling 1975). Oxidation of in vitro transcribed RNAs was verified by observing an increase in UV absorbance at 305 nm (**Table 3.1**) (Boateng 2014).

Our data showed that the oxidized in vitro transcribed RNA reads had a higher G>T mutation rate (unweighted average: 1.93×10^{-2}; weighted average: 1.62×10^{-2}) compared to the untreated reads (unweighted average: 0.77×10^{-2}; weighted average: 1.15×10^{-2}) (**Figure 3.1, D**; see **Chapter III/Methods and Materials/Deep-sequencing and data analysis** for calculation details). C>T was the second most prevalent mutation in the oxidized RNA reads, with an unweighted average rate of 1.3×10^{-2} (weighted average: 1.19×10^{-2}). This could be due to deamination of cytidine to uridine, which has been shown to occur on single-stranded DNA exposed to heat or alkaline solutions (Hurst and Kuksis 1958; Ullman and McCarthy 1973; Lindahl and Nyberg 1974). The C>T mutation was also the second highest mutation in the untreated sample, but only when error rates were averaged across sequences (0.76×10^{-2}); weighted averages revealed G>A to be the second highest mutation in the untreated sample (0.93×10^{-2}). To estimate the overall sequencing error rate, we calculated the error rate in the untreated and 40mer RNA reads (unweighted average: 1.45×10^{-2}; weighted average: 1.59×10^{-2}). This error rate was higher than previous reports (Minoche et al. 2011; Schmitt et al. 2012; Schirmer et al. 2016), and may be explained by the inclusion of low-quality reads in our analysis (quality score > 2). Overall, we conclude oxidized RNA results in a signature G>T mutation that can be detected via deep-sequencing.

We next tested whether a deep-sequencing approach can detect a higher G>T mutation rate in cells subjected to oxidative stress. H_2O_2 treatment has been previously shown to induce oxidative stress in yeast (McKinlay et al. 2012). We established a survival curve of yeast treated with different concentrations of H_2O_2 and found that 1.5 mM allows for >50% survival (**Figure 3.2, A**). H_2O_2 treatment can introduce 8oxoG lesions in both RNA and DNA, with RNA procuring more adducts than DNA per cell (Hofer et al. 2005; 2006; Liu et al. 2012). To confirm our H_2O_2 treatment generated damaged nucleic acids, we measured the genomic mutation frequency by monitoring the rate of spontaneous resistance to canavanine. Yeast incorporate this toxic arginine analog into proteins, resulting in aberrant proteins and cell death. Canavanine, as well as arginine, is transported into the cell via an arginine membrane permease (*CAN1*); however, mutations in the *CAN1* gene can lead to a malfunctioning transporter, thus rendering yeast resistant to canavanine (CanR strains) (Ahmad and Bussey 1986). Resistance to canavanine spontaneously arises in unadulterated yeast, but this rate increases upon treatment with damaging agents (**Figure 3.2, B**). Treatment with H_2O_2 for ten minutes increased the frequency of CanR strains nearly six-fold, suggesting the DNA, and likely the RNA, was damaged.

We prepared strand-specific libraries from H_2O_2-treated and untreated yeast as described in (Heyer et al. 2015) with some modifications. Although oxidative stress generates 8oxoG lesions in vivo, certain procedures in library preparation can also oxidize nucleic acids (Chen et al. 2017). For instance, the Broad Institute determined that acoustic shearing of DNA samples generates 8oxoG lesions (Costello et al. 2013) that manifest as mutations in deep-sequencing data. This effect is due to the production of H_2O_2 from dissolved oxygen and heat (Bruskov et al. 2002); H_2O_2 subsequently reacts with metals, often present in trace amounts in standard buffers, to form free radicals (Costello et al. 2013). Adding a metal chelator before heating the solution appears to prevent the formation of 8oxoG lesions (Bruskov et al. 2002; Hofer et al. 2006; Costello et al. 2013). Gel-purification is another common procedure in library preparation that can oxidize nucleic acids. Acrylamide polymerization is facilitated by the strong oxidizing agent ammonium persulfate. Gels used within a few hours after polymerization can introduce base lesions in nucleic acids, but this effect essentially disappears if gels are allowed to polymerize for more than twelve hours (Kladwang et al. 2012). With these observations in mind, we modified our library preparation protocol to minimize oxidation of our samples. First, we included EDTA in our lysis buffer during total RNA extraction. Second, we fragmented RNA by alkaline hydrolysis using sodium bicarbonate and EDTA. Finally, we allowed acrylamide gels to polymerize overnight prior to gel-purification.

Evidence from published work shows a basal level of approximately 6 8oxoG per 10^4 G's in *S. cerevisiae* poly(A)-selected RNA (Simms et al. 2014) and < 1 8oxoG per 10^5 G's in *E. coli* total RNA (Liu et al. 2012). However, these rates are lower than the sequencing error rate for the Illumina sequencing platform (Shendure and Ji 2008; Minoche et al. 2011; Schmitt et al. 2012; Schirmer et al. 2016). To enhance the sensitivity of our approach, our strategy includes sequencing overlapping paired-end (PE) reads, which has been shown to significantly decrease sequencing error (Chen-Harris et al. 2013; Preston et al. 2016). We identified sequencing errors as base calls present in one read but not in the reverse complement read. 125 bp PE sequencing of 100-150 nt inserts generated paired reads with substantial overlapping sequences that were merged using a paired-end read merger (Zhang et al. 2014). Subsequent quality filtering and end-trimming resulted in majority of bases with Phred-like quality scores $\geq$ 35 (data not shown). Thus, detected errors were likely from reverse transcription and PCR amplification. Since default mapping parameters have a low threshold for base mismatches, we optimized parameters to permit more mutations without affecting mapping quality. Our data revealed higher G>T mutation rates in H_2O_2-treated (2.17 G>T per 10^3 G's) yeast compared to untreated yeast (1.36 G>T per 10^3 G's) (**Figure 3.2, C**). Furthermore, the G>T rate difference between the treated and untreated yeast was higher than the differences of other mutation rates, suggesting the high G>T mutation rate was likely due to 8oxoG sites. Overall, we conclude that it is possible to use a deep-sequencing approach to detect 8oxoG lesions in vivo.

Discussion

We have developed a deep-sequencing approach to detect 8oxoG in RNA. Prior to this work, methods to study oxidized RNA were limited to low-resolution techniques. HPLC-MS/MS and HPLC-EDC are highly sensitive at detecting and quantifying adducts; however, they afford no information on the RNA sequence and require substantial (several micrograms) of sample RNA (Fiala et al. 1989; Shen et al. 2000; Hofer et al. 2005; 2006; Liu et al. 2012). Antibodies specific to 8oxoG also exist, but have only been used for qualitative assessments, such as whether or not oxidized RNA is present in the tissue sample (Park et al. 1992; Yin et al. 1995; Nunomura et al. 2002; Shan et al. 2007; Chang et al. 2008; Nunomura et al. 2012). While a few studies were able to identify transcripts susceptible to oxidation (Shan et al. 2007; McKinlay et al. 2012), information regarding sequence features is still lacking.

Although previous studies monitored reverse transcriptase stops to determine the location of base modifications (Rhee et al. 1995; Gong et al. 2006), we sought to establish conditions permitting read-through of oxidized bases. Specifically, we found that SuperScript™ II reads through 8oxoG in standard reaction conditions (buffer condition 1) (**Figure 3.1, B** and **C**). Sequencing a 40mer RNA containing a single 8oxoG site demonstrated that the most prevalent mutation from 8oxoG was G>T. We also observed increased G>T mutations from in vitro synthesized RNAs that were oxidized via Fenton's reagent (**Figure 3.1, D**). Finally, our preliminary data suggested that yeast treated with H_2O_2 exhibited higher G>T mutation rates compared to untreated yeast (**Figure 3.2, C**).

We took several steps to minimize error rates from sequencing and library preparation. For instance, heating buffer solutions can generate H_2O_2 that, in turn, can react with trace amounts of metals to produce reactive oxygen species. To prevent oxidation of our samples, we added the metal chelator EDTA to the lysis and fragmentation buffers, which has been shown to reduce the occurrence of 8oxoG-induced G>T mutations (Bruskov et al. 2002; Costello et al. 2013). We also sequenced and merged overlapping paired-reads to obtain consensus sequences. This approach greatly reduces sequencing error because the probability of the sequencer inserting the same mismatch in the forward and reverse strand is extremely low (Chen-Harris et al. 2013; Preston et al. 2016). The cost of sequencing overlapping reads, however, is reduced coverage. Nevertheless, we were able to analyze our yeast datasets comprised of approximately 20 million merged reads per sample.

Although our preliminary analysis showed increased G>T mutations in yeast treated with H_2O_2, many aspects of this work need improvement. For one, more replicates are necessary to assess reproducibility; so far, this study only includes one in vivo experiment. However, technical sequencing replicates of our yeast libraries revealed similar error rates between both datasets (data not shown). Thus, we predict that any variability detected through additional biological replicates will stem from inherent biological variance or variance in library preparation. Second, the presented analysis is limited to the overall transcriptome-wide mutation rate; therefore, information about sequence features requires further investigation. For example, do G>T mutations reside within the ORF or UTRs? Would we see more mutations in coding versus noncoding RNA (or vice versa)? Do structured regions contain fewer mutations compared to unstructured regions? Data from the present work could potentially answer these questions. The Yeast Genome Browser contains over two hundred annotated tracks that can be downloaded and used to isolate reads mapping to a region of interest (i.e. UTRs). Comparing G>T mutation rates among different regions may reveal sequence features that are more prone to oxidation. Finally, our analysis does not exclude mutations arising from SNPs, which can be resolved by modifying our current software.

We generated strand-specific RNA-sequencing libraries using a protocol that our laboratory previously optimized (Heyer et al. 2015). This protocol can easily be adapted to other types of specialized sequencing, such as ribosome profiling (Ingolia et al. 2009) or 5'-phosphate sequencing (5PSeq) (Pelechano et al. 2015). Since earlier work indicated that 8oxoG sites severely slow ribosome elongation kinetics (Simms et al. 2014), it would be interesting to see whether G>T mutations occur in-frame and/or within the A-site.

Methods and Materials

All solution and enzyme concentrations are noted as their final concentration in the reactions.

RNA oligos

Two RNA oligos, with (40mer RNA) or without 8oxoG (8oxoG RNA), was synthesized by Boston Open Labs (BOL; Cambridge MA). The sequence of both RNA oligos was 5' HO-GGAAUCUCUCUCUCUCUCUAUGUUCUUC**G**CUUUCUUCUAA-OH 3', where "**G**" was either guanosine or 8oxoG.

Hot Reverse Transcription

A miRCat-33 3' preadenylated adaptor (5' -AppTGGAATTCTCGGGTGCCAAGGddC - 3') was ligated to the 40mer and 8oxoG RNA as described below in "Ligation to preadenylated 3' adaptor". The 3' adaptor served as a priming site for the reverse transcription reaction. T4 PNK (NEB M0201S) was used for ^{32}P end-labeling of an RT primer that is reverse complementary to the adaptor sequence. A mixture of 43 nM of ligated 40mer and 8oxoG RNA, 130 nM of labeled RT primer, and 0.5 mM dNTPs was heated at 65°C for 5 minutes, then immediately chilled on ice. Next, 50 mM Tris-HCl pH = 8.3, 75 mM KCl, 5 mM DTT, and 5.3 units/uL of either SuperScript™ II (ThermoFisher 18064014), SuperScript™ III (ThermoFisher 18080093), or PrimeScript™ (CloneTech 2680A) was added to the mixture and incubated at 42°C (SuperScript™ II and PrimeScript™) or 55°C (SuperScript™ III) for 45 minutes. Enzymes were inactivated by heating the reaction to 70°C for 15 minutes. Samples were loaded on a 20% denaturing polyacrylamide gel. Analysis was performed using ImageQuant. Full-length cDNA product and the band corresponding to the 8oxoG site were normalized to free primers.

In vitro transcription

A PCR product containing a T7 promoter and part of the yeast RP51A DNA sequence was in vitro transcribed using the RiboMax Large Scale RNA Production – T7 kit (Promega P1300). The final RP51A RNA product (381 nt) was subsequently gel-purified from a 5% denaturing polyacrylamide gel. A PCR product containing a T7 promoter and the P2-o41-o26 DNA sequence was also in vitro transcribed using the same conditions. The final P2-o41-o26 RNA product (120 nt) was gel-purified from a 10% denaturing polyacrylamide gel.

Oxidation of in vitro transcribed RNA

A solution of 60 uM $Fe_2(SO_4)_3$, 1 mM H_2O_2, and 73 ng/uL of RP51A or P2-o41-o26 RNA was incubated at room temperature for 1 minute 30 seconds. 6 mM EDTA was added to stop the reaction. Successful oxidation of RNAs was verified by observing an increased in UV absorbance at 305 nm. Integrity of the oxidized RNA was assessed by denaturing gel electrophoresis.

Percent survival of H_2O_2-treated yeast

The percent survival of yeast treated with various H_2O_2 concentrations was determined. First, cultures of BY4741 wild-type yeast were grown in YPD overnight at 30°C to mid-log phase. Cultures were then diluted with fresh YPD to 7.5×10^6 cells/mL and treated with various concentrations of H_2O_2 for 10 minutes at 30°C. Next, 25 units/mL of Catalase from bovine liver (Sigma Aldrich C1345-10G, resuspended in 50 mM KH_2PO_4 pH = 7.0 and filtered) was used to removed H_2O_2 from the cultures. 100 uL of a 1:2000 dilution of treated and untreated yeast was plated onto pre-warmed YPD plates. Plates were incubated for 3 days at 30°C. The number of colonies were counted and results were used to determine colony forming units per milliliter (CFU/mL). CFU/mL of H_2O_2-treated yeast was normalized to the CFU/mL of untreated yeast to obtain the percent survival.

Genomic mutation frequency of H_2O_2-treated yeast

The genomic mutation frequency of yeast treated with 1.5 mM H_2O_2 was determined by calculating the rate of spontaneous resistance to Canavanine. An aliquot of H_2O_2-treated and untreated yeast (see above) was plated onto YPD or Arg- plates containing 60 ug/mL Canavanine. Plates were incubated for 3 days at 30°C. The number of colonies was counted and results were used to determine the number of Canavanine resistant colonies (CanR) per 10^6 cells.

Yeast treatment with H_2O_2 for deep-sequencing libraries

A culture of BY4741 wild-type yeast was grown in YPD overnight at 30°C to mid-log phase. Cells were diluted to 7.5×10^6 cells/mL in fresh YPD and split into two cultures. 1.5 mM H_2O_2 was added to one culture, and both cultures were incubated for 10 minutes at 30°C. 13 units/mL of Catalase was added to both cultures and an aliquot of cells was immediately removed and frozen in liquid nitrogen. Another aliquot of cells was used to determine the percent survival and genomic mutation frequency (see above).

Isolation of yeast RNA for deep-sequencing libraries

Total RNA from untreated and H_2O_2-treated yeast (see above) was isolated as previously described (Amberg et al. 2006). Ribosomal RNA and RNAs < 200 nt were depleted from total RNA using the RiboZero Gold Magnetic Kit (Yeast) (Epicenter MRZ116C) and a size selection column (Zymo Research RNA Clean and Concentrator – 5 R1016) respectively. The resulting pool of rRNA- and <200 nt-depleted yeast RNA was analyzed on the Agilent Bioanalyzer 2100.

Fragmentation

Synthesized RNA samples: ~1 uM of untreated and oxidized RP51A RNA was fragmented in 1X Fragmentation Buffer 1 (50 mM Tris-HCl pH = 8.3, 15 mM $MgCl_2$) at 90°C to obtain fragment sizes of 30-150 nt. Samples were immediately put on ice to stop the reaction, then precipitated by EtOH. The P2-o41-o26, 40mer, and 8oxoG RNA samples were not fragmented.

Yeast RNA samples: rRNA- and < 200 nt-depleted yeast RNA was fragmented by alkaline hydrolysis. A solution containing ~2 ng/uL of RNA, 55.6 mM $NaHCO_3$ pH = 9.2, and 1 mM EDTA was heated to 95°C for 5 minutes. To stop the reaction, 280 mM NaOAc pH = 5.2 and 0.22 mg/mL Glycogen was added and samples were immediately chilled on ice. Fragmented RNAs were then precipitated by EtOH. This condition yielded a fragment size range of 100 – 150 nt as assessed by the Agilent Bioanalyzer 2100.

Dephosphorylation of 3' ends

All RNA samples were dephosphorylated using T4 PNK and standard T4 PNK buffer without ATP.

Preadenylation of 3' adaptor

A miRCat-33 3' adaptor with a 4N randomer (5' P-NNNNTGGAATTCTCGGGTGCCAAGG-OH 3') was synthesized by IDT and subsequently adenylated using the 5' DNA Adenylation Kit (NEB E2610L). Adenylated products were gel-purified.

Ligation to preadenylated 3' adaptor

0.13 uM of fragmented and dephosphorylated RNA was ligated to 0.47 uM 3' preadenylated adaptor for 6 hours at 30°C using 6 units/uL T4 RNA Ligase 2, truncated K227Q (NEB M0351L) in standard reaction buffer (50 mM Tris-HCl pH = 7.5, 10 mM $MgCl_2$, 2 mM DTT, and 25% PEG-8000). The reaction was heated to 65°C for 20 minutes to inactivate the enzyme. Samples were then precipitated by EtOH.

Reverse Transcription

Synthesized RNA samples: Untreated in vitro transcribed RNA and 40mer RNA samples were pooled together before the reverse transcription reaction. Similarly, oxidized in vitro transcribed RNA and 8oxoG RNA samples were also pooled before the reverse transcription reaction. A mixture of 0.1 uM of ligated RNA samples, 0.5 uM barcoded RT primer, and 0.5 mM dNTPs was heated to 65°C for 5 minutes, then immediately chilled on ice. *Condition 1*) 1X SII buffer (50 mM Tris-HCl pH = 8.3, 75 mM KCl, 10 mM DTT), 3 mM $MgCl_2$, and 10 units/uL of SuperScript™ II was added to the mixture and the reaction was incubated at 42°C for 1 hour. *Condition 2*) 1X SII buffer, 6 mM $MnCl_2$, and 10 units/uL of SuperScript™ II was added to the mixture and incubated at 42°C for 1 hour. *Condition 3*) The same as Condition 2 except the reaction was incubated for 3 hours. *Condition 4*) 1X SIII buffer (50 mM Tris-HCl pH = 8.3, 75 mM KCl, 5 mM DTT), 3 mM $MgCl_2$, and 10 units/uL of SuperScript™ III were added to the mixture and the reaction was incubated at 55°C for 1 hour. All reactions were stopped by incubating the reactions at 70°C for 15 minutes, then adding denaturing loading buffer immediately afterward. cDNA products (size range 105 – 220 nt) were purified from a 10% denaturing polyacrylamide gel and precipitated by EtOH.

Yeast RNA samples: A mixture of ~0.1 uM of ligated RNA, 0.5 uM barcoded RT primer, and 0.5 mM dNTPs was heated to 65°C for 5 minutes, then immediately chilled on ice. 1X SII buffer, 3 mM $MgCl_2$, and 10 units/uL of SuperScript™ II were added to the mixture and the reaction was incubated at 42°C for 1 hour. All reactions were stopped by incubating the samples at 70°C for 15 minutes, then adding denaturing loading buffer immediately afterward. cDNA products (size range 195 – 245 nt) were purified from a 10% denaturing polyacrylamide gel and precipitated by EtOH.

Circularization

Gel-purified cDNA products were incubated with 1X CircLigaseI Reaction Buffer (50 mM MOPS pH = 7.5, 10 mM KCl, 5 mM $MgCl_2$, 1 mM DTT), 2.5 mM $MnCl_2$, 50 uM ATP, 1 M Betaine, 50 nM single-stranded DNA, and 5 units/uL Cerclages ssDNA Ligase (Epicentre Biotechnologies CL4115K) at 60°C for 4 hours. The reaction was stopped by incubating the samples at 80°C for 10 minutes.

PCR Amplification of circularized cDNA products

All PCR reactions were performed using the KAPA HiFi Library Amplification Kit (KAPA Biosystems KK2611), gel-purified PE1.0 and PE2.0 Illumina primers, and circularized cDNA products (comprising up to one-fifth of the PCR reaction volume). Small-scale PCR reactions were performed to determine the appropriate PCR cycle that yielded a product of expected size without depleting the primer pool. After completing a large-scale PCR amplification, PCR products were prepared for and purified from the PippinHT instrument (synthesized RNA samples: size range 160-271 bp; yeast RNA samples: size range 251-301 bp).

Deep-sequencing and data analysis

Synthesized RNA Libraries: Samples were prepared and pooled for single-end 100 bp sequencing on the Illumina HiSeq2000 sequencing platform (UMassMed Sequencing Core). Barcoded libraries were sequenced with 90% PhiX. The adaptor sequence was trimmed and reads were separated by barcode. Reads were first mapped to the PhiX174 reference genome using Bowtie 2 (default parameters). All reads not mapped to the PhiX174 genome were mapped to a reference genome comprised of the RP51A, P2-o41-o26, and the 40mer sequences using Bowtie 2 (default parameters). Reads with quality scores > 2 were isolated and reads mapping to the reverse strand were removed. Reads were visualized on IGV and mutations were counted using an in-house developed script. Unweighted averages were obtained by calculating the average mutation rate between RP51A and P2-o41-o26 at each base and across bases. Weighted averages were calculated the same way except the contribution of each RNA species was weighted according to its total number of read bases.

Yeast RNA Libraries: Samples were prepared and pooled for paired-end 125 bp sequencing on the Illumina HiSeq2500 sequencing platform (New York Genome Center). Barcoded libraries were sequenced with 5% PhiX. Paired-end reads were first separated by barcode, then merged using PEAR v0.9.4. The 3' adaptor sequence and 5' CC was trimmed using CutAdapt v1.7.1 and the resulting reads with $\leq$ 5 bases were removed using CutAdapt v1.9. The 4N randomer was appended to the header using GCAT UMI-tools. Read ends with a Phred score < 40 were trimmed using Trimmomatic v0.32. Next, reads were mapped to the yeast reference genome (sacCer3) using TopHat v2.0.14 with the following parameters: -N 5 --read-edit-dist 5 --read-realign-edit-dist 0 –i 40 –I 2000 –p 4 --no-coverage-search --library-type fr-secondstrand --segment-mismatches 3 --max-segment-intron 2000 --b2-D 20 --b2-R 4 --b2-N 1 --b2-L 10 --b2-I S,1,1.15. Mapped reads were then analyzed using a script that determines the number and type of base mutations.

A

GGAAUCUCUCUCUCUCUCUAUGUUCUUC**G**CUUUCUUCUAA*TGGAATTCTCGGGTGCCAAGG*

B

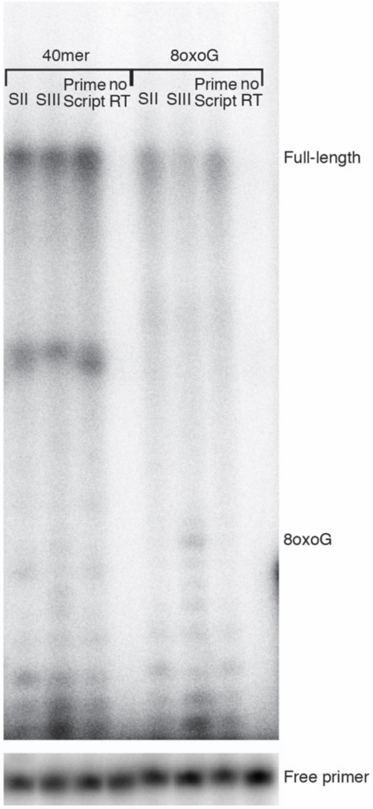
40mer
8oxoG
SII
SIII
Prime Script
no RT
SII
SIII
Prime Script
no RT
Full-length
8oxoG
Free primer

	SII	SIII	Prime Script
Full-length	95%	58%	90%
8oxoG	5%	42%	10%

C

		SII 3mM $MgCl_2$	SII 6mM $MnCl_2$	SII 6mM $MnCl_2$ 3hrs	SIII 3mM $MgCl_2$
40mer RNA		n = 1,279,2200	n = 1,258,043	n = 1,087,751	n = 620,323
		x 10^{-2}	x 10^{-2}	x 10^{-2}	x 10^{-2}
	G → G	95.90	95.91	95.85	96.22
	G → T	0.30	0.39	0.42	0.42
	G → A	2.83	2.62	2.51	2.64
	G → C	0.25	0.25	0.35	0.16
	In/Del	0.71	0.83	0.86	0.56
8oxoG RNA		n = 250,077	n = 314,618	n = 214,054	n = 195,746
		x 10^{-2}	x 10^{-2}	x 10^{-2}	x 10^{-2}
	G → G	21.73	23.11	23.69	28.38
	G → T	71.82	68.66	67.51	66.30
	G → A	0.18	0.23	0.19	0.22
	G → C	2.13	2.43	2.61	2.57
	In/Del	4.14	5.58	6.01	2.54
	stops	2.61	1.67	1.45	3.78

D

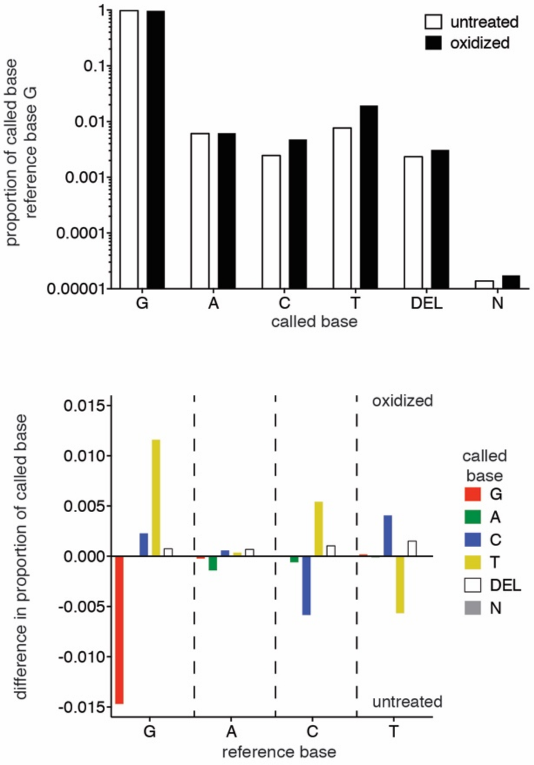

Figure 3.1: Reverse transcription of oxidized RNA
(A) Diagram of 40mer and 8oxoG RNA ligated to 21 nt DNA adaptor (italicized). Site of 8oxoG (G29) indicated in red bold. **(B)** Hot reverse transcription of 40mer and 8oxoG reporters. The adaptor sequence served as the priming site for the 3' end-labeled primer. cDNA products analyzed on a 20% denaturing polyacrylamide gel. Signal intensity corresponding to full-length product and 8oxoG stop were normalized to free primer (n=1). **(C)** Deep-sequencing of 40mer and 8oxoG oligos. Showing results of mutational analysis at 8oxoG site. **(D)** Mutational analysis of deep-sequenced in vitro synthesized RNA. *Top*: Frequency of called base for reference base G (unweighted averages). *Bottom*: Difference in mutation rate between H_2O_2-treated and untreated yeast for all possible base substitutions. A positive value indicates that H_2O_2-treated had a higher mutation rate than untreated yeast.

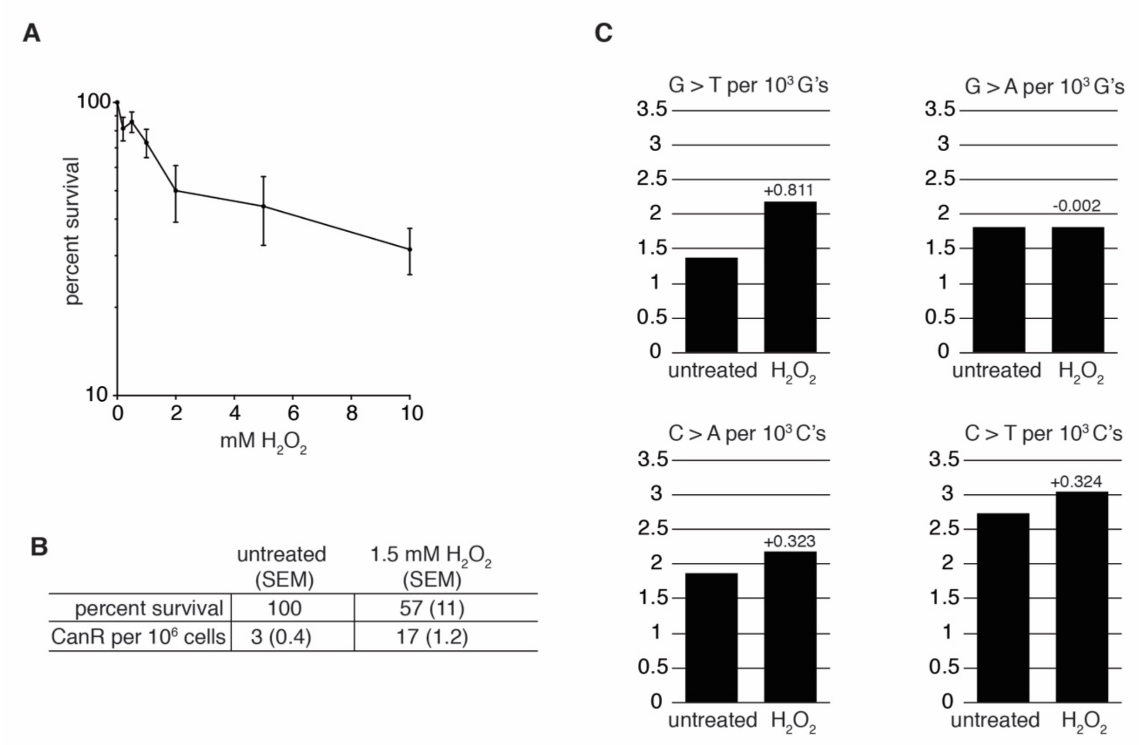

	untreated (SEM)	1.5 mM H_2O_2 (SEM)
percent survival	100	57 (11)
CanR per 10^6 cells	3 (0.4)	17 (1.2)

Figure 3.2: cDNA variant sequencing of yeast treated with H_2O_2
(A) Percent survival of yeast treated with various concentrations of H_2O_2. Error bars represent standard error of the mean (n=3). **(B)** Percent survival and frequency of CanR strains upon treatment with 1.5 mM H_2O_2. Average results of three biological replicates and standard error of the mean (SEM). **(C)** Deep-sequencing of RNA from H_2O_2-treated and untreated yeast. Results of mutational analysis with the top four occurring mutations shown.

	Abs 260 nm	Abs 305 nm
40mer RNA	2.470	0.088
8oxoG RNA	2.430	0.127
Untreated RP51A	4.286	0.069
Oxidized RP51A	3.817	0.145
Untreated P2-o41-o26	2.323	0.054
Oxidized P2-o41-o26	2.181	0.116

Table 3.1: Absorbance of untreated and oxidized RNA
UV absorbance of 40mer RNA oligos and in vitro synthesized RNAs.

CHAPTER IV. DISCUSSION

Part 1. *ASC1* and *RPS3*: New actors in 18S nonfunctional rRNA decay

18S rRNA containing inactivating mutations within the decoding center is subject to quality control known as nonfunctional rRNA decay (18S NRD). Previous work from our lab demonstrated a convergence between 18S NRD and other translation-dependent pathways (LaRiviere et al. 2006; Cole et al. 2009). Although deletion of NGD factors *DOM34*, *HBS1*, or both decreases 18S NRD kinetics, the observation that cycloheximide treatment completely abrogates 18S NRD suggested other factors must contribute (Cole et al. 2009). Moreover, our unpublished data suggested that RQC/PDTA factor *ASC1* contributes to 18S NRD (Merrikh 2012).

The goal of Chapter II was to identify additional 18S NRD factors to further our understanding of rRNA quality control. We demonstrated that deletion of *ASC1* partially stabilizes 18S:A1492C, whereas deletion of either *DOM34* or *HBS1* in the *asc1*Δ strain completely stabilizes 18S:A1492C (**Figure 2.2, A** and **B; Figure 2.4, A**). These data indicate that 18S NRD can be divided into genetically separable pathways, with *ASC1* functioning in parallel with *DOM34*:*HBS1*. We also identified *RPS3* as a central component of 18S NRD.

Deletion of a six amino-acid region within the Rps3p C-terminal tail decreased 18S NRD kinetics by >11-fold (**Figure 2.6, B**), the largest effect from any single-mutant tested. Finally, we found deletion of *SKI2* partially stabilizes 18S:A1492C, but is synthetic with neither *DOM34* nor *ASC1* (**Figure 2.4, A**). Overall, we conclude that multiple, redundant pathways exist for the target and decay of nonfunctional 18S rRNA.

This work along with others suggests a central role of *RPS3* in translation-dependent quality control. In particular, the post-translational modification of the Rps3p C-terminal tail appears to mark stalled ribosomes for quality control. Recent studies determined that *S. cerevisiae* Hel2p ubiquitinates Rps3p (uS3) K212 and Rps20p (uS10) K6/K8 of stalled ribosomes (Matsuo et al. 2017; Simms et al. 2017). In mammalian cells, ZNF598 (yeast *HEL2*) and RACK1 (yeast *ASC1*) both participate in the ubiquitination of stalled ribosomes, with ZNF598 primarily participating in RPS10 (eS10) and RPS20 (uS10) ubiquitination, and RACK1 primarily participating in RPS3 (uS3) and RPS2 (uS5) ubiquitination (Juszkiewicz and Hegde 2017; Sundaramoorthy et al. 2017). Notably, small-molecule activators of the unfolded protein response pathway or inhibitors of translation elongation both lead to the ubiquitination of RPS3 at the site equivalent to yeast K212 (Higgins et al. 2015; Juszkiewicz and Hegde 2017; Sundaramoorthy et al. 2017). In our study, deleting amino acids 212-217 of

RPS3 nearly abrogated 18S NRD (**Figure 2.6, B**), whereas single deletion of *ASC1* only partially stabilized 18S:A1492C (**Figure 2.2, B**). The different kinetic contributions of *ASC1* and *RPS3* would be consistent with the scenario in which Asc1p and another factor (possibly Hel2p) converge to ubiquitinate Rps3p on stalled ribosomes and initiate quality control.

Since ubiquitination of Rps3p K212 appears to mark stalled ribosomes (Matsuo et al. 2017; Simms et al. 2017), it would be worth investigating whether the same ubiquitination pattern occurs during 18S NRD. A mutational analysis of the 212-217 region would ascertain whether one, some, or all of the amino acids are required for 18S NRD, and testing whether 18S NRD disappears in *hel2*Δ and *rps3* K212A yeast strains may provide evidence of Hel2p-dependent ubiquitination. Deletion of amino acids 212-217 in Rps3p may prevent K212 ubiquitination, but it is equally possible that the remaining five amino acids might have functional relevance, such as serving as a binding site for Hel2p or other factors. Another experiment would be to purify 18S:A1492C-containing ribosomes and perform mass spectrometry to see if Rps3p K212 and/or other ribosomal proteins are ubiquitinated during 18S NRD.

Interestingly, a small body of literature suggests RPS3 moonlights as a DNA damage repair factor. Purified *Drosophila* RPS3 exhibits cleavage activity on double-stranded DNA containing 8oxoG or apurinic/apyrimidinic (AP) lesions.

The authors proposed that *Drosophila* RPS3 removes 8oxoG using its *N*-glycosylase activity, then proceeds to cleave the phosphodiester bond via a type 1 beta-elimination reaction (Wilson et al. 1993; 1994; Yacoub et al. 1996; Deutsch et al. 1997; Hegde et al. 2001). This lyase activity appears to be conserved since another group independently discovered the AP lyase activity of human RPS3 after performing a series of biochemical fractionation experiments (Kim et al. 1995; Hegde et al. 2004). Although recombinant human RPS3 does not contain *N*-glycosylase activity, it exhibits strong binding affinity to 8oxoG substrates (Hegde et al. 2006). While evidence of lyase activity came from purified RPS3, it would be interesting to know whether RPS3 harbors this activity in the context of the ribosome. Indeed, one group investigated whether human RPS3 exhibits AP lyase activity while bound to the 40S subunit; however, the authors observed no cleavage events. Rather, it appears that 40S-bound RPS3 is able to recognize AP sites since RPS3 crosslinked with AP DNA substrates in the presence of sodium cyanoborohydride[20] (Grosheva et al. 2017). The activity differences between free and 40S-bound RPS3 might imply that the joining of the 60S subunit to form 80S ribosomes could modulate the activity of RPS3. For example, during the translation of an abasic mRNA, RPS3 might recognize and bind to the abasic site to promote ribosome stalling. If so, RPS3 may connect translation-dependent quality control to RNA damage by recognizing aberrant modifications on mRNA.

---

[20] The lyase mechanism includes the formation of a Schiff base intermediate between the enzyme and the ribose C1' moiety. Reducing agents, such as sodium cyanoborohydride, can covalently trap lyases in this intermediate step (Grosheva et al. 2017).

18S NRD shares many qualities with other translation-dependent surveillance pathways. For instance, factors that participate in NGD (*DOM34* and *HBS1*), NSD (*SKI7* and *SKI2*), and PDTA/RQC (*ASC1*) also participate in 18S NRD (**Chapter II**) (Cole et al. 2009). Despite being discovered independently of each other, emerging evidence suggests these pathways merely describe different outcomes of the same initiating event – a stalled or severely slowed ribosome. How do stalling events trigger quality control and how are they different from normal stalling events (e.g. targeting for endoplasmic reticulum)? To help answer this question, one group examined kinetic models of three stalling scenarios: 1) an individual ribosome encounters a stall site and triggers quality control; 2) the stalled ribosome causes a traffic jam so severe that it prevents ribosomes from initiating; or 3) trailing ribosomes collide with each other, and the collision event triggers quality control (Ferrin and Subramaniam 2017). The authors showed that the ribosome collision model closely matched experimentally determined protein-synthesis rates from a library of stalling reporters (Ferrin and Subramaniam 2017). Evidence from yeast further corroborates this finding (Simms et al. 2017). Sequencing of stalling reporters revealed multiple cleavage sites occurring approximately every 30 nt (the size of a ribosome footprint) upstream of the stall site and in one frame. In addition, cleavage efficiency increased as the distance between the start codon and stall site increased (Simms et al. 2017). These data indicate that several ribosomes engage on the same aberrant mRNA and cleavage takes place between closely stacked ribosomes. To model collision events in vivo, the authors created a yeast strain that housed a mixed population of cycloheximide-resistant and cycloheximide-sensitive ribosomes. In the presence of cycloheximide, resistant ribosomes continue to elongate and eventually collide with sensitive ribosomes. This system allowed the authors to demonstrate that collision events lead to the Hel2p-dependent ubiquitination of Rps3p at amino acid K212 (Simms et al. 2017). Thus, ribosome collision likely initiates translation-dependent quality control.

How might 18S NRD fit into this model? Does 18S:A1492C lead to ribosome collision? While ribosome density positively correlates with NGD efficiency, the nature of the stall site appears to modulate this interaction; that is, a stronger stall site diminishes the effect of ribosome density on NGD efficiency by increasing ribosome dwell time (Simms et al. 2017). Thus, strong stallers bypass the need for ribosome collision to initiate NGD. 18S:A1492C likely fits into the category of strong stallers. The highly conserved A1492 in 16S rRNA (A1755 in *S. cerevisiae* 18S rRNA) assists in codon:anticodon pairing at the second position. A1492 mutations impair tRNA-binding at the A-site in vitro and are dominant lethal in *E. coli* (Powers and Noller 1990; 1993; Yoshizawa et al. 1999b; LaRiviere et al. 2006). Thus, the strong stalling effect of 18S:A1492C could bypass the need for collision-based initiation of 18S NRD. Nevertheless, the slow decay rate of 18S:A1492C (half-life: 41 to 96 minutes) (**Chapter II**) (LaRiviere et al. 2006; Cole et al. 2009) compared to other stalling mRNA reporters (half-life: 2 to 9 minutes) (Frischmeyer et al. 2002; Doma and Parker 2006; Sweet et al. 2012; Tsuboi et al. 2012) suggests targeting of 18S:A1492C for NRD is relatively inefficient.

The numerous studies examining the fate of nascent peptides associated with stalled ribosomes has given us some idea on what happens to the 60S subunit. For example, the 60S subunit likely remains intact since stalled 80S complexes are dissociated before the final steps of the RQC pathway (CAT-tailing, Ltn1p ubiquitination, and hydrolysis of the peptidyl-tRNA) isolate and remove the aberrant nascent peptide (Brandman and Hegde 2016). This would be consistent with the observation that the decay of 25S rRNA harboring mutations in the peptidyl-transfer center (25S NRD) happens via a mechanism that is distinct from 18S NRD and other translation-dependent pathways

(LaRiviere et al. 2006; Cole et al. 2009; Fujii et al. 2009; 2012) (see **Chapter I**).[21] Thus, a probable outcome for the 60S subunit is that it is recycled into new 80S complexes.

Conversely, the fate of the 40S subunit remains elusive. What happens to the 40S subunit? In order for exonucleases to gain access to 18S:A1492C during 18S NRD, one could predict that some or all of the 40S proteins disassemble either before or simultaneous to decay. If so, are the 40S proteins degraded or are they reassembled with new 18S rRNA? Can cells distinguish between nonfunctional 18S rRNA from aberrant mRNA? Is the associated mRNA cleaved during 18S NRD? Given the overlapping features between 18S NRD and NGD/NSD/PDTA/RQC, it is possible that cells degrade both the 18S rRNA and mRNA. Alternatively, subtle differences (e.g. in the ubiquitination pattern) may communicate whether the source of ribosome stalling comes from the nonfunctional 18S rRNA or aberrant mRNA. A key long-term question for the field is whether 18S NRD is functionally different from NGD/NSD/PDTA/RQC pathways. Providing answers to these questions will add to our growing understanding of 18S NRD and other translation-dependent quality control pathways.

---

[21] We have preliminary data suggesting 25S NRD still happens in the *rps3*$_{1\text{-}211}$ mutant (data not shown).

Part 2. A deep-sequencing approach to detect oxidized RNA

The studies in Chapter III serve as the foundation for the development of a deep-sequencing approach to detect oxidized RNA. Prior to this work, low-resolution methods were routinely used to detect 8oxoG and other types of damaging adducts. HPLC-MS/MS and HPLC-ECD can detect and quantify modifications, and have been used to demonstrate that RNA is more susceptible to various damaging agents than DNA (Fiala et al. 1989; Abe et al. 2002; 2003; Hofer et al. 2005; 2006). Data establishing the presence of oxidized RNA in Alzheimer's, Parkinson's, and ALS came from immunohistochemistry experiments using antibodies specific to 8oxoG (Park et al. 1992; Yin et al. 1995; Nunomura et al. 1999; 2002; Shan et al. 2007; Chang et al. 2008; Nunomura et al. 2012). These techniques, however, do not provide information regarding transcript or sequence features. So far, measuring reverse transcriptase (RT) stops at modified sites is the only tool that can provide sequence and nucleotide information, but analysis is limited to one transcript at a time (Iordanov et al. 1998; Gong et al. 2006; Hostetter et al. 2012; Kladwang et al. 2012).

Our work aimed at developing a deep-sequencing method to detect damaged RNA at nucleotide resolution. This approach relies on the ability of RT to read through and introduce mutations across damaged sites. Being the most prevalent adduct formed from reactive oxygen species (ROS) – and since numerous stressors generate intracellular ROS (Fiala et al. 1989; Nunoshiba and Demple 1993; Bruskov et al. 2002; Cadet et al. 2005; Rada and Leto 2008; Carozzi et al. 2010) – made 8oxoG a suitable model lesion for our studies. Analysis of cDNA products from an oligo containing a single 8oxoG demonstrated that SuperScript™ II can read through and introduce G>T mutations at 8oxoG sites (**Figure 3.1**, **B** and **C**); cDNA products from oxidized in vitro synthesized RNA confirmed these findings (**Figure 3.1**, **D**). Although previous research determined that substituting $MgCl_2$ with $MnCl_2$ improved read-through at bulky adducts (e.g. SHAPE) (Siegfried et al. 2014), we found that standard reaction conditions (condition 1; 3 mM $MgCl_2$, 1-hour incubation) yielded the most G>T mutations (**Figure 3.1, C**). Finally, our preliminary analysis showed increased G>T mutations in yeast treated with H_2O_2 (**Figure 3.2, C**)[22].

One of the challenges of detecting true mutations from false positives derives from the inherent error rate of sequencing platforms. For example, the Illumina HiSeq sequencing platform can exhibit substitution error rates as high as 1.6×10^{-3}, even after stringent quality-filtering of aligned reads (Minoche et al. 2011; Schirmer et al. 2016). This error rate is higher than reported 8oxoG rates occurring in vivo (0.2 to 60 8oxoG per 10^5 G's) (Hofer et al. 2005; 2006; Liu et al. 2012; Simms et al. 2014). To overcome the high error rate of deep-sequencing, we sequenced libraries containing short inserts to generate overlapping paired-end reads. This method has been previously established to significantly reduce sequencing error, with the number of paired reads containing mismatched base-calls declining from ~6.7 x 10^{-3} (unfiltered read pairs) to ~2.5 x 10^{-7} (filtered by quality score $\geq$35) (Chen-Harris et al. 2013; Preston et al. 2016), well below the reported 8oxoG rates (Hofer et al. 2005; 2006; Liu et al. 2012; Simms et al. 2014). FastQ assessment of merged reads from our yeast experiments reported Phred-like quality scores of $\geq$38 per base for the first 95 bases (data not shown). Our preliminary analysis showed G>T rates of 1.36 per 10^3 G's in untreated yeast and 2.17 per 10^3 G's in H_2O_2-treated yeast (**Figure 3.2**, **C**), suggesting that the errors likely originated from reverse transcription and PCR. Indeed, we observed similar mutation rates after resequencing the same yeast library (data not shown).[23]

---

[22] Based on one biological replicate

We prepared strand-specific RNA-Seq libraries from in vitro synthesized RNA and yeast total RNA using our in-house developed protocol (Heyer et al. 2015). For our yeast libraries, we depleted rRNA and tRNA from total RNA to increase the sensitivity of our mutational analysis given the recent evidence of poly(A)-selected RNA being more susceptible to oxidation than total RNA (Simms et al. 2014). However, certain procedures in library preparation damage nucleic acids, which can manifest as base substitutions in deep-sequencing data. For instance, excessive heating (e.g. during nucleic acid fragmentation) generates ROS that, in turn, react with guanosine to form 8oxoG; in this regard, G>T mutations result from polymerases incorporating adenosine across 8oxoG (Costello et al. 2013; Chen et al. 2017). Therefore, we adjusted our library preparation protocol to minimize exposure to damaging agents. We added the metal chelator EDTA during our lysis and fragmentation steps, we allowed acrylamide gels to polymerize for >24 hours, and we used low-energy lamps to visualize RNA during gel-purification. Although we did not empirically determine whether each change affected the signal-to-noise ratio, earlier research has provided evidence that such changes help reduce the formation of 8oxoG and uridine dimers (Bruskov et al. 2002; Hofer et al. 2006; Kladwang et al. 2012; Costello et al. 2013).

---

[23] To really evaluate the merit of sequencing overlapping paired-end reads, we could compare mutation rates from merged reads to unmerged reads.

Our analysis employed a simple mutation-counting software to quantify the global mutation rate for each base. Although this software was sufficient for our oligo and in vitro synthesized RNA libraries, our yeast libraries require more sophisticated analyses. For example, we did not distinguish random base substitutions from bona fide SNPs in our yeast dataset (Chen-Harris et al. 2013; Preston et al. 2016). A possible solution would be to isolate reads that contain the same mutation in the same position over a certain threshold. With this information, we could modify the reference genome, remap the dataset, then repeat our mutation analysis. Doing so may increase the single-to-noise ratio without having to discard reads. Additionally, a subset of mutations in the RNA-Seq data may have derived from oxidized DNA. RNA transcribed from DNA containing an oxidized-induced mutation would manifest as mutations in the dataset. A possible approach to overcome this issue is to overexpress the yeast DNA repair enzyme *OGG1*. Ogg1p is a combined DNA glycosylase and lyase that specifically excises 8oxoG residues in nuclear or mitochondrial DNA (van der Kemp et al. 1996; Singh et al. 2001). Ogg1p overexpression might protect the yeast genome from accumulating mutations due to 8oxoG DNA; if so, this approach would further increase the likelihood that the G>T mutations in the RNA-Seq dataset are due to oxidized RNA rather than DNA.

Preliminary analysis of the yeast libraries came from one biological replicate. Our results look promising, however, since the simple mutation-counting software detected increased G>T incidences in H_2O_2-treated yeast compared to untreated yeast (**Figure 3.2, C**). We are currently making libraries from additional yeast experiments to assess reproducibility. Our replicate libraries also contain varying amounts of the 40mer and 8oxoG oligos in order to measure the sensitivity of our assay. Analysis of datasets produced from these libraries will determine the minimum coverage necessary to reliably detect 8oxoG-induced mutations. To further increase the sensitivity of our assay, we can prepare libraries from pull-down experiments using antibodies specific to 8oxoG. We could then compare the RNA-Seq datasets to the 8oxoG-enriched datasets to see if we obtain similar conclusions.

Many questions remain to be answered. For example, do reactive oxygen species preferentially modify single-stranded RNA? If so, we may observe fewer G>T mutations in structured regions versus unstructured regions. We may also observe fewer G>T mutations in rRNA and tRNA compared to mRNA, assuming we are able to account for less coverage at these regions in our calculations since our libraries were depleted of rRNA and tRNA species. In addition, we could examine whether certain motifs are prone to oxidation. Guanosines are highly susceptible to oxidation (Wurtmann and Wolin 2009), but in what context? Are runs of guanosines more susceptible than discontinuous guanosines? Does the number of guanosines in a transcript correlate with the number of G>T mutations? In-depth analysis may provide answers to some of these questions.

Our ultimate goal was to investigate how cells deal with damaged RNA. Accumulating evidence suggests damaged RNA negatively affects translation, with ribosomes stalling at the adduct (see **Chapter I**). However, given the limited tools, we sought to develop a deep-sequencing approach to detect damaged RNA to see if we can gain additional insight into the relationship between damaged RNA and translation surveillance mechanisms. For example, if translation-dependent quality control targets oxidized RNA, we would predict higher G>T mutations in coding regions (e.g. ORFs) versus noncoding regions (e.g. UTRs). Moreover, we could test whether *dom34*Δ, *xrn1*Δ, *rps3*$_{1\text{-}211}$, or other strains deficient in quality control exhibit higher mutation rates compared to wild-type yeast. Additional insight could come from investigating ribosome dynamics. Our library preparation protocol can be easily adapted to other specialized sequencing. Ribosome profiling would tell us whether G>T mutations appear in frame and, if so, at what codon position. If ribosomes stall at 8oxoG sites, we could assess whether ribosome density positively correlates with G>T incidences. Examining the relationship between G>T positions within the ORF and ribosome density might also tell us something about the stalling mechanism. For example, if ribosomes collide at 8oxoG sites, we may observe an increase in both G>T mutations and ribosome density toward the middle or end of ORFs. We could also generate 5'-phosphate sequencing libraries (5PSeq) from wild-type yeast and yeast lacking *XRN1*. 5PSeq selectively sequences RNAs containing 5'-phosphates; the yeast cytoplasmic exonuclease Xrn1p generates mRNAs with 5' phosphates, thus decay intermediates represent a major portion of reads. 5PSeq has allowed researchers to study ribosome dynamics during co-translational mRNA decay (Pelechano et al. 2015). By comparing mutation rates from each strain, we can determine whether 8oxoG RNAs are preferential targets for decay.

Since 8oxoG is well-studied, appears under a variety of stressors, and is known to stall (or severely slow down) ribosome transit (Fiala et al. 1989; Nunoshiba and Demple 1993; Bruskov et al. 2002; Cadet et al. 2005; Shan et al. 2007; Tanaka et al. 2007; Rada and Leto 2008; Wurtmann and Wolin 2009; Simms et al. 2014), we selected 8oxoG as a model lesion to develop our deep-sequencing method. Eventually, however, we would like to see if this method can be applied to other types of damage. One would have to determine the conditions for RT read-through at specific adducts, such as pyrimidine dimers or platination. Furthermore, the read-through of adducts does not necessarily lead to the insertion of a mutation. For example, SuperScript™ II can read through bulky SHAPE adducts, but this usually manifests as deletions in deep-sequencing data (Siegfried et al. 2014). Nevertheless, once these conditions are established, subsequent analyses may uncover information regarding sequence features, ribosome dynamics, etc. for the adduct of interest. Overall, our deep-sequencing approach may serve as the foundation for the study of other types of damaging adducts.

REFERENCES

Aas PA, Otterlei M, Falnes PO, Vågbø CB, Skorpen F, Akbari M, Sundheim O, Bjørås M, Slupphaug G, Seeberg E, et al. 2003. Human and bacterial oxidative demethylases repair alkylation damage in both RNA and DNA. *Nature* **421**: 859–863.

Abe T, Isobe C, Murata T, Sato C, Tohgi H. 2003. Alteration of 8-hydroxyguanosine concentrations in the cerebrospinal fluid and serum from patients with Parkinson's disease. *Neurosci Lett* **336**: 105–108.

Abe T, Tohgi H, Isobe C, Murata T, Sato C. 2002. Remarkable increase in the concentration of 8-hydroxyguanosine in cerebrospinal fluid from patients with Alzheimer's disease. *J Neurosci Res* **70**: 447–450.

Ahmad M, Bussey H. 1986. Yeast arginine permease: nucleotide sequence of the CAN1 gene. *Curr Genet* **10**: 587–592.

Aitken CE, Lorsch JR. 2012. A mechanistic overview of translation initiation in eukaryotes. *Nature Publishing Group* **19**: 568–576.

Albuquerque CP, Smolka MB, Payne SH, Bafna V, Eng J, Zhou H. 2008. A multidimensional chromatography technology for in-depth phosphoproteome analysis. *Mol Cell Proteomics* **7**: 1389–1396.

Amberg DC, Burke DJ, Strathern JN. 2006. Yeast RNA isolation: small-scale. *CSH Protoc* **2006**: pdb.prot4155.

Amrani N, Sachs MS, Jacobson A. 2006. Early nonsense: mRNA decay solves a translational problem. *Nat Rev Mol Cell Biol* **7**: 415–425.

Anger AM, Armache J-P, Berninghausen O, Habeck M, Subklewe M, Wilson DN, Beckmann R. 2013. Structures of the human and Drosophila 80S ribosome. *Nature* **497**: 80–85.

Araki Y, Takahashi S, Kobayashi T, Kajiho H, Hoshino S, Katada T. 2001. Ski7p G protein interacts with the exosome and the Ski complex for 3“-to-5” mRNA decay in yeast. *EMBO J* **20**: 4684–4693.

Ban N, Beckmann R, Cate JHD, Dinman JD, Dragon F, Ellis SR, Lafontaine DLJ, Lindahl L, Liljas A, Lipton JM, et al. 2014. A new system for naming ribosomal proteins. *Curr Opin Struct Biol* **24**: 165–169.

Becker T, Armache J-P, Jarasch A, Anger AM, Villa E, Sieber H, Motaal BA, Mielke T, Berninghausen O, Beckmann R. 2011. Structure of the no-go mRNA decay complex Dom34-Hbs1 bound to a stalled 80S ribosome. *Nat Struct Mol Biol* **18**: 715–720.

Ben-Shem A, Jenner L, Yusupova G, Yusupov M. 2010. Crystal structure of the eukaryotic ribosome. *Science* **330**: 1203–1209.

Bengtson MH, Joazeiro CAP. 2010. Role of a ribosome-associated E3 ubiquitin ligase in protein quality control. *Nature* **467**: 470–473.

Bernard JJ, Cowing-Zitron C, Nakatsuji T, Muehleisen B, Muto J, Borkowski AW, Martinez L, Greidinger EL, Yu BD, Gallo RL. 2012. Ultraviolet radiation damages self noncoding RNA and is detected by TLR3. *Nat Med* **18**: 1286–1290.

Bessho Y, Shibata R, Sekine S-I, Murayama K, Higashijima K, Hori-Takemoto C, Shirouzu M, Kuramitsu S, Yokoyama S. 2007. Structural basis for functional mimicry of long-variable-arm tRNA by transfer-messenger RNA. *Proc Natl Acad Sci USA* **104**: 8293–8298.

Boateng DA. 2014. Kinetics of Formation and Oxidation of 8-oxo-7,8-dihydroguanine (8oxoG). East Tennessee State University School of Graduate Studies. Electronic Theses and Dissertations. Paper 2314. http://dc.etsu.edu/etd/2314.

Bonekamp NA, Völkl A, Fahimi HD, Schrader M. 2009. Reactive oxygen species and peroxisomes: struggling for balance. *Biofactors* **35**: 346–355.

Brandman O, Hegde RS. 2016. Ribosome-associated protein quality control. *Nature Publishing Group* **23**: 7–15.

Brandman O, Stewart-Ornstein J, Wong D, Larson A, Williams CC, Li G-W, Zhou S, King D, Shen PS, Weibezahn J, et al. 2012. A ribosome-bound quality control complex triggers degradation of nascent peptides and signals translation stress. *Cell* **151**: 1042–1054.

Brina D, Miluzio A, Ricciardi S, Biffo S. 2015. eIF6 anti-association activity is required for ribosome biogenesis, translational control and tumor progression. *Biochim Biophys Acta* **1849**: 830–835.

Brown A, Shao S, Murray J, Hegde RS, Ramakrishnan V. 2015. Structural basis for stop codon recognition in eukaryotes. *Nature* **524**: 493–496.

Brown JT, Bai X, Johnson AW. 2000. The yeast antiviral proteins Ski2p, Ski3p, and Ski8p exist as a complex in vivo. *RNA* **6**: 449–457.

Bruskov VI, Malakhova LV, Masalimov ZK, Chernikov AV. 2002. Heat-induced formation of reactive oxygen species and 8-oxoguanine, a biomarker of damage to DNA. *Nucleic Acids Res* **30**: 1354–1363.

Cadet J, Sage E, Douki T. 2005. Ultraviolet radiation-mediated damage to cellular DNA. *Mutat Res* **571**: 3–17.

Calabretta A, Küpfer PA, Leumann CJ. 2015. The effect of RNA base lesions on mRNA translation. *Nucleic Acids Res* **43**: 4713–4720.

Carozzi VA, Marmiroli P, Cavaletti G. 2010. The role of oxidative stress and anti-oxidant treatment in platinum-induced peripheral neurotoxicity. *Curr Cancer Drug Targets* **10**: 670–682.

Casati P. 2004. Crosslinking of Ribosomal Proteins to RNA in Maize Ribosomes by UV-B and Its Effects on Translation. *PLANT PHYSIOLOGY* **136**: 3319–3332.

Ceci M, Gaviraghi C, Gorrini C, Sala LA, Offenhäuser N, Marchisio PC, Biffo S. 2003. Release of eIF6 (p27BBP) from the 60S subunit allows 80S ribosome assembly. *Nature* **426**: 579–584.

Chadani Y, Matsumoto E, Aso H, Wada T, Kutsukake K, Sutou S, Abo T. 2011a. trans-translation-mediated tight regulation of the expression of the alternative ribosome-rescue factor ArfA in Escherichia coli. *Genes Genet Syst* **86**: 151–163.

Chadani Y, Ono K, Kutsukake K, Abo T. 2011b. Escherichia coli YaeJ protein mediates a novel ribosome-rescue pathway distinct from SsrA- and ArfA-mediated pathways. *Mol Microbiol* **80**: 772–785.

Chadani Y, Ono K, Ozawa S-I, Takahashi Y, Takai K, Nanamiya H, Tozawa Y, Kutsukake K, Abo T. 2010. Ribosome rescue by Escherichia coli ArfA (YhdL) in the absence of trans-translation system. *Mol Microbiol* **78**: 796–808.

Chang Y, Kong Q, Shan X, Tian G, Ilieva H, Cleveland DW, Rothstein JD, Borchelt DR, Wong PC, Lin C-LG. 2008. Messenger RNA Oxidation Occurs Early in Disease Pathogenesis and Promotes Motor Neuron Degeneration in ALS ed. M.R. Cookson. *PLoS ONE* **3**: e2849.

Chen L, Liu P, Evans TC, Ettwiller LM. 2017. DNA damage is a pervasive cause of sequencing errors, directly confounding variant identification. *Science* **355**: 752–756.

Chen L, Muhlrad D, Hauryliuk V, Cheng Z, Lim MK, Shyp V, Parker R, Song H. 2010. Structure of the Dom34-Hbs1 complex and implications for no-go decay. *Nat Struct Mol Biol* **17**: 1233–1240.

Chen-Harris H, Borucki MK, Torres C, Slezak TR, Allen JE. 2013. Ultra-deep mutant spectrum profiling: improving sequencing accuracy using overlapping read pairs. *BMC Genomics* **14**: 96.

Choe Y-J, Park S-H, Hassemer T, Körner R, Vincenz-Donnelly L, Hayer-Hartl M, Hartl FU. 2016. Failure of RQC machinery causes protein aggregation and proteotoxic stress. *Nature* **531**: 191–195.

Chu J, Hong NA, Masuda CA, Jenkins BV, Nelms KA, Goodnow CC, Glynne RJ, Wu H, Masliah E, Joazeiro CAP, et al. 2009. A mouse forward genetics screen identifies LISTERIN as an E3 ubiquitin ligase involved in neurodegeneration. *Proc Natl Acad Sci USA* **106**: 2097–2103.

Cole SE, LaRiviere FJ. 2008. Chapter 12. Analysis of nonfunctional ribosomal RNA decay in Saccharomyces cerevisiae. *Methods Enzymol* **449**: 239–259.

Cole SE, LaRiviere FJ, Merrikh CN, Moore MJ. 2009. A convergence of rRNA and mRNA quality control pathways revealed by mechanistic analysis of nonfunctional rRNA decay. *Mol Cell* **34**: 440–450.

Costello M, Pugh TJ, Fennell TJ, Stewart C, Lichtenstein L, Meldrim JC, Fostel JL, Friedrich DC, Perrin D, Dionne D, et al. 2013. Discovery and characterization of artifactual mutations in deep coverage targeted capture sequencing data due to oxidative DNA damage during sample preparation. *Nucleic Acids Res* **41**: e67.

Coyle SM, Gilbert WV, Doudna JA. 2009. Direct link between RACK1 function and localization at the ribosome in vivo. *Mol and Cell Biol* **29**: 1626–1634.

Cozen AE, Quartley E, Holmes AD, Hrabeta-Robinson E, Phizicky EM, Lowe TM. 2015. ARM-seq: AlkB-facilitated RNA methylation sequencing reveals a complex landscape of modified tRNA fragments. *Nat Meth* **12**: 879–884.

Decatur WA, Fournier MJ. 2002. rRNA modifications and ribosome function. *Trends in biochemical sciences* **27**: 344–351.

Defenouillère Q, Yao Y, Mouaikel J, Namane A, Galopier A, Decourty L, Doyen A, Malabat C, Saveanu C, Jacquier A, et al. 2013. Cdc48-associated complex bound to 60S particles is required for the clearance of aberrant translation products. *Proc Natl Acad Sci USA* **110**: 5046–5051.

Defenouillère Q, Zhang E, Namane A, Mouaikel J, Jacquier A, Fromont-Racine M. 2016. Rqc1 and Ltn1 Prevent C-terminal Alanine-Threonine Tail (CAT-tail)-induced Protein Aggregation by Efficient Recruitment of Cdc48 on Stalled 60S Subunits. *J Biol Chem* **291**: 12245–12253.

Demo G, Svidritskiy E, Madireddy R, Diaz-Avalos R, Grant T, Grigorieff N, Sousa D, Korostelev AA. 2017. Mechanism of ribosome rescue by ArfA and RF2. *eLife* **6**: e14874.

Demple B, Harrison L. 1994. Repair of oxidative damage to DNA: enzymology and biology. *Annu Rev Biochem* **63**: 915–948.

Deutsch WA, Yacoub A, Jaruga P, Zastawny TH, Dizdaroglu M. 1997. Characterization and mechanism of action of Drosophila ribosomal protein S3 DNA glycosylase activity for the removal of oxidatively damaged DNA bases. *J Biol Chem* **272**: 32857–32860.

Dever TE, Green R. 2012. The elongation, termination, and recycling phases of translation in eukaryotes. *Cold Spring Harb Perspect Biol* **4**: a013706–a013706.

Dimitrova LN, Kuroha K, Tatematsu T, Inada T. 2009. Nascent peptide-dependent translation arrest leads to Not4p-mediated protein degradation by the proteasome. *J Biol Chem* **284**: 10343–10352.

Ding Q, Markesbery WR, Chen Q, Li F, Keller JN. 2005. Ribosome dysfunction is an early event in Alzheimer's disease. *Journal of Neuroscience* **25**: 9171–9175.

Doetsch PW, Cunningham RP. 1990. The enzymology of apurinic/apyrimidinic endonucleases. *Mutat Res* **236**: 173–201.

Doma MK, Parker R. 2006. Endonucleolytic cleavage of eukaryotic mRNAs with stalls in translation elongation. *Nature* **440**: 561–564.

Drabløs F, Feyzi E, Aas PA, Vaagbø CB, Kavli B, Bratlie MS, Peña-Diaz J, Otterlei M, Slupphaug G, Krokan HE. 2004. Alkylation damage in DNA and RNA—repair mechanisms and medical significance. *DNA Repair* **3**: 1389–1407.

Duechler M, Leszczyńska G, Sochacka E, Nawrot B. 2016. Nucleoside modifications in the regulation of gene expression: focus on tRNA. *Cell Mol Life Sci* **73**: 3075–3095.

Eberle AB, Lykke-Andersen S, Mühlemann O, Jensen TH. 2009. SMG6 promotes endonucleolytic cleavage of nonsense mRNA in human cells. *Nat Struct Mol Biol* **16**: 49–55.

Fang NN, Chan GT, Zhu M, Comyn SA, Persaud A, Deshaies RJ, Rotin D, Gsponer J, Mayor T. 2014. Rsp5/Nedd4 is the main ubiquitin ligase that targets cytosolic misfolded proteins following heat stress. *Nat Cell Biol* **16**: 1227–1237.

Ferrin MA, Subramaniam AR. 2017. Kinetic modeling predicts a stimulatory role for ribosome collisions at elongation stall sites in bacteria. *eLife* **6**.

Fiala ES, Conaway CC, Mathis JE. 1989. Oxidative DNA and RNA damage in the livers of Sprague-Dawley rats treated with the hepatocarcinogen 2-nitropropane. *Cancer Res* **49**: 5518–5522.

Franckenberg S, Becker T, Beckmann R. 2012. Structural view on recycling of archaeal and eukaryotic ribosomes after canonical termination and ribosome rescue. *Curr Opin Struct Biol* **22**: 786–796.

Frischmeyer PA, van Hoof A, O'Donnell K, Guerrerio AL, Parker R, Dietz HC. 2002. An mRNA surveillance mechanism that eliminates transcripts lacking termination codons. *Science* **295**: 2258–2261.

Fu Y, Dominissini D, Rechavi G, He C. 2014. Gene expression regulation mediated through reversible m^{6}A RNA methylation. *Nat Rev Genet* **15**: 293–306.

Fujii K, Kitabatake M, Sakata T, Miyata A, Ohno M. 2009. A role for ubiquitin in the clearance of nonfunctional rRNAs. *Genes Dev* **23**: 963–974.

Fujii K, Kitabatake M, Sakata T, Ohno M. 2012. 40S subunit dissociation and proteasome-dependent RNA degradation in nonfunctional 25S rRNA decay. *EMBO J* **31**: 2579–2589.

Gagnon MG, Seetharaman SV, Bulkley D, Steitz TA. 2012. Structural Basis for the Rescue of Stalled Ribosomes: Structure of YaeJ Bound to the Ribosome. *Science* **335**: 1370–1372.

Gandhi R, Manzoor M, Hudak KA. 2008. Depurination of Brome Mosaic Virus RNA3 in Vivo Results in Translation-dependent Accelerated Degradation of the Viral RNA. *J Biol Chem* **283**: 32218–32228.

Garza-Sánchez F, Schaub RE, Janssen BD, Hayes CS. 2011. tmRNA regulates synthesis of the ArfA ribosome rescue factor. *Mol Microbiol* **80**: 1204–1219.

Gatfield D, Izaurralde E. 2004. Nonsense-mediated messenger RNA decay is initiated by endonucleolytic cleavage in Drosophila. *Nature* **429**: 575–578.

Gilbert WV, Bell TA, Schaening C. 2016. Messenger RNA modifications: Form, distribution, and function. *Science* **352**: 1408–1412.

Gong X, Tao R, Li Z. 2006. Quantification of RNA damage by reverse transcription polymerase chain reactions. *Analytical Biochemistry* **357**: 58–67.

Graille M, Chaillet M, van Tilbeurgh H. 2008. Structure of yeast Dom34: a protein related to translation termination factor Erf1 and involved in No-Go decay. *J Biol Chem* **283**: 7145–7154.

Graille M, Séraphin B. 2012. Surveillance pathways rescuing eukaryotic ribosomes lost in translation. *Nat Rev Mol Cell Biol* **13**: 727–735.

Greenberg JR. 1979. Ultraviolet light-induced crosslinking of mRNA to proteins. *Nucleic Acids Res* **6**: 715–732.

Gregersen N, Bross P, Vang S, Christensen JH. 2006. Protein misfolding and human disease. *Annu Rev Genomics Hum Genet* **7**: 103–124.

Gros L, Saparbaev MK, Laval J. 2002. Enzymology of the repair of free radicals-induced DNA damage. *Oncogene* **21**: 8905–8925.

Grosheva AS, Zharkov DO, Stahl J, Gopanenko AV, Tupikin AE, Kabilov MR, Graifer DM, Karpova GG. 2017. Recognition but no repair of abasic site in single-stranded DNA by human ribosomal uS3 protein residing within intact 40S subunit. *Nucleic Acids Res* **45**: 3833–3843.

Guydosh NR, Green R. 2014. Dom34 rescues ribosomes in 3' untranslated regions. *Cell* **156**: 950–962.

Guydosh NR, Green R. 2017. Translation of poly(A) tails leads to precise mRNA cleavage. *RNA* **23**: 749–761.

Hafner M, Landthaler M, Burger L, Khorshid M, Hausser J, Berninger P, Rothballer A, Ascano M, Jungkamp A-C, Munschauer M, et al. 2010. PAR-CliP--a method to identify transcriptome-wide the binding sites of RNA binding proteins. *J Vis Exp*.

Halbach F, Reichelt P, Rode M, Conti E. 2013. The Yeast Ski Complex: Crystal Structure and RNA Channeling to the Exosome Complex. *Cell* **154**: 814–826.

Handa Y, Inaho N, Nameki N. 2011. YaeJ is a novel ribosome-associated protein in Escherichia coli that can hydrolyze peptidyl-tRNA on stalled ribosomes. *Nucleic Acids Res* **39**: 1739–1748.

Hegde V, Kelley MR, Xu Y, Mian IS, Deutsch WA. 2001. Conversion of the bifunctional 8-oxoguanine/beta-delta apurinic/apyrimidinic DNA repair activities of Drosophila ribosomal protein S3 into the human S3 monofunctional beta-elimination catalyst through a single amino acid change. *J Biol Chem* **276**: 27591–27596.

Hegde V, Wang M, Deutsch WA. 2004. Characterization of human ribosomal protein S3 binding to 7,8-dihydro-8-oxoguanine and abasic sites by surface plasmon resonance. *DNA Repair* **3**: 121–126.

Hegde V, Wang M, Mian IS, Spyres L, Deutsch WA. 2006. The high binding affinity of human ribosomal protein S3 to 7,8-dihydro-8-oxoguanine is abrogated by a single amino acid change. *DNA Repair* **5**: 810–815.

Heminger KA, Hartson SD, Rogers J, Matts RL. 1997. Cisplatin inhibits protein synthesis in rabbit reticulocyte lysate by causing an arrest in elongation. *Arch Biochem Biophys* **344**: 200–207.

Heyer EE, Ozadam H, Ricci EP, Cenik C, Moore MJ. 2015. An optimized kit-free method for making strand-specific deep sequencing libraries from RNA fragments. *Nucleic Acids Res* **43**: e2.

Higgins R, Gendron JM, Rising L, Mak R, Webb K, Kaiser SE, Zuzow N, Riviere P, Yang B, Fenech E, et al. 2015. The Unfolded Protein Response Triggers Site-Specific Regulatory Ubiquitylation of 40S Ribosomal Proteins. *Mol Cell* **59**: 35–49.

Hilal T, Yamamoto H, Loerke J, Bürger J, Mielke T, Spahn CMT. 2016. Structural insights into ribosomal rescue by Dom34 and Hbs1 at near-atomic resolution. *Nat Commun* **7**: 13521.

Hoernes TP, Clementi N, Faserl K, Glasner H, Breuker K, Lindner H, Hüttenhofer A, Erlacher MD. 2016. Nucleotide modifications within bacterial messenger RNAs regulate their translation and are able to rewire the genetic code. *Nucleic Acids Res* **44**: 852–862.

Hofer T, Badouard C, Bajak E, Ravanat J-L, Mattsson Å, Cotgreave IA. 2005. Hydrogen peroxide causes greater oxidation in cellular RNA than in DNA. *Biol Chem* **386**: 333–337.

Hofer T, Seo AY, Prudencio M, Leeuwenburgh C. 2006. A method to determine RNA and DNA oxidation simultaneously by HPLC-ECD: greater RNA than DNA oxidation in rat liver after doxorubicin administration. *Biol Chem* **387**: 103–111.

Holmes RK, Singer MF. 1971. Inability to detect RNase V in Escherichia coli and comparison of other ribonucleases before and after infection with coliphage T7. *Biochemical and Biophysical Research Communications* **44**: 837–843.

Holt LJ, Tuch BB, Villén J, Johnson AD, Gygi SP, Morgan DO. 2009. Global analysis of Cdk1 substrate phosphorylation sites provides insights into evolution. *Science* **325**: 1682–1686.

Horikawa W, Endo K, Wada M, Ito K. 2016. Mutations in the G-domain of Ski7 cause specific dysfunction in non-stop decay. *Sci Rep* **6**: 29295.

Hosoda N, Kobayashi T, Uchida N, Funakoshi Y, Kikuchi Y, Hoshino S, Katada T. 2003. Translation termination factor eRF3 mediates mRNA decay through the regulation of deadenylation. *J Biol Chem* **278**: 38287–38291.

Hostetter AA, Osborn MF, DeRose VJ. 2012. RNA-Pt Adducts Following

Cisplatin Treatment of Saccharomyces cerevisiae. *ACS Chem Biol* **7**: 218–225.

Hsu GW, Ober M, Carell T, Beese LS. 2004. Error-prone replication of oxidatively damaged DNA by a high-fidelity DNA polymerase. *Nature* **431**: 217–221.

Hudson BH, Zaher HS. 2015. O6-Methylguanosine leads to position-dependent effects on ribosome speed and fidelity. *RNA* **21**: 1648–1659.

Hurst RO, Kuksis A. 1958. Degradation of some purine and pyrimidine derivatives by hot alkali. *Can J Biochem Physiol* **36**: 931–936.

Huter P, Müller C, Beckert B, Arenz S, Berninghausen O, Beckmann R, Wilson DN. 2017. Structural basis for ArfA-RF2-mediated translation termination on mRNAs lacking stop codons. *Nature* **541**: 546–549.

Ikeuchi K, Inada T. 2016. Ribosome-associated Asc1/RACK1 is required for endonucleolytic cleavage induced by stalled ribosome at the 3' end of nonstop mRNA. *Sci Rep* **6**: 28234–28234.

Inada T. 2013. Quality control systems for aberrant mRNAs induced by aberrant translation elongation and termination. *Biochim Biophys Acta* **1829**: 634–642.

Ingolia NT, Brar GA, Rouskin S, McGeachy AM, Weissman JS. 2012. The ribosome profiling strategy for monitoring translation in vivo by deep sequencing of ribosome-protected mRNA fragments. *Nat Protoc* **7**: 1534–1550.

Ingolia NT, Ghaemmaghami S, Newman JRS, Weissman JS. 2009. Genome-wide analysis in vivo of translation with nucleotide resolution using ribosome profiling. *Science* **324**: 218–223.

Iordanov MS, Pribnow D, Magun JL, Dinh TH, Pearson JA, Chen SL, Magun BE. 1997. Ribotoxic stress response: activation of the stress-activated protein kinase JNK1 by inhibitors of the peptidyl transferase reaction and by sequence-specific RNA damage to the alpha-sarcin/ricin loop in the 28S rRNA. *Mol and Cell Biol* **17**: 3373–3381.

Iordanov MS, Pribnow D, Magun JL, Dinh TH, Pearson JA, Magun BE. 1998. Ultraviolet radiation triggers the ribotoxic stress response in mammalian cells. *J Biol Chem* **273**: 15794–15803.

Ito K, Chadani Y, Nakamori K, Chiba S, Akiyama Y, Abo T. 2011. Nascentome analysis uncovers futile protein synthesis in Escherichia coli. *PLoS ONE* **6**: e28413–e28413.

Ivanova N, Pavlov MY, Felden B, Ehrenberg M. 2004. Ribosome Rescue by tmRNA Requires Truncated mRNAs. *J Mol Biol* **338**: 33–41.

Jamar NH, Kritsiligkou P, Grant CM. 2017. The non-stop decay mRNA surveillance pathway is required for oxidative stress tolerance. *Nucleic Acids Res* **45**: 6881–6893.

James NR, Brown A, Gordiyenko Y, Ramakrishnan V. 2016. Translational termination without a stop codon. *Science* **354**: 1437–1440.

Jia G, Fu Y, Zhao X, Dai Q, Zheng G, Yang Y, Yi C, Lindahl T, Pan T, Yang Y-G, et al. 2011. N6-methyladenosine in nuclear RNA is a major substrate of the obesity-associated FTO. *Nat Chem Biol* **7**: 885–887.

Jiao X, Xiang S, Oh C, Martin CE, Tong L, Kiledjian M. 2010. Identification of a quality-control mechanism for mRNA 5'-end capping. *Nature* **467**: 608–611.

Juszkiewicz S, Hegde RS. 2017. Initiation of Quality Control during Poly(A) Translation Requires Site-Specific Ribosome Ubiquitination. *Molecular Cell* **65**: 743–750.e4.

Karzai AW, Susskind MM, Sauer RT. 1999. SmpB, a unique RNA-binding protein essential for the peptide-tagging activity of SsrA (tmRNA). *EMBO J* **18**: 3793–3799.

Katibah GE, Qin Y, Sidote DJ, Yao J, Lambowitz AM, Collins K. 2014. Broad and adaptable RNA structure recognition by the human interferon-induced tetratricopeptide repeat protein IFIT5. *Proc Natl Acad Sci USA* **111**: 12025–12030.

Keiler KC. 2015. Mechanisms of ribosome rescue in bacteria. *Nat Rev Microbiol* **13**: 285–297.

Keiler KC, Waller PR, Sauer RT. 1996. Role of a peptide tagging system in degradation of proteins synthesized from damaged messenger RNA. *Science* **271**: 990–993.

Kervestin S, Jacobson A. 2012. NMD: a multifaceted response to premature translational termination. *Nat Rev Mol Cell Biol* **13**: 700–712.

Kiely PA, Baillie GS, Barrett R, Buckley DA, Adams DR, Houslay MD, O'Connor R. 2009. Phosphorylation of RACK1 on tyrosine 52 by c-Abl is required for insulin-like growth factor I-mediated regulation of focal adhesion kinase. *J Biol Chem* **284**: 20263–20274.

Kim J, Chubatsu LS, Admon A, Stahl J, Fellous R, Linn S. 1995. Implication of mammalian ribosomal protein S3 in the processing of DNA damage. *J Biol Chem* **270**: 13620–13629.

Kim SK, Kim JY, Yokoyama S, Takaku H, Moon BJ. 2006. Misreading of RNA Templates Containing 8-Oxo-7,8-Dihydroguanosine Or 8-Oxo-2′-O-Methylguanosine in cDNA Synthesis by Reverse Transcriptases. *Nucleosides and Nucleotides* **18**: 1335–1337.

Kim SKS, Lee SHS, Kwon O-SO, Moon BJB. 2004. DNA . RNA heteroduplex containing 8-oxo-7,8-dihydroguanosine: base pairing, structures, and thermodynamic stability. *J Biochem Mol Biol* **37**: 657–662.

Kladwang W, Hum J, Das R. 2012. Ultraviolet shadowing of RNA can cause significant chemical damage in seconds. *Sci Rep* **2**: 517–517.

Korostelev AA. 2011. Structural aspects of translation termination on the ribosome. *RNA* **17**: 1409–1421.

Kostova KK, Hickey KL, Osuna BA, Hussmann JA, Frost A, Weinberg DE, Weissman JS. 2017. CAT-tailing as a fail-safe mechanism for efficient degradation of stalled nascent polypeptides. *Science* **357**: 414–417.

Kowalinski E, Kögel A, Ebert J, Reichelt P, Stegmann E, Habermann B, Conti E. 2016. Structure of a Cytoplasmic 11-Subunit RNA Exosome Complex. *Mol Cell* **63**: 125–134.

Kowalinski E, Schuller A, Green R, Conti E. 2015. Saccharomyces cerevisiae Ski7 Is a GTP-Binding Protein Adopting the Characteristic Conformation of Active Translational GTPases. *Structure* **23**: 1336–1343.

Kuroha K, Akamatsu M, Dimitrova L, Ito T, Kato Y, Shirahige K, Inada T. 2010. Receptor for activated C kinase 1 stimulates nascent polypeptide-dependent translation arrest. *EMBO Rep* **11**: 956–961.

LaRiviere FJ, Cole SE, Ferullo DJ, Moore MJ. 2006. A Late-Acting Quality Control Process for Mature Eukaryotic rRNAs. *Molecular Cell* **24**: 619–626.

Lee HH, Kim Y-S, Kim KH, Heo I, Kim SK, Kim O, Kim HK, Yoon JY, Kim HS, Do Jin Kim, et al. 2007. Structural and Functional Insights into Dom34, a Key Component of No-Go mRNA Decay. *Molecular Cell* **27**: 938–950.

Letzring DP, Dean KM, Grayhack EJ. 2010. Control of translation efficiency in yeast by codon-anticodon interactions. *RNA* **16**: 2516–2528.

Letzring DP, Wolf AS, Brule CE, Grayhack EJ. 2013. Translation of CGA codon repeats in yeast involves quality control components and ribosomal protein L1. *RNA* **19**: 1208–1217.

Lindahl T, Nyberg B. 1974. Heat-induced deamination of cytosine residues in deoxyribonucleic acid. *Biochemistry* **13**: 3405–3410.

Liu F, Clark W, Luo G, Wang X, Fu Y, Wei J, Wang X, Hao Z, Dai Q, Zheng G, et al. 2016. ALKBH1-Mediated tRNA Demethylation Regulates Translation. *Cell* **167**: 1897.

Liu M, Gong X, Alluri RK, Wu J, Tene' Sablo, Li Z. 2012. Characterization of RNA damage under oxidative stress in Escherichia coli. *Biol Chem* **393**: 123–132.

Liu YV, Baek JH, Zhang H, Diez R, Cole RN, Semenza GL. 2007. RACK1 competes with HSP90 for binding to HIF-1alpha and is required for O(2)-independent and HSP90 inhibitor-induced degradation of HIF-1alpha. *Molecular Cell* **25**: 207–217.

Lu J, Kobertz WR, Deutsch C. 2007. Mapping the electrostatic potential within the ribosomal exit tunnel. *Journal of Molecular Biology* **371**: 1378–1391.

Ma C, Kurita D, Li N, Chen Y, Himeno H, Gao N. 2017. Mechanistic insights into the alternative translation termination by ArfA and RF2. *Nature* **541**: 550–553.

Matsuo Y, Ikeuchi K, Saeki Y, Iwasaki S, Schmidt C, Udagawa T, Sato F, Tsuchiya H, Becker T, Tanaka K, et al. 2017. Ubiquitination of stalled ribosome triggers ribosome-associated quality control. *Nat Commun* **8**: 159.

McCahill A, Warwicker J, Bolger GB, Houslay MD, Yarwood SJ. 2002. The RACK1 scaffold protein: a dynamic cog in cell response mechanisms. *Mol Pharmacol* **62**: 1261–1273.

McGinnis JL, Dunkle JA, Cate JHD, Weeks KM. 2012. The mechanisms of RNA SHAPE chemistry. *J Am Chem Soc* **134**: 6617–6624.

McKinlay A, Gerard W, Fields S. 2012. Global analysis of RNA oxidation in Saccharomyces cerevisiae. *Biotech* **52**.

Melamed D, Bar-Ziv L, Truzman Y, Arava Y. 2010. Asc1 supports cell-wall integrity near bud sites by a Pkc1 independent mechanism. ed. M. Kaeberlein. *PLoS ONE* **5**: e11389.

Melnikov SV, Söll D, Steitz TA, Polikanov YS. 2016. Insights into RNA binding by the anticancer drug cisplatin from the crystal structure of cisplatin-modified ribosome. *Nucleic Acids Res* **44**: 4978–4987.

Merino EJ, Wilkinson KA, Coughlan JL, Weeks KM. 2005. RNA structure analysis at single nucleotide resolution by selective 2'-hydroxyl acylation and primer extension (SHAPE). *J Am Chem Soc* **127**: 4223–4231.

Merrikh CN. 2012. Characterization of new factors in the 18S nonfunctional ribosomal RNA decay pathway in S. cerevisiae: a dissertation. University of Massachusetts Medical School. GSBS Dissertations and Theses. Paper 613. http://escholarship.umassmed.edu/gsbs_diss/613.

Miller N, Cerutti P. 1968. Structure of the photohydration products of cytidine and uridine. *Proc Natl Acad Sci USA* **59**: 34–38.

Minoche AE, Dohm JC, Himmelbauer H. 2011. Evaluation of genomic high-throughput sequencing data generated on Illumina HiSeq and genome analyzer systems. *Genome biology* **12**: R112.

Mohr S, Ghanem E, Smith W, Sheeter D, Qin Y, King O, Polioudakis D, Iyer VR, Hunicke-Smith S, Swamy S, et al. 2013. Thermostable group II intron reverse transcriptase fusion proteins and their use in cDNA synthesis and next-generation RNA sequencing. *RNA* **19**: 958–970.

Mortimer SA, Weeks KM. 2007. A Fast-Acting Reagent for Accurate Analysis of RNA Secondary and Tertiary Structure by SHAPE Chemistry. *J Am Chem Soc* **129**: 4144–4145.

Neubauer C, Gillet R, Kelley AC, Ramakrishnan V. 2012. Decoding in the absence of a codon by tmRNA and SmpB in the ribosome. *Science* **335**: 1366–1369.

Niki E. 2014. Role of vitamin E as a lipid-soluble peroxyl radical scavenger: in vitro and in vivo evidence. *Free Radical Biology and Medicine* **66**: 3–12.

Nunomura A, Chiba S, Kosaka K, Takeda A, Castellani RJ, Smith MA, Perry G. 2002. Neuronal RNA oxidation is a prominent feature of dementia with Lewy bodies. *Neuroreport* **13**: 2035–2039.

Nunomura A, Hofer T, Moreira PI, Castellani RJ, Smith MA, Perry G. 2009. RNA oxidation in Alzheimer disease and related neurodegenerative disorders. *Acta Neuropathol* **118**: 151–166.

Nunomura A, Tamaoki T, Motohashi N, Nakamura M, McKeel DW Jr, Tabaton M, Lee H-G, Smith MA, Perry G, Zhu X. 2012. The Earliest Stage of Cognitive Impairment in Transition From Normal Aging to Alzheimer Disease Is Marked by Prominent RNA Oxidation in Vulnerable Neurons. *Journal of Neuropathology & Experimental Neurology* **71**: 233–241.

Nunomura AA, Perry GG, Pappolla MAM, Wade RR, Hirai KK, Chiba SS, Smith MAM. 1999. RNA oxidation is a prominent feature of vulnerable neurons in Alzheimer's disease. *Journal of Neuroscience* **19**: 1959–1964.

Nunoshiba T, Demple B. 1993. Potent Intracellular Oxidative Stress Exerted by the Carcinogen 4-Nitroquinoline-N-oxide. *Cancer Res* **53**: 3250–3252.

Ogle JM, Brodersen DE, Clemons WM, Tarry MJ, Carter AP, Ramakrishnan V. 2001. Recognition of cognate transfer RNA by the 30S ribosomal subunit. *Science* **292**: 897–902.

Osborn MF, White JD, Haley MM, DeRose VJ. 2014. Platinum-RNA modifications following drug treatment in S. cerevisiae identified by click chemistry and enzymatic mapping. *ACS Chem Biol* **9**: 2404–2411.

Osuna BA, Howard CJ, Kc S, Frost A, Weinberg DE. 2017. In vitro analysis of RQC activities provides insights into the mechanism and function of CAT tailing. *eLife* **6**.

Ougland R, Zhang C-M, Liiv A, Johansen RF, Seeberg E, Hou Y-M, Remme J, Falnes PO. 2004. AlkB restores the biological function of mRNA and tRNA inactivated by chemical methylation. *Molecular Cell* **16**: 107–116.

Paier A, Leppik M, Soosaar A, Tenson T, Maiväli Ü. 2015. The effects of disruptions in ribosomal active sites and in intersubunit contacts on ribosomal degradation in Escherichia coli. *Sci Rep* **5**: 7712–7712.

Park EM, Shigenaga MK, Degan P, Korn TS, Kitzler JW, Wehr CM, Kolachana P, Ames BN. 1992. Assay of excised oxidative DNA lesions: isolation of 8-oxoguanine and its nucleoside derivatives from biological fluids with a monoclonal antibody column. *Proc Natl Acad Sci USA* **89**: 3375–3379.

Passos DO, Doma MK, Shoemaker CJ, Muhlrad D, Green R, Weissman J, Hollien J, Parker R. 2009. Analysis of Dom34 and its function in no-go decay. *Mol Biol Cell* **20**: 3025–3032.

Pearson M, Johns HE. 1966. Suppression of hydrate and dimer formation in ultraviolet-irradiated poly (A plus U) relative to poly U. *Journal of Molecular Biology* **20**: 215–229.

Pearson M, Whillans DW, LeBlanc JC, Johns HE. 1966. Dependence on wavelength of photoproduct yields in ultraviolet-irradiated poly U. *Journal of Molecular Biology* **20**: 245–261.

Pelechano V, Wei W, Steinmetz LM. 2015. Widespread Co-translational RNA Decay Reveals Ribosome Dynamics. *Cell* **161**: 1400–1412.

Peng J, Schwartz D, Elias JE, Thoreen CC, Cheng D, Marsischky G, Roelofs J, Finley D, Gygi SP. 2003. A proteomics approach to understanding protein ubiquitination. *Nat Biotechnol* **21**: 921–926.

Peña C, Hurt E, Panse VG. 2017. Eukaryotic ribosome assembly, transport and quality control. *Nature Publishing Group* **24**: 689–699.

Pisareva VP, Skabkin MA, Hellen CUT, Pestova TV, Pisarev AV. 2011. Dissociation by Pelota, Hbs1 and ABCE1 of mammalian vacant 80S ribosomes and stalled elongation complexes. *EMBO J* **30**: 1804–1817.

Powers T, Noller HF. 1990. Dominant lethal mutations in a conserved loop in 16S rRNA. *Proc Natl Acad Sci USA* **87**: 1042–1046.

Powers T, Noller HF. 1993. Evidence for functional interaction between elongation factor Tu and 16S ribosomal RNA. *Proc Natl Acad Sci USA* **90**: 1364–1368.

Preis A, Heuer A, Barrio-Garcia C, Hauser A, Eyler DE, Berninghausen O, Green R, Becker T, Beckmann R. 2014. Cryoelectron microscopic structures of eukaryotic translation termination complexes containing eRF1-eRF3 or eRF1-ABCE1. *Cell Rep* **8**: 59–65.

Preston JL, Royall AE, Randel MA, Sikkink KL, Phillips PC, Johnson EA. 2016. High-specificity detection of rare alleles with Paired-End Low Error Sequencing (PELE-Seq). *BMC Genomics* **17**: 464.

Rachfall N, Schmitt K, Bandau S, Smolinski N, Ehrenreich A, Valerius O, Braus GH. 2013. RACK1/Asc1p, a ribosomal node in cellular signaling. *Mol Cell Proteomics* **12**: 87–105.

Rada B, Leto TL. 2008. Oxidative innate immune defenses by Nox/Duox family NADPH oxidases. *Contrib Microbiol* **15**: 164–187.

Remsen JF, Miller N, Cerutti PA. 1970. Photohydration of uridine in the RNA of coliphage R17. II. The relationship between ultraviolet inactivation and uridine photohydration. *Proc Natl Acad Sci USA* **65**: 460–466.

Requião RD, de Souza HJA, Rossetto S, Domitrovic T, Palhano FL. 2016. Increased ribosome density associated to positively charged residues is evident in ribosome profiling experiments performed in the absence of translation inhibitors. *RNA Biol* **13**: 561–568.

Rhee Y, Valentine MR, Termini J. 1995. Oxidative base damage in RNA detected by reverse transcriptase. *Nucleic Acids Res* **23**: 3275–3282.

Roberts JJ, Thomson AJ. 1979. The mechanism of action of antitumor platinum compounds. *Prog Nucleic Acid Res Mol Biol* **22**: 71–133.

Roberts RW, Szostak JW. 1997. RNA-peptide fusions for the in vitro selection of peptides and proteins. *Proc Natl Acad Sci USA* **94**: 12297–12302.

Rodnina MV, Wintermeyer W. 2009. Recent mechanistic insights into eukaryotic ribosomes. *Curr Opin Cell Biol* **21**: 435–443.

Ron D, Chen CH, Caldwell J, Jamieson L, Orr E, Mochly-Rosen D. 1994. Cloning of an intracellular receptor for protein kinase C: a homolog of the beta subunit of G proteins. *Proc Natl Acad Sci USA* **91**: 839–843.

Ron D, Jiang Z, Yao L, Vagts A, Diamond I, Gordon A. 1999. Coordinated movement of RACK1 with activated betaIIPKC. *J Biol Chem* **274**: 27039–27046.

Rosenberg B. 1985. Fundamental studies with cisplatin. *Cancer* **55**: 2303–l6.

Rosenberg JM, Sato PH. 1993. Cisplatin inhibits in vitro translation by preventing the formation of complete initiation complex. *Mol Pharmacol* **43**: 491–497.

Saito K, Horikawa W, Ito K. 2015. Inhibiting K63 polyubiquitination abolishes no-go type stalled translation surveillance in Saccharomyces cerevisiae. *PLoS Genet* **11**: e1005197–e1005197.

Saito S, Hosoda N, Hoshino S-I. 2013a. The Hbs1-Dom34 protein complex functions in non-stop mRNA decay in mammalian cells. *J Biol Chem* **288**: 17832–17843.

Saito S, Hosoda N, Hoshino S-I. 2013b. The Hbs1-Dom34 protein complex functions in non-stop mRNA decay in mammalian cells. *J Biol Chem* **288**: 17832–17843.

Schirmer M, D'Amore R, Ijaz UZ, Hall N, Quince C. 2016. Illumina error profiles: resolving fine-scale variation in metagenomic sequencing data. *BMC Bioinformatics* **17**: 125.

Schmeing TM, Ramakrishnan V. 2009. What recent ribosome structures have revealed about the mechanism of translation. *Nature* **461**: 1234–1242.

Schmidt C, Kowalinski E, Shanmuganathan V, Defenouillère Q, Braunger K, Heuer A, Pech M, Namane A, Berninghausen O, Fromont-Racine M, et al. 2016a. The cryo-EM structure of a ribosome-Ski2-Ski3-Ski8 helicase complex. *Science* **354**: 1431–1433.

Schmidt C, Kowalinski E, Shanmuganathan V, Defenouillère Q, Braunger K, Heuer A, Pech M, Namane A, Berninghausen O, Fromont-Racine M, et al. 2016b. The cryo-EM structure of a ribosome-Ski2-Ski3-Ski8 helicase complex. *Science* **354**: 1431–1433.

Schmitt MW, Kennedy SR, Salk JJ, Fox EJ, Hiatt JB, Loeb LA. 2012. Detection of ultra-rare mutations by next-generation sequencing. *Proc Natl Acad Sci USA* **109**: 14508–14513.

Schmittgen TD, Ju J-F, Danenberg KD, Danenberg PV. 2003. Inhibition of pre-mRNA splicing by cisplatin and platinum analogs. *Int J Oncol* **23**: 785–789.

Sedgwick B. 2004. Repairing DNA-methylation damage. *Nat Rev Mol Cell Biol* **5**:

148–157.

Seyfried NT, Xu P, Duong DM, Cheng D, Hanfelt J, Peng J. 2008. Systematic approach for validating the ubiquitinated proteome. *Anal Chem* **80**: 4161–4169.

Shan X, Chang Y, Lin CLG. 2007. Messenger RNA oxidation is an early event preceding cell death and causes reduced protein expression. *The FASEB Journal* **21**: 2753–2764.

Shan X, Lin C-LG. 2006. Quantification of oxidized RNAs in Alzheimer's disease. *Neurobiol Aging* **27**: 657–662.

Shan X, Tashiro H, Lin C-LG. 2003. The identification and characterization of oxidized RNAs in Alzheimer's disease. *Journal of Neuroscience* **23**: 4913–4921.

Shao S, Brown A, Santhanam B, Hegde RS. 2015. Structure and assembly pathway of the ribosome quality control complex. *Mol Cell* **57**: 433–444.

Shao S, Hegde RS. 2014. Reconstitution of a minimal ribosome-associated ubiquitination pathway with purified factors. *Mol Cell* **55**: 880–890.

Shao S, Malsburg von der K, Hegde RS. 2013. Listerin-dependent nascent protein ubiquitination relies on ribosome subunit dissociation. *Mol Cell* **50**: 637–648.

Shao S, Murray J, Brown A, Taunton J, Ramakrishnan V, Hegde RS. 2016. Decoding Mammalian Ribosome-mRNA States by Translational GTPase Complexes. *Cell* **167**: 1229–1240.e15.

Shen PS, Park J, Qin Y, Li X, Parsawar K, Larson MH, Cox J, Cheng Y, Lambowitz AM, Weissman JS, et al. 2015. Protein synthesis. Rqc2p and 60S ribosomal subunits mediate mRNA-independent elongation of nascent chains. *Science* **347**: 75–78.

Shen Z, Wu W, Hazen SL. 2000. Activated Leukocytes Oxidatively Damage DNA, RNA, and the Nucleotide Pool through Halide-Dependent Formation of Hydroxyl Radical †. *Biochemistry* **39**: 5474–5482.

Shendure J, Ji H. 2008. Next-generation DNA sequencing. *Nat Biotechnol* **26**: 1135–1145.

Shi X, Khade PK, Sanbonmatsu KY, Joseph S. 2012. Functional role of the sarcin-ricin loop of the 23S rRNA in the elongation cycle of protein synthesis. *Journal of Molecular Biology* **419**: 125–138.

Shoemaker CJ, Eyler DE, Green R. 2010. Dom34:Hbs1 promotes subunit dissociation and peptidyl-tRNA drop-off to initiate no-go decay. *Science* **330**: 369–372.

Shoemaker CJ, Green R. 2011. Kinetic analysis reveals the ordered coupling of translation termination and ribosome recycling in yeast. *Proc Natl Acad Sci USA* **108**: E1392–E1398.

Shoemaker CJ, Green R. 2012. Translation drives mRNA quality control. *Nat Struct Mol Biol* **19**: 594–601.

Siddik ZH. 2003. Cisplatin: mode of cytotoxic action and molecular basis of resistance. *Oncogene* **22**: 7265–7279.

Siegfried NA, Busan S, Rice GM, Nelson JAE, Weeks KM. 2014. RNA motif discovery by SHAPE and mutational profiling (SHAPE-MaP). *Nat Meth* **11**: 959–965.

Simms CL, Hudson BH, Mosior JW, Rangwala AS, Zaher HS. 2014. An active role for the ribosome in determining the fate of oxidized mRNA. *Cell Rep* **9**: 1256–1264.

Simms CL, Yan LL, Zaher HS. 2017. Ribosome Collision Is Critical for Quality Control during No-Go Decay. *Mol Cell* **68**: 361–373.e5.

Simms CL, Zaher HS. 2016. Quality control of chemically damaged RNA. *Cell Mol Life Sci* **73**: 3639–3653.

Singh KK, Sigala B, Sikder HA, Schwimmer C. 2001. Inactivation of Saccharomyces cerevisiae OGG1 DNA repair gene leads to an increased frequency of mitochondrial mutants. *Nucleic Acids Res* **29**: 1381–1388.

Sitron CS, Park JH, Brandman O. 2017. Asc1, Hel2, and Slh1 couple translation arrest to nascent chain degradation. *RNA* **23**: 798–810.

Song H, Mugnier P, Das AK, Webb HM, Evans DR, Tuite MF, Hemmings BA, Barford D. 2000. The crystal structure of human eukaryotic release factor eRF1--mechanism of stop codon recognition and peptidyl-tRNA hydrolysis.

Cell **100**: 311–321.

Soulard A, Cremonesi A, Moes S, Schütz F, Jenö P, Hall MN. 2010. The rapamycin-sensitive phosphoproteome reveals that TOR controls protein kinase A toward some but not all substrates. *Mol Biol Cell* **21**: 3475–3486.

Stiege W, Atmadja J, Zobawa M, Brimacombe R. 1986. Investigation of the tertiary folding of Escherichia coli ribosomal RNA by intra-RNA cross-linking in vivo. *Journal of Molecular Biology* **191**: 135–138.

Subauste MC, Ventura-Holman T, Du L, Subauste JS, Chan S-L, Yu VC, Maher JF. 2009. RACK1 downregulates levels of the pro-apoptotic protein Fem1b in apoptosis-resistant colon cancer cells. *Cancer Biol Ther* **8**: 2297–2305.

Sundaramoorthy E, Leonard M, Mak R, Liao J, Fulzele A, Bennett EJ. 2017. ZNF598 and RACK1 Regulate Mammalian Ribosome- Associated Quality Control Function by Mediating Regulatory 40S Ribosomal Ubiquitylation. *Molecular Cell* **65**: 751–760.e4.

Sweet T, Kovalak C, Coller J. 2012. The DEAD-box protein Dhh1 promotes decapping by slowing ribosome movement. *PLoS Biol* **10**: e1001342–e1001342.

Tanaka M, Chock PB, Stadtman ER. 2007. Oxidized messenger RNA induces translation errors. *Proc Natl Acad Sci USA* **104**: 66–71.

Tsuboi T, Kuroha K, Kudo K, Makino S, Inoue E, Kashima I, Inada T. 2012. Dom34:hbs1 plays a general role in quality-control systems by dissociation of a stalled ribosome at the 3' end of aberrant mRNA. *Mol Cell* **46**: 518–529.

Turrens JF. 2003. Mitochondrial formation of reactive oxygen species. *J Physiol (Lond)* **552**: 335–344.

Ullman JS, McCarthy BJ. 1973. Alkali deamination of cytosine residues in DNA. *Biochim Biophys Acta* **294**: 396–404.

Valerius O, Kleinschmidt M, Rachfall N, Schulze F, López Marín S, Hoppert M, Streckfuss-Bömeke K, Fischer C, Braus GH. 2007. The Saccharomyces homolog of mammalian RACK1, Cpc2/Asc1p, is required for FLO11-dependent adhesive growth and dimorphism. *Mol Cell Proteomics* **6**: 1968–1979.

van den Elzen AMG, Henri J, Lazar N, Gas ME, Durand D, Lacroute F, Nicaise M, van Tilbeurgh H, Séraphin B, Graille M. 2010. Dissection of Dom34-Hbs1 reveals independent functions in two RNA quality control pathways. *Nat Struct Mol Biol* **17**: 1446–1452.

van den Elzen AMG, Schuller A, Green R, Séraphin B. 2014. Dom34-Hbs1 mediated dissociation of inactive 80S ribosomes promotes restart of translation after stress. *EMBO J* **33**: 265–276.

van der Kemp PA, Thomas D, Barbey R, de Oliveira R, Boiteux S. 1996. Cloning and expression in Escherichia coli of the OGG1 gene of Saccharomyces cerevisiae, which codes for a DNA glycosylase that excises 7,8-dihydro-8-oxoguanine and 2,6-diamino-4-hydroxy-5-N-methylformamidopyrimidine. *Proc Natl Acad Sci USA* **93**: 5197–5202.

van Hoof A, Frischmeyer PA, Dietz HC, Parker R. 2002. Exosome-mediated recognition and degradation of mRNAs lacking a termination codon. *Science* **295**: 2262–2264.

Vågbø CB, Svaasand EK, Aas PA, Krokan HE. 2013. Methylation damage to RNA induced in vivo in Escherichia coli is repaired by endogenous AlkB as part of the adaptive response. *DNA Repair* **12**: 188–195.

Verma R, Oania RS, Kolawa NJ, Deshaies RJ. 2013. Cdc48/p97 promotes degradation of aberrant nascent polypeptides bound to the ribosome. *eLife* **2**: e00308.

Voorhees RM, Ramakrishnan V. 2013. Structural basis of the translational elongation cycle. *Annu Rev Biochem* **82**: 203–236.

Walling C. 1975. Fenton's reagent revisited. *Acc Chem Res* **8**: 125–131.

Walter P, Ron D. 2011. The unfolded protein response: from stress pathway to homeostatic regulation. *Science* **334**: 1081–1086.

Wang L, Lewis MS, Johnson AW. 2005. Domain interactions within the Ski2/3/8 complex and between the Ski complex and Ski7p. *RNA* **11**: 1291–1302.

Wehner P, Shnitsar I, Urlaub H, Borchers A. 2011. RACK1 is a novel interaction partner of PTK7 that is required for neural tube closure. *Development* **138**: 1321–1327.

Weimann A, Belling D, Poulsen HE. 2002. Quantification of 8-oxo-guanine and guanine as the nucleobase, nucleoside and deoxynucleoside forms in human urine by high-performance liquid chromatography-electrospray tandem mass spectrometry. *Nucleic Acids Res* **30**: E7–E7.

Weinert BT, Schölz C, Wagner SA, Iesmantavicius V, Su D, Daniel JA, Choudhary C. 2013. Lysine succinylation is a frequently occurring modification in prokaryotes and eukaryotes and extensively overlaps with acetylation. *Cell Rep* **4**: 842–851.

Wilson DM, Deutsch WA, Kelley MR. 1993. Cloning of the Drosophila ribosomal protein S3: another multifunctional ribosomal protein with AP endonuclease DNA repair activity. *Nucleic Acids Res* **21**: 2516–2516.

Wilson DM, Deutsch WA, Kelley MR. 1994. Drosophila ribosomal protein S3 contains an activity that cleaves DNA at apurinic/apyrimidinic sites. *J Biol Chem* **269**: 25359–25364.

Wilson MA, Meaux S, van Hoof A. 2007. A genomic screen in yeast reveals novel aspects of nonstop mRNA metabolism. *Genetics* **177**: 773–784.

Wilusz JE. 2015. Removing roadblocks to deep sequencing of modified RNAs. *Nat Meth* **12**: 821–822.

Windebank AJ, Grisold W. 2008. Chemotherapy-induced neuropathy. *J Peripher Nerv Syst* **13**: 27–46.

Wolf AS, Grayhack EJ. 2015. Asc1, homolog of human RACK1, prevents frameshifting in yeast by ribosomes stalled at CGA codon repeats. *RNA* **21**: 935–945.

Wolf DH, Stolz A. 2012. The Cdc48 machine in endoplasmic reticulum associated protein degradation. *Biochim Biophys Acta* **1823**: 117–124.

Wool IG, Glück A, Endo Y. 1992. Ribotoxin recognition of ribosomal RNA and a proposal for the mechanism of translocation. *Trends in Biochemical Sciences* **17**: 266–269.

Wu R, Jiang D, Wang Y, Wang X. 2016. N (6)-Methyladenosine (m(6)A) Methylation in mRNA with A Dynamic and Reversible Epigenetic Modification. *Molecular Biotechnology* **58**: 450–459.

Wurtmann EJ, Wolin SL. 2009. RNA under attack: Cellular handling of RNA damage. *Critical Reviews in Biochemistry and Molecular Biology* **44**: 34–49.

Yacoub A, Augeri L, Kelley MR, Doetsch PW, Deutsch WA. 1996. A Drosophila ribosomal protein contains 8-oxoguanine and abasic site DNA repair activities. *EMBO J* **15**: 2306–2312.

Yaka R, Thornton C, Vagts AJ, Phamluong K, Bonci A, Ron D. 2002. NMDA receptor function is regulated by the inhibitory scaffolding protein, RACK1. *Proc Natl Acad Sci USA* **99**: 5710–5715.

Yamamoto Y, Sunohara T, Jojima K, Inada T, Aiba H. 2003. SsrA-mediated trans-translation plays a role in mRNA quality control by facilitating degradation of truncated mRNAs. *RNA* **9**: 408–418.

Yanagawa H, Ogawa Y, Ueno M. 1992. Redox ribonucleosides. Isolation and characterization of 5-hydroxyuridine, 8-hydroxyguanosine, and 8-hydroxyadenosine from Torula yeast RNA. *J Biol Chem* **267**: 13320–13326.

Yanagawa H, Ogawa Y, Ueno M, Sasaki K, Sato T. 1990. A novel minimum ribozyme with oxidoreduction activity. *Biochemistry* **29**: 10585–10589.

Yin B, Whyatt RM, Perera FP, Randall MC. 1995. Determination of 8-hydroxydeoxyguanosine by an immunoaffinity chromatography-monoclonal antibody-based ELISA. *Free Radical Biology and Medicine* **18**: 1023–1032.

Yonashiro R, Tahara EB, Bengtson MH, Khokhrina M, Lorenz H, Chen K-C, Kigoshi-Tansho Y, Savas JN, Yates JR, Kay SA, et al. 2016. The Rqc2/Tae2 subunit of the ribosome-associated quality control (RQC) complex marks ribosome-stalled nascent polypeptide chains for aggregation. *eLife* **5**: e11794.

Yoshizawa S, Fourmy D, Puglisi JD. 1999a. Recognition of the codon-anticodon helix by ribosomal RNA. *Science* **285**: 1722–1725.

Yoshizawa S, Fourmy D, Puglisi JD. 1999b. Recognition of the codon-anticodon helix by ribosomal RNA. *Science* **285**: 1722–1725.

You C, Dai X, Wang Y. 2017. Position-dependent effects of regioisomeric methylated adenine and guanine ribonucleosides on translation. *Nucleic Acids Res* **45**: 9059–9067.

Zhang J, Kobert K, Flouri T, Stamatakis A. 2014. PEAR: a fast and accurate Illumina Paired-End reAd mergeR. *Bioinformatics* **30**: 614–620.

Zhang J, Perry G, Smith MA, Robertson D, Olson SJ, Graham DG, Montine TJ. 1999. Parkinson's disease is associated with oxidative damage to cytoplasmic DNA and RNA in substantia nigra neurons. *Am J Pathol* **154**: 1423–1429.